Universidade do Minho
Escola de Engenharia

Edgar Manuel Neto Carneiro

Reach Regulation: Alternative Coatings to Hexavalent Chromium

julho de 2024

Edgar Manuel Neto Carneiro Reach Regulation: Alternative Coatings to Hexavalent Chromium

UMinho | 2024

Universidade do Minho
Escola de Engenharia

Edgar Manuel Neto Carneiro

Reach Regulation: Alternative Coatings to Hexavalent Chromium

Tese de Doutoramento
Programa Doutoral em Engenharia de Materiais

Trabalho efetuado sob a orientação da
Professora Doutora Sandra Maria Fernandes Carvalho

julho de 2024

DIREITOS DE AUTOR E CONDIÇÕES DE UTILIZAÇÃO DO TRABALHO POR TERCEIROS

ACKNOWLEDGEMENTS

Este trabalho é o resultado de um esforço coletivo, e não seria possível sem o apoio fundamental de várias pessoas e instituições que merecem o meu mais sincero agradecimento. Durante essa jornada, fui verdadeiramente privilegiado pela generosidade e apoio de indivíduos notáveis, cujas contribuições, em diversas formas e momentos, iluminaram o caminho e enriqueceram esta experiência de maneiras que transcendem as palavras.

Em primeiro lugar quero agradecer à minha orientadora, Professora Sandra Carvalho. Agradecer por tudo! Aceitou ser minha orientadora, ciente de todas as minhas imperfeições, mas ainda assim acreditou que seria capaz. Agradeço pelas oportunidades, as discussões, os ensinamentos científicos e para a vida e até os puxões de orelhas. Fez de mim um melhor investigador, e sem dúvida uma melhor pessoa.

Ao Professor Albano Cavaleiro do Departamento de Engenharia Mecânica da Universidade de Coimbra, pela disponibilidade e com um olhar crítico e que me permitiu crescer durante os longos anos em que colaborou no nosso grupo.

Ao Professor Luís Rebouta que me ajudou imenso no início do meu trabalho. Ensinou-me a trabalhar com o equipamento de pulverização catódica e passou todo o seu conhecimento para que pudesse desenvolver o meu trabalho com confiança.

Quero agradecer a todas as pessoas que contribuíram com o seu conhecimento para desenvolver este trabalho dando contribuições valiosos e fundamentais para a evolução científica que culminou na coautoria de publicações científicas em jornais internacionais, nomeadamente ao Nuno Parreira, Todor Vuchkov, Engenheiro Jorge Ferreira e Professor Martin Andritschky.

Um especial agradecimento ao José David, meu amigo e colega que sempre mostrou disponibilidade para as horas intermináveis na câmara, para as discussões de científicas que muito nos fizeram crescer e acima de todo por todos os bons momentos que passamos. Obrigado pelos conselhos e pela tua visão mais pragmática da vida, e pelo incentivo nas horas mais difíceis.

Não posso deixar de agradecer à Mariana Marques por estar sempre lá, e dar-me confiança e muitos puxões de orelhas e no fundo a mostrar-me que tudo se consegue mesmo que a luz esteja lá ao fundo. Obrigado, minha irmã de coração. Rimos, choramos e aprendemos muita coisa juntos quer na vida como na ciência.

Agradecer à Maria José Lima, companheira de gabinete pelo incentivo na fase final, não só como coautora do artigo mas principalmente como colega que deu um apoio fundamental e muita energia positiva.

Os meus agradecimentos a todas as pessoas que integraram o Grupo SMF e que de uma ou outra forma contribuíram para este projeto, em especial à Luísa Fialho e ao Diogo Cavaleiro.

Agradeço os apoios financeiros no âmbito dos projetos: On-SURF (cofinanciado via FEDER (PT2020) POCI-01-0247-FEDER-024521); Projeto POCI-01-0247-FEDER-042785, acrónimo "GREENCoat" (COMPETE 2020); Projeto POCI-01-0247-FEDER-072607, acrónimo "i9LOGO".

Por último agradecer à minha mãe pela paciência que sempre demonstrou em deixar-me escolher o meu caminho ao meu ritmo. E por sempre me apoiar mesmo não concordando com algumas opções. À minha namorada Fernanda pela paciência, apoio, e por me trazer de volta à realidade tantas e tantas vezes e por estar sempre presente em todos os momentos.

Esta tese foi financiada pelo Programa Operacional Norte 2020, nos termos do Aviso de Abertura Norte-69-2015-15, Formação Avançada - Programas Doutorais, cofinanciado pelo Fundo Social Europeu, "Programa Doutoral em Engenharia e Proteção de Superfícies", com ref: NORTE-08-5369-FSE-000047, referência UMINHO/BD/30/2016.

Esta tese foi suportada pelo projeto DRIVOLUTION (7141- 02/C05-i01.02/2022.PC644913740-00000022 - 23), que foi financiado pelo PRR - Recovery and Resilience Plan – e por Next Generation EU European Funds, segundo o NOTICE No. 02/C05-i01/2022.

STATEMENT OF INTEGRITY

I hereby declare having conducted this academic work with integrity. I confirm that I have not used plagiarism or any form of undue use of information or falsification of results along the process leading to its elaboration.

I further declare that I have fully acknowledged the Code of Ethical Conduct of the University of Minho.

RESUMO

Após o regulamento REACH ser implementado na União Europeia, acelerou a necessidade de encontrar soluções alternativas para os processos de eletrodeposição do crómio hexavalente. Estes processos, amplamente usados na indústria devido às propriedades físicas e mecânicas dos produtos finais que permitem uma vida útil mais longa dos produtos. Revestimentos por eletrodeposição podem também ser encontrados na indústria automóvel ou eletrodomésticos nos quais um acabamento metálico é desejado pelo consumidor. Este trabalho pretendeu oferecer soluções para substituir a eletrodeposição de crómio hexavalente, quer para aplicações que exigem crómio duro ou acabamentos decorativos.

Em primeiro lugar, estudou-se um revestimento alternativo ao crómio duro, com boas propriedades mecânicas, nomeadamente elevada resistência a cargas cíclicas, para cunhagem de moedas. Revestimentos de Cr(Al,Si)N foram depositados por pulverização reativa em magnetrão DC. Por solução sólida, a dureza destes revestimentos aumentou progressivamente com a adição de elementos na matriz base (CrN), passando de ≈10 GPa nos revestimentos de CrN para ≈17 GPa nos revestimentos de CrAlSiN. Para CrAlN, os testes de impacto demonstraram que uma dureza superior nem sempre garante um melhor desempenho em aplicações sujeitas a desgaste por impacto ou fadiga. Quando comparadas com as pressões de contato típicas de cunhagem (1,4 GPa), este estudo sugere aplicações práticas tanto para os revestimentos de CrAlN quanto para os revestimentos de CrAlSiN em cenários de alto impacto.

Investigou-se ainda o uso decorativo de revestimentos de crómio em polímero (policarbonato, PC) para aplicações automóveis. Os maiores desafios foram conseguir revestimentos suficientemente espessos com aparência metálica em PC sem a necessidade de aplicar nenhuma camada de base. Foram depositados revestimentos de CrN e oxinitretos de crómio para aumentar a dureza e obter diferentes aparências sem defeitos. Todos os revestimentos, exceto gCrN, passaram no teste de deslizamento em seco de acordo com os padrões da indústria mostrando que poderiam ser usados em superfícies decorativas e propensas ao toque. Com este conhecimento, substratos de alumínio muito usado em automóveis, revestimentos de Cr(N,O) e CrN/CrO multicamadas, mais espessos, foram também depositados por meio de pulverização reativa por magnetrão. Testes de corrosão com suor artificial simularam a exposição de toque humano a longo prazo, com os revestimentos mostrando melhor resistência à corrosão do que o substrato. Os revestimentos de Cr e CrO demonstraram ser promissores para resistir ao toque humano em várias aplicações, como peças automóveis e eletrodomésticos.

Palavras-chave: Regulamento REACH; Crómio Hexavalente; Pulverização Catódica; Fadiga; Corrosão

ABSTRACT

Aiming to improve the protection of human health and the environment, REACH regulation was enforced across European Union, accelerating the need to find alternative solutions to the electrodeposition processes of hexavalent chromium employed in several industrial applications. Electroplated hard chromium coatings are widely used due to their physical and mechanical properties that allow a longer service life of products. In a similar way electroplated coatings can be found in the automotive industry and can be used in appliances where a metallic finish is desired by the consumer as a mainly decorative property. This work intends to offer solutions for replace electroplating in a broad spectrum of substrate materials, whether it's for applications requiring hard chromium or decorative finishes.

First, we introduce an alternative coating to hard chromium, emphasizing remarkable mechanical properties, particularly high cyclic load resistance. Cr(Al,Si)N coatings were deposited via reactive DC magnetron sputtering. Focusing on mechanical aspects, hardness increased progressively with the addition of elements to the base matrix (CrN), going from ≈10 GPa in CrN coatings to ≈17 GPa for CrAlSiN coatings. The wear resistance of CrAlN coating under impact stress highlights that superior hardness doesn't always ensure better performance in impact or fatigue-related wear applications. Given typical minting contact pressures (1.4 GPa), this initial study suggests practical applications for both CrAlN and CrAlSiN coatings in high-impact scenarios.

We investigated the decorative use of Cr-sputtered coatings on plastic (polycarbonate, PC) for automotive applications, focusing on the effects of O and N addition. The biggest challenges were achieving thick metallic-looking coatings on PC without requiring a base coat. We sputtered CrN and chromium oxynitrides to enhance hardness and achieve different appearances. All coatings, except gCrN, passed a dry sliding test typical for automotive components, meeting industry standards and demonstrating their suitability for use on decorative and touch-sensitive surfaces. Based on previous knowledge, we also developed hexavalent chromium-free coatings for frequently touched aluminium substrates. Thicker Cr(N,O) and multilayered CrN/CrO coatings were deposited through reactive magnetron sputtering. Artificial sweat corrosion tests simulated long-term human touch exposure, with the coatings displaying better corrosion resistance than the bare substrate. The Cr and CrO coatings demonstrated promise for enduring frequent human touch in various applications, such as automotive and general appliances.

Keywords: Reach Regulation; Hexavalent Chromium; Sputtering; Fatigue; Corrosion

TABLE OF CONTENTS

LIST OF FIGURES

LIST OF TABLES

LIST OF Abbreviations

AFM – Atomic force microscopy

Al – Aluninium

at. – atomic

bcc – Body Centered Cubic

BE – Binding energy

BSE – Backscattered electrons

Cr – Chromium

CVD – Chemical Vapor Deposition

DC- Direct current

EDS - Energy dispersive spectroscopy

EIS – Electrochemical Impedance Spectroscopy

E – Elastic modulus

EC – Equivalent circuit

PVD – Physical Vapor Deposition

SE – Secondary electrons

SEM – Scanning electron microscopy

Si – Silicon

Ti – Titanium

TEM – Transmission electron microscopy

XPS - X-ray Photoelectron Spectroscopy

XRD - X-ray diffraction

Z – Atomic number

CHAPTER I - Introduction

1 Introduction

1.1 Motivation

Reach regulation was designed to enhance the safeguarding of both human health and the environment by advancing the early detection of the inherent characteristics of chemical substances. Additionally, it mandates the gradual replacement of the most hazardous chemicals with safer alternatives once they are identified. Among the substances of concern is hexavalent chromium. Numerous industries utilize electroplated chromium coatings due to their excellent physical, chemical and mechanical properties, which extend the lifespan of their products, typically failing due to wear and corrosion. However, the electroplating of components with hard chromium poses health risks to workers due to the carcinogenic nature of Cr VI, leading to potential occupational diseases. Furthermore, environmental considerations come into play, as hexavalent chromium is a toxic pollutant associated with water and soil contamination.

Electroplated hard chromium is employed to enhance the mechanical and tribological performance of minting dies, for instance. The coin industry is dedicated to developing improved dies with longer service lives while adhering to relevant laws and regulations. The challenge lies in creating a suitable tool material that strikes a balance among all the required properties (including fatigue, corrosion resistance, friction, and wear resistance) to achieve the most optimal and versatile material comparable to hard chromium.

In automotive and decorative industries, metal-coated plastic parts, replacing traditional metals, offer benefits like low weight, flexibility, cost-effectiveness, and design versatility while retaining the metal's shiny finish, reflectivity, and conductivity. These parts are typically created through injection molding and subsequent electroplating, often involving toxic hexavalent chromium. Industry and researchers seek eco-friendly alternatives to chrome plating, exploring various coating methods. However, alternative coating processes need to address some common challenges, such as weak adhesion between the coating and the polymeric substrate, and thermal stress caused by the low melting point of plastics just to mention a few.

Apart from polymeric materials, aluminium is another widely utilized materials in automotive components. Its combination of high-strength alloys and ease of manufacturing renders it well-suited for safety features and impact absorption. With superb corrosion resistance, aluminium and its alloys find application not only in cast engine blocks but also in sheet and extruded parts. These include hoods, trunk lids, and outer panels like doors, fenders, and protective covers. Regularly handled pieces such as doorhandles suffer

from corrosion and this aesthetic effect influences the end user's perception of finishing quality in decorative automotive parts.

In this research work we suggest replacing electroplated surfaces with hexavalent chromium-free sputtered coatings. We will consider two major categories of functional properties and explore PVD technique to find alternative methods for achieving the same functional characteristics as those obtained through chromium electroplating in various applications. PVD sputtering presents itself as a promising green and healthy alternative to electrochemical methods of surface functionalization. Several other advantages can be attributed such as enhanced control and precision resulting in uniform high-quality coatings and is a versatile technique that can be adjusted to be applied to a wide range of substrates.

1.2 Work objectives, methodology and thesis organization

The primary objective of this thesis is to advance the field by proposing alternative coatings capable of competing with electroplated surfaces containing hexavalent chromium. Our primary focus is on the deposition of coatings through the technique of reactive DC magnetron sputtering, aiming to achieve coatings with enhanced functional attributes that either rival or surpass the characteristics of electroplated components according to industry specifications.

Our research is motivated by the need to find alternative solutions for two applications currently reliant on electroplated chromium: hard and decorative. We will deposit thin films as replacements for electroplated coatings in both application domains by magnetron sputtering. This research will bifurcate into two primary research streams within the scope of the PhD thesis, each catering to the specific requirements and challenges posed by those two application areas.

To guide this investigation, we asked ourselves:

"**What are good alternatives for replacing electroplated hard chromium coatings in minting dies while maintaining performance?**" and "**How can we replace electroplated chromium coatings on metal-coated parts in the automotive industry, with equivalent functional properties?**"

To answer those, we established specific objectives for each research branch to provide comprehensive answers.

For hard chromium applications,

- ✓ Deposition of Cr(Al,Si)N coatings by reactive DC magnetron sputtering;
- ✓ Characterize and correlate structure, mechanical and tribological behavior, atomic composition and structure with deposition parameters;
- ✓ Obtain coating with competitive mechanical properties for the requested application (minting)
- ✓ Study the behavior of the selected coatings in controlled conditions to understand the viability to be used in real conditions of a minting facility.

For decorative coatings, the adopted strategy was

- ✓ Deposition of $Cr_xO_yN_z$ coatings by reactive DC magnetron sputtering in N_2 and/or O_2 atmosphere;
- ✓ Deposition of these coatings in polymeric (PC) and metallic substrates (Aluminium sheet);
- ✓ Characterize and correlate structure, mechanical and tribological behavior, atomic composition and structure with deposition parameters;
- ✓ Obtain coatings with good attributes such as good adhesion in a wide range of colours;
- ✓ Assess the coatings' performance under simulated extreme conditions that resemble the real-world environments.

Figure I-1 provides a schematic overview that summarizes the various research branches within this study and the methodology employed throughout this thesis. Detailed descriptions of these aspects will be presented in the subsequent chapters.

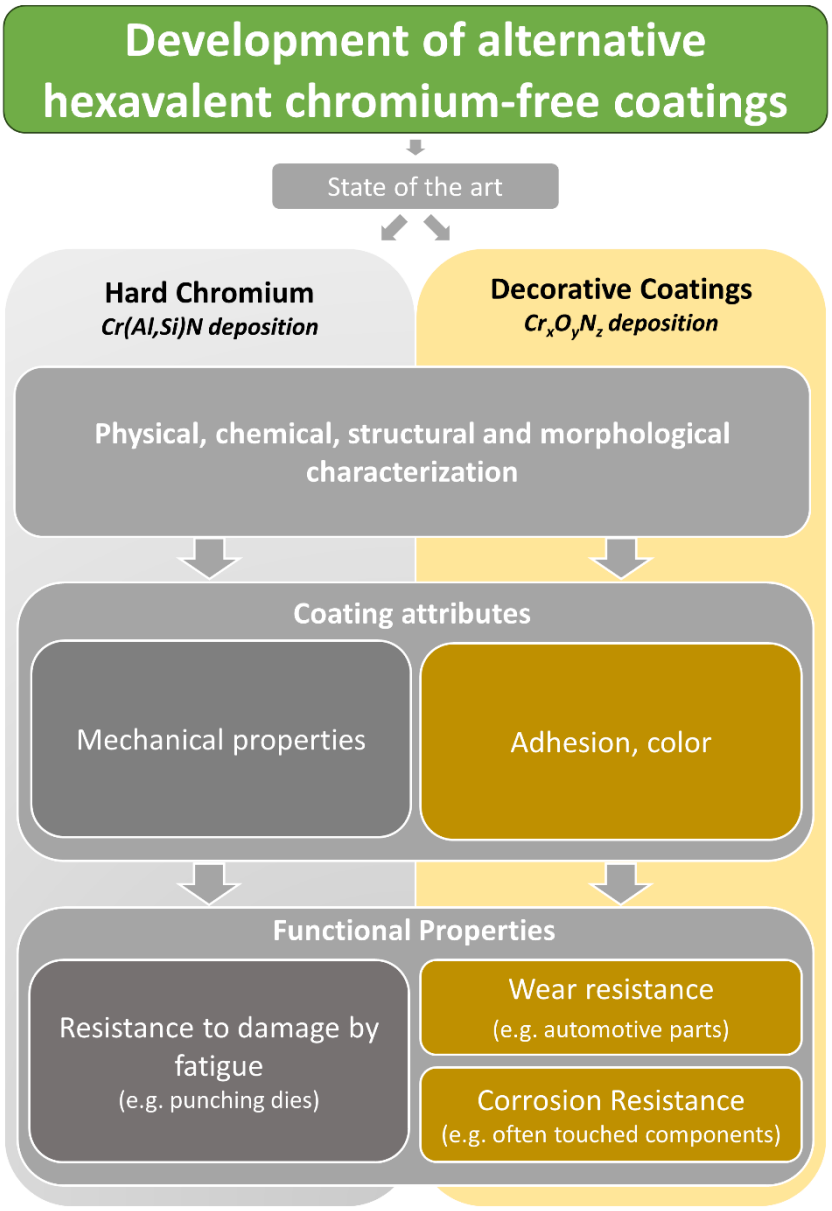

Figure I-1. Schematic representation of the paths followed to find the best coating for each application group.

This thesis is structured into six chapters, offering a comprehensive description of the advancements achieved in this research. The arrangement of these chapters is intended to showcase the research progress. Among these chapters, three are derived from scientific papers published in international journals. The following chapters explore into the development of hexavalent chromium-free coatings for diverse applications and provide a detailed account of their fundamental characterization, functional properties, and behavior.

The present chapter, Chapter I, introduces the topic of the thesis, identifying the main objectives to be achieved and how, setting the context for the study, and establishing the objectives and scope of the research.

The Chapter II offers an overview of the literature, including different electroplated chromium coatings in the industrial setting, examining the health and safety considerations prompting the implementation of Reach Regulation and summarizing its key elements, as well as consolidating the relevant research findings in the areas of hard and decorative chromium applications.

Chapter III is focused on investigating alternatives to hexavalent chromium coatings for coinage punches, exploring physical vapor deposition (PVD) with a focus on gradient-based designs to enhance surface properties aiming to improve coating properties and durability in minting applications through mechanical behavior evaluation via multiple impulse testing and comparative analysis with conventional die materials.

In Chapter IV, by using reactive magnetron sputtering to deposit hexavalent chromium-free coatings onto PC substrates for automotive industry applications we aim of emulate the desirable properties of metal-coated plastic parts popular in the automotive and decorative industries. We explore the effects of deposition parameters and multilayers on adhesion and decorative possibilities.

Chapter V investigate the corrosion effects of human perspiration on decorative coatings, with a specific focus on hexavalent chromium-free coatings applied to aluminium substrates for automotive and consumer products using reactive magnetron sputtering, and evaluates their corrosion resistance against artificial sweat, ultimately addressing the industry's demand for sustainable and durable coatings.

Lastly, the Chapter VI gives an overall conclusion of this thesis and discusses the possible future research perspectives.

CHAPTER II - State of the Art

2 State of the Art

2.1 Introduction

In this chapter, an overview of the literature concerning the main motivations of the research is provided. Specifically, we explore into the use and significance of various electroplated chromium coatings within the industrial context. Furthermore, we go over the health and safety concerns that have driven the enactment of Reach Regulation, summarizing its essential aspects. Additionally, we condense the pertinent research findings within the domains of hard chromium and decorative chromium applications.

2.2 Chromium electroplating in industry

Electroplating is an electrodeposition process in which a dense, uniform, and highly adhesive coating of a metal or alloy is produced [1]. There are specific types of electroplating, such as copper plating, silver plating, or chromium plating, allowing manufacturers to use inexpensive metals such as steel or zinc as base material and then apply different metals on the surface. The electroplated coating produced is commonly used for decorative or protective purposes and it can enhance the properties of the original surface itself. Electroplating can occur in conductive materials, such as metals, or nonconductive materials, such as polymers. This process is widely used worldwide in the automotive, aerospace, machinery, electronics, jewellery, defence, and toy industries.

Regardless of the material slated for deposition, the electroplating procedure resembles the one illustrated in Figure II-1, which provides a general schematic overview.

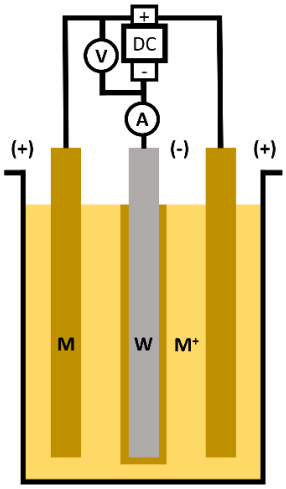

Figure II-1. Electroplating process. (M – metal anode; M+ - metal ion; W – workpiece or cathode; DC – rectifier; V – voltmeter; A – amperemeter.

The central element of this procedure is the electrolytic cell. Within this cell, an electric current pass through a solution bath housing an electrolyte, an anode, and a cathode [1], [2]. The cathode (negatively charged terminal) is designated as the workpiece (W) to be plated. On the other hand, the anode can fall into one of two categories: sacrificial anodes, composed of the metal to be deposited, or permanent/inert anodes solely employed to close the electrical circuit. In the latter case, platinum or carbon are used as inert anodes.

An electrolyte is the conductor for electrical flow in the electrolytic cell, depicted as the yellow region in Figure II-1. In this medium, ions, rather than free electrons, carry the electric current, linking the two electrodes within the circuit. Upon applying an electric current, positively charged ions within the electrolyte migrate toward the cathode, while negatively charged ions move toward the anode. This migration constitutes the electric current within this portion of the circuit.

Simultaneously, electrons travel through the wiring and an electric generator to reach the anode, ultimately completing their journey back to the cathode, thus establishing the current in the external circuit. The metallic ions within the salt dissolved in the electrolyte bear a positive charge, attracting them towards the cathode. Upon reaching the negatively charged workpiece, the workpiece releases electrons to reduce these positively charged ions, transforming them into metallic form. Subsequently, the metal atoms are deposited onto the surface of the negatively charged workpiece.

The cathode, or the object intended for plating, carries a negative charge. Some of the electrons from the cathode are transferred to the positively charged metal ions (designated as M+), liberating them as individual metal atoms. These liberated metallic atoms adhere to the cathode's surface, effectively plating it. Simultaneously, an equal number of negative ions are discharged at the metal anodes, completing the electrical circuit.

This process generates new salt that dissolves into the solution, returning it to its original composition. This method mirrors the conventional electroplating procedures involving sacrificial anodes, where the current deposits a specific amount of metal onto the cathode, and the anode dissolves to an equivalent extent, maintaining the solution's uniformity.

2.3 Electrodeposition of chromium

Electroplated chromium coatings represent a crucial category of electrodeposited metals, primarily enhancing the final quality of various components. These coatings offer a set of unique physical attributes,

enabling manufacturers to extend the lifespan of their products, which would otherwise suffer from premature wear and corrosion-related issues. In the absence of electroplated chromium coatings, components require frequent replacements or repairs, or they need to be constructed from costlier materials. This would result in the squandering of valuable resources and a subsequent increase in product costs.

Electroplated chromium deposits can be classified into two categories based on their thickness: decorative and functional. Decorative deposits typically have a thickness of less than 0.80 µm. They not only present a reflective and metallic appearance but also provide excellent resistance to corrosion and durability. Decorative chromium deposits are often plated over a nickel layer for enhanced adhesion. However, they can be directly plated onto the substrate [2]. In the case of functional hard chrome coatings, they are thicker than their decorative counterparts and are applied in extensive industries. In contrast to decorative chrome, functional chromium is typically directly electroplated onto the substrate, though it can also be applied on other electrodeposits like nickel. The industrial sector capitalizes on chromium's unique attributes, which include exceptional heat resistance, hardness, wear resistance, corrosion resistance, erosion resistance, and a low coefficient of friction. These functional chromium electrodeposits apply to various components, such as cutting tools and punches, for various specific applications.

Since the mid-1920s up to the present day, the prevailing method for chromium electroplating has involved the use of hexavalent chromium (Cr^{6+}) within an aqueous solution containing specific catalysts [2], [3].

In contrast to many other metals, chromium cannot be readily deposited from a simple aqueous solution containing only its metal ions. The process of chromium deposition requires the presence of one or more acid radicals from chromic acid and sulfuric acid, which serve as catalysts (for Cr VI) or complexing agents like carboxylic acids (for Cr III), facilitating the cathodic deposition of chromium metal. Whether for decorative or hard chromium plating, CrO_3 is employed as the electrolyte. The limitation of depositing chromium exclusively from Cr^{6+} solutions rather than basic aqueous solutions of lower valency salts pose efficiency and quality challenges.

As indicated by the REACH regulation, Cr(VI) is highly toxic and poses significant risks [4]–[8]. Over the past decade, there has been growing apprehension surrounding the electroplating of chromium coatings. This concern is driven by environmental, health, and safety considerations associated with the handling, storing, and disposing of hexavalent chromium compounds used in the plating process [9]. The

unexpended chromium ions remain in the hexavalent state (Cr^{6+}) in the electrolyte whereas the chromium deposited is in the metallic form. The handling and disposing of Cr^{6+} based electrolytes must be carefully made due to its carcinogenic properties, among other associated health issues. Elevated oxidative stress, the occurrence of chromosome breaks, and the formation of DNA adducts are among the key mechanisms by which Cr(VI) inflicts damage on cells [10]–[12]. A typical occupational ailment in the electroplating industry is nasal septum perforation [7], [9].

Consequently, numerous research efforts have been directed toward electrodepositing Cr coatings from Cr(III) electrolytes, which are considered one of the most promising alternative technologies [13]. Nonetheless, it remains a technical challenge to produce thick Cr coatings of high quality with a uniform and smooth appearance using Cr(III) electrolytes.

2.3.1 Electroplated Hard chromium for minting applications

Plating can be performed on conductive, such as metals, or nonconductive, such as polymers, materials. This process is widely used in worldwide industries, namely for automotive, air space, machinery, electronics, jewellery, defence, and toy applications [1]. Electroplated chromium coatings are among the most important electrodeposited metals and their physical properties allow manufacturers to increase the service life of their products, affected by wear and corrosion. As already mentioned, electroplated chromium deposits fall into two classifications if thickness is considered: decorative and functional [2]. Functional ‘‘hard chrome’’ deposits have a thickness greater than decorative ones and are used for industrial applications. Industry takes advantage of the special properties of chromium, including heat resistance, high hardness, high wear, corrosion, and erosion resistance, and a low coefficient of friction. Punches (figure II-2) are a type of tool where electroplated chromium properties are exceptional and difficult to substitute.

These applications include minting and tablet pressing [14]–[22]. Hard chromium (HC) plating has been used extensively in the coining industry for many years [22]. However, despite their excellent properties

to allow production of several hundred thousand of coins [23], the negative health impact and environmental problems, associated with chromic acid, is something to be attentive.

Figure II-2. CAD illustration of a coining punch

In minting applications, frictional stresses are generated because of deforming metal sliding over the die surfaces. The frictional conditions on the die/blank interface influence metal flow, surface defects, die stresses, load and minting energy requirements. Comparing to other cold forming operation, in minting the deformation causes a minimal amount of metal flow across the die surface. However, the effects of friction can lead to surface defects transferred from the die. Plastic deformation and friction contribute to heat generation which influence lubrication conditions (in minting, no lubricant or coolant is used), tool life and more importantly, influence the maximum deformation speed which can be used without excessive tool damage. The load necessary to overcome friction increases rapidly with decreasing material thickness so, friction effects should be kept at an acceptable minimum. Abrasive wear from friction is the most common wear mechanism in coining [3][23]. Die material is removed from the die surface due to pressure and sliding of the blank's material. This is greatly influenced by the wear resistance of the die material. Details on the coin are designed to minimize wear while maintaining its distinctive features. Transfer of nonmetallic inclusions on the die surface from the blank causes adhesive and abrasive wear failure. In addition, thermal and mechanical fatigue and plastic deformation cause the punching dies to fail. After repetitive cycles cracking can occur and the surface layers withstanding compressive stresses may suffer from delamination [3]. Minting punches should have enough toughness, optimized frictional behaviour to reduce stress and consequent failure. These properties could be achieved through the usage

of functional coatings such as Cr(Al,Si)N or multilayered coatings deposited onto the die providing the surfaces with the optimal properties to increase tool life and decrease failure due to wear and friction.

2.3.2 Electroplated decorative coatings

Many objects encountered daily include metal coated plastic parts. Most of these are fabricated using injection molding and are subsequently metallized using electroless and electroplating methods. However, the practice of electroless plating of nonconductive parts is recognized as a tremendous environmental hazard due to the use of chromic acid in essential surface etching steps [24]. Electroplating is used to produce decoratively plated plastic parts with available finishes, including nickel, bright and matte chrome, gold, copper, and brass. Typically, electroless plating is used to deposit thin metal coatings of less than 12.5 μm total metal thickness. Unlike its electrolytic counterpart, which relies on an external electrical current, electroless plating utilizes a chemical bath containing a metal source, a reducing agent, and complexing/stabilizing agents. This bath initiates a controlled autocatalytic reduction reaction on the substrate surface, leading to uniform metal deposition in applications where the plating film thickness must be controlled, such as antennas, for example. Alternatively, if thicker coatings are required, electroplating processes can be used to deposit copper, nickel, tin, chrome, silver, and gold layers. Electroplating typically offers faster deposition rates and lower costs compared to achieving the same thickness through electroless plating. However, electroplating is a line-of-sight process that will yield wider thickness variation over a part than would electroless plating. With electroplating, plating thickness can exceed 75 μm [25].

Thin film-coated (metallized) polymers are replacing traditional metallic materials in many industrial fields, particularly in automotive. The low density, flexibility, design versatility and low-cost production of most polymers, combined with the properties of a shining, highly reflective and conductive metallic coating (figure II-3), gives them a considerable advantage over common metals [26].

Figure II-3. Examples of automotive metallized parts. From left to right: accent in bumper and emblems in the exterior of a car; door handle and knob with metallized details from a car interior.

An overview of requirements is presented in Table II-1, which lists the key functionalities for chromium plated surfaces for automotive sector [27]. This adapted list is intended to provide an evaluation basis for alternative coatings.

Table II-1. Sector specific key functionalities of chromium-based electroplating.

Key Functionality	Auto-motive exterior	Auto-motive interior
Wear resistance / abrasion resistance (scratch resistance)	- Taber abrasion: 80% remain-ing gloss after 20 double strokes EN 2813 - car wash resistance ISO 20566	- Taber abrasion: 10,000 hubs - further tests acc. to OEM specifications, for example Abrex or Martindale
Ni leaching (not toxic)	0.5 µg/cm² per week (Bed GgstV)	0.5 µg/cm² per week (Bed GgstV)
Adhesion	GT0 to GT1 (after tempera-ture cycle test) in cross-cut test EN ISO 2409 Peel resistance: > 3.5 N/cm to 9 N/cm (ABS: 7 N/cm)	GT0 to GT1 (after tempera-ture cycle test) in Cross-cut test EN ISO 2409 Peel resistance: > 3.5 N/cm to 9 N/cm (ABS: 7 N/cm)
Sunlight resistance (UV exposure)	- 3200 h Florida simulation (PV 3930)	- 10 exposure cycles according to ISO 75202
Temperature change resistance / heat resistance	OEM specification	OEM specification
Aesthetics	- Surface must be free of any kind of defects such as pores, cracks and blistering - Colour testing according to EN ISO 11664 - Finish quality (bright or matt) can be tested acc. to primordial pattern	- Surface has to be free of any kind of defects such as pores, cracks and blistering - Colour testing according to EN ISO 11664 - Finish quality (bright or matt) can be tested acc. to primordial pattern

A wide selection of materials can be electroplated either polymeric or metallic. The most common polymers used in the automobile industry are Acrylonitrile butadiene styrene (ABS), Polycarbonate (PC) and PC/ABS blends. Additionally, there is an interest in Polyamide (PA) fiber-glass reinforced [28]. Typically, PC exhibits a variety of optical and technical applications, and its demand is increasing year by year. It is widely used in optical data storage devices, bulletproof windows, and food packaging. Because

of its good properties such as optical transmittance, excellent thermal and flame resistance, high impact strength and high stability to different environmental conditions, PC is used in a wide range of industrial applications, such as the automotive [29]. Aluminium-based automotive components are also considered one of the most promising materials to reach this equilibrium [30]. Combining a high-strength alloy with ease part' manufacturing makes aluminium ideal for safety and impact-absorbing components. Aluminium and aluminium-based alloys can be used for cast engine blocks, but more importantly for sheet and extruded parts like hoods, trunk lids, and outer panels such as doors, fenders, and protection covers for a wide range of appliances and even in aircraft industry [31][32][33].

2.4 Reach Regulation

REACH is a European Union (EU) regulation aiming to improve the protection of human health and the environment from the risks of chemical usage while enhancing the competitiveness of the EU chemicals industry. REACH stands for Registration, Evaluation, Authorization, and Restriction of Chemicals, and it entered into force on June 1st 2007. This regulation applies to all chemical substances, not only those used in industrial procedures but also in our daily lives (cleaning products, paints, clothes, furniture, and electrical appliances) impacting several companies across the EU. Companies must identify and manage the risks related to the substances they manufacture and market to comply with the regulation. They must demonstrate to the European Chemicals Agency (ECHA) how the substance can be safely used, and they must communicate the risk management measures to the end users. If the risks cannot be managed, authorities can restrict the use of these substances. In the long term, the most hazardous substances should be substituted with less dangerous ones.

REACH defines procedures for collecting and assessing information on the properties and dangers of substances. Companies need to register their substances and they need to work together with other companies who are registering the same substance. ECHA receives and evaluates individual registrations for their compliance, and the EU Member States evaluate selected substances to clarify initial concerns for human health or the environment. Authorities and ECHA's scientific committees assess whether the risks of substances can be managed or otherwise restricted or banned.

It is essential to highlight that the general intention is not to socioeconomically hamper the current conditions of those involved in the current industrial reality but rather to make day-to-day work safer and obey more rigorous environmental aspects. REACH regulation should be seen as an incentive tool for technological research and innovation in achieving healthy competitiveness between companies. In

summary, this regulation aims to improve the protection of human health and the environment against chemical substance risks while fostering competitiveness in the European Union's chemical industry. Within the ideals of UE, it also intends to ensure the free movement of substances within the internal market of the European Union.

2.5 Registration, Evaluation, Authorization, and Restriction of Chemicals

It is possible to describe the four steps of the REACH regulation briefly. The REACH regulation covers the entire lifecycle of a chemical substance, from its conception and placement on the market to its use and disposal, imposing rules and guidelines on manufacturers, importers, and downstream users located in the European Union. REACH regulation has allowed the consolidation of dozens of distinct and scattered legal acts into a single document.

Once registered, the substances can be assessed by ECHA and the competent authorities of the Member States to determine whether there is a need for additional information on them. We can describe all the necessary steps until it is determined whether a substance can be marketed in flowchart (figure II-4) to facilitate the understanding of the entire process.

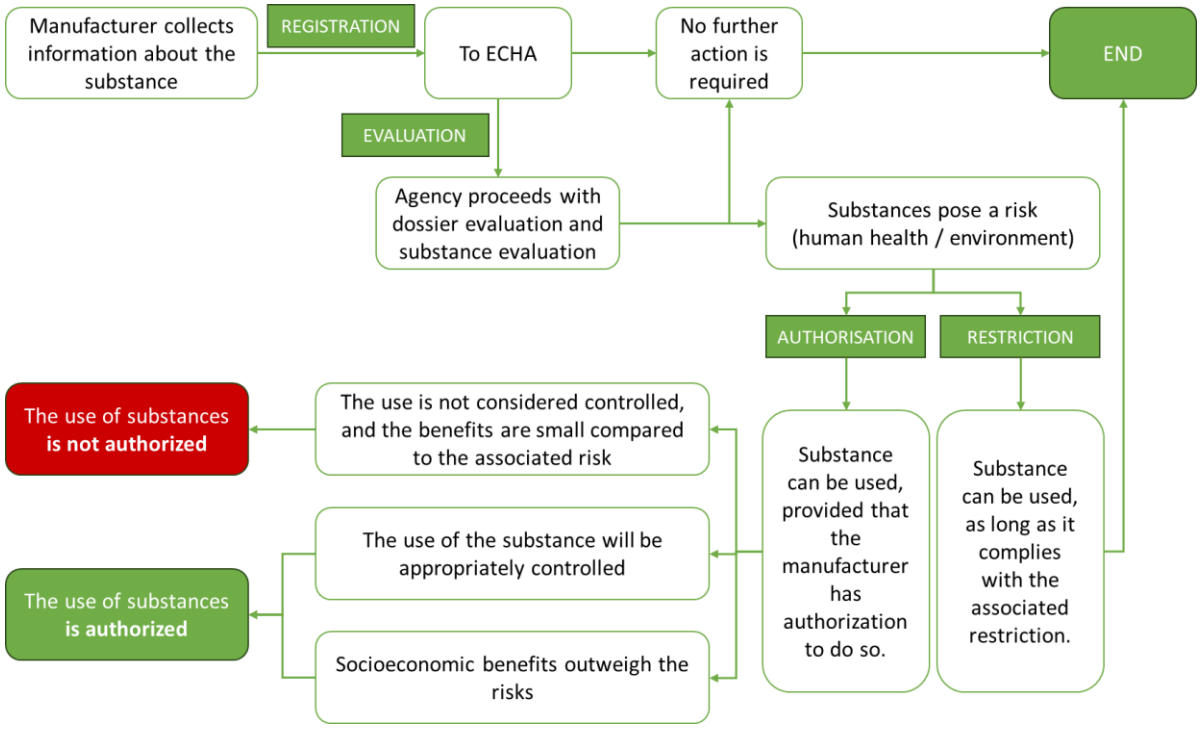

Figure II-4. REACH Regulation scheme

2.5.1 Registration

REACH regulation is primarily based on the registration of chemical substances. Therefore, this is the most crucial step in the process since if it is not completed, it is impossible to produce or market these

substances. Registration becomes mandatory for substances manufactured or imported in quantities exceeding 1 ton per year and for substances intended to be released under normal or reasonably foreseeable conditions of use. There are substances that not only do not require registration but are also those that are not part of REACH. Examples of such chemicals are radioactive substances, substances under customs supervision temporarily stored in the free zone, the transport of substances, or waste. Likewise, some substances, such as medicines, are exempt from registration because they already have specific regulations. The responsibility for registration lies with the producer or importer and is carried out through ECHA. This registration includes information about the producer or importer, the substance's identity, classification, annual production quantity, and a brief description. If, during this assessment, it is concluded that the substance meets any of the criteria mentioned above, an exposure assessment must be attached to the registration. This assessment should include the definition of all possible exposure scenarios, their estimation, and a characterization of the risks associated with the substance.

2.5.2 Evaluation

ECHA and the Member States' competent authorities carry out the substance evaluation. This evaluation is only conducted when obtaining additional information about the substance in question is necessary. The assessment is performed using the risk associated with each substance as a criterion. These criteria may include hazards, exposure, or production quantity information. At this stage, there are two types of assessment: dossier and substance assessment. With this evaluation, ECHA can create a draft decision within twelve months from the start of the evaluation process. If this draft decision is finalized, registrants are requested to provide sufficient information to register in compliance with the applicable information requirements. Substance assessment is only conducted if there is any indication that it may pose a risk to human health and the environment. If this is confirmed, ECHA includes that substance in the list referred to as the 'substance evaluation. This evaluation helps clarify the reasons why the substance is designated as hazardous. This process involves data collection and analysis to identify whether measures should be taken regarding restriction or authorization, clarifying the classification, or labelling of substances. It may be necessary to inform other authorities to take necessary actions within the scope of other regulations.

2.5.3 Authorization

Only substances listed in Annex XIV of the REACH regulations require manufacturing and/or importation authorization. These substances are of great concern (SVHC – Substances of Very High Concern) due to

their potential impact on human health and the environment. Consequently, manufacturers, importers, and downstream users are prohibited from introducing an SVHC substance into the market or using it unless they meet the applicable usage requirements. SVHC substances can include those known to be carcinogenic, mutagenic, or toxic to reproduction (categories 1 and 2). Additionally, substances exhibiting moderated or high persistence, bioaccumulation, and toxicity or any other substances with demonstrated potential for adverse effects on human health or the environment, may also be classified as SVHC. The list is subject to review and updates every six months, with the possibility of adding new SVHC substances.

Nonetheless, employing an SVHC substance remains a possibility. To pursue this option, one must apply for authorization from ECHA. It's essential to note, however, that this should be considered a last recourse and should only be pursued if there are no feasible alternatives available in the market, whether from a technical or economic perspective. This measure ensures that the risks linked to these substances are managed, and gradually, harmful substances are substituted with alternatives that serve the same purposes without causing harm to humans and the environment. An essential component of REACH involves maintaining the Candidate List of "Substances of Very High Concern" (SVHC). The objective is to prioritize substituting these SVHCs with less hazardous materials or technologies whenever viable alternatives exist. The most recent edition of this list was released on June 14, 2023, and comprises 235 SVHCs.

2.5.4 Restriction

When a substance found within a preparation or product is subject to a restriction, it cannot be produced, introduced into the market, or utilized unless it complies with the stipulated requirements of that restriction. Substances designated for use in cosmetic products, as defined by Directive 76/68/EEC, are exempt from any health-related limits within the scope of this directive. Similarly, substance restrictions do not apply when employed for scientific research or development. In such cases, these substances may be manufactured and placed on the market, even if listed in Annex XVII, along with specifications regarding the applicable substances within this field and the maximum allowable quantity that can be used without restraint. Whenever a substance poses a risk to human health or the environment, and this risk remains uncontrolled, the European Parliamentary Commission calls upon ECHA to prepare a dossier for these circumstances. The evaluation of compliance for this dossier falls under the purview of the Risk Assessment Committee and the Socioeconomic Analysis Committee, which are part of the European Parliament and the Council. These committees review the dossier's conformity and notify ECHA or the

respective Member State about its alignment with Annex XV. In the event of an unfavourable assessment, modifications can be made to validate the document.

2.6 Reactive magnetron sputtering

Direct current magnetron sputtering (DCMS) stands as a leading technique within the realm of physical vapor deposition (PVD) as recognized by industry [34]. At its core, sputtering revolves around the transformation of a target material into vapor species and their subsequent deposition onto a substrate. In the DCMS process, atoms are ejected from the target material due to interaction with high-energy ions, such as Ar+ or He+, which form the plasma.

The sputtering process involves the application of an electric field between a cathode (referred to as the target) and an anode within a high-vacuum, non-reactive atmosphere, typically composed of argon (Ar) or helium (He). In this setting, the electric field plays a crucial role in accelerating charged particles, including ionized species and secondary electrons emitted by the target surface during the discharge. These charged species enable collisions and momentum transfer to the target, leading to the ejection of atoms (sputtering) and the emission of secondary electrons[35].

The secondary electrons, in turn, contribute to the ionization of non-reactive species and the maintenance of the plasma. Consequently, the sputtered atoms accumulate on the substrate surface, where subsequent nucleation and coalescence processes give rise to the formation of the desired coating. Ar is commonly chosen as the non-reactive gas due to its substantial mass, which enhances the sputtering efficiency by facilitating momentum transfer. However, it is important to note that there exists a minimum voltage requirement, known as the breakdown voltage, to initiate plasma. Without this threshold voltage, non-reactive species lack the necessary kinetic energy for ionization and the generation of charged particles.

While sputtering offers efficient and uniform atom ejection from the target surface, its effectiveness is limited in a direct current (DC) diode system, where ionization and collision rates of Ar are typically low. This results in reduced deposition rates and suboptimal film densities. However, by introducing a magnetic field perpendicular to the electric field and parallel to the target surface, it becomes possible to confine and capture secondary electrons, thereby amplifying plasma ionization and target sputtering. The magnetron sputtering system also aids in minimizing electronic bombardment of the substrate holder. The bombardment of the substrate holder with secondary electrons results in an increase in temperature

and can cause atoms to be re-sputtered from the growing film, leading to defects in film growth. To mitigate these issues, applying a negative bias voltage (within certain limits) to the substrate holder is effective in reducing electronic bombardment while increasing ionic bombardment on the substrates, ultimately enhancing film density[36].

The versatility and utility of reactive DC magnetron sputtering (DCMS) are well-recognized, as it enables the deposition of a wide range of compounds that might be challenging to obtain through other physical processes. For instance, by introducing various reactive gases, it is possible to deposit metal oxide coatings with different compositions using only a metallic target, modifying the reactive atmosphere, and carefully controlling deposition parameters. This capability becomes crucial in optimizing the final properties of the films, such as their chemical state, structure, and morphology.

2.7 Alternatives to electroplating of hard chromium

In order to overcome the environment and health problems of Cr(VI)-based coatings, a large number of researches on electrodepositing Cr coating from Cr(III) electrolyte, such as aqueous $CrCl_3$, have been carried out as a very promising alternative [13]. However, it is difficult technically to prepare high-quality thick Cr coating with uniform and smooth appearance from Cr(III) electrolyte. Various processes have been suggested as alternatives to chromium plating. Therefore, chemical vapor deposition (CVD), physical vapor deposition (PVD e.g sputtering) and thermal spraying (HVOF) have been used to alter the surface of different substrates with different coatings, for many application, such valves, decorative surfaces or tools where hard chromium dominated the market [3], [9], [37], [38][39].

Since 90's, researchers try to improve the system either through heat treatment of the steels used in coining dies [22], [40] or, more recently, using advanced materials such as diamond-like-carbon (DLC) [41]. DLC film exhibits superior properties; however, the environmental sensitivity and poor adhesion, due to carbon diffusion between the DLC and steel interface, restrict its practical applications [42]–[44]. Other recent approach has been PVD deposition of CrN, TiN and TiCN as alternative coatings onto cold working tool steel punches, heat-treated for the hardness increase [45]. In coining applications, frictional stresses are generated when deforming metal slides over the die surfaces. Fatigue and plastic deformation cause the punching dies to fail. After repetitive cycles, cracking can occur and the surface layers withstanding compressive stresses may suffer from delamination [22].

Multilayered coatings designs are attractive from an industrial point of view because they allow to tailor the surface properties freely: properties such as residual stress, hardness, elasticity modulus and adhesion to the substrate are easily controlled. On one hand, ceramic materials such as nitrides in multilayers structures provide hardness, wear resistance and a better adhesion to the substrate. On the other hand, they are brittle and have a high friction coefficient. To overcome the latter, in the topmost layer we find materials with low friction coefficient like DLC and solid lubricants [46]–[48]. CrN/TiN multilayer coatings were widely used as an excellent protective candidate to improve the performance and lifetime of components in complex environments due to their increased mechanical properties and wear resistance in comparison to traditional monolithic coatings (e.g., TiN, CrN, TiCrN) [49]. Recently, various ternary Cr-X-N films were developed and investigated to further improve the properties of CrN films, where X is one alloying element such as Si (for super hardness >40GPa) , Al and Zr (for enhanced corrosion resistance [33]. Of all the above, aluminium seems to have a leading role in recent research works. Parallel to Cr-Al-N, Ti-Al-N coatings were also researched in the latest years. These nitrides exhibit enhanced hardness and thermal stability when compared to CrN and TiN, due to the incorporation of aluminium in the matrix [50]. In the case of Al substituting Cr in a CrN structure, some studies reveal an excellent oxidation resistance and high hardness (27.3 GPa) [51]. CrAlN could solve the industrial problems in minting because of its higher hardness and fatigue resistance when compared to the CrN coating [52][53]. Researchers also found out that Si incorporation to CrAlN coatings, can improve even more the mechanical properties of the coatings [54]–[56]. Despite promising, the majority of these studies were always focused on hardness and Young´s modulus.

In table II-2, a summary of the available literature regarding minting is presented. Authors developing coatings or modified surfaces for minting choose to perform wear tests directly in the production line. Most papers present an estimation for the lifetime of the punches when operation and in some cases some microscopy is done after testing to assess the failure mechanism. Due to intellectual property and overall industrial confidentiality coating parameters are omitted which makes reproducibility harder.

Table II-2. Surface modification for minting applications in recent literature

Author	Year	Substrate	Coating	Method	Coating Parameters	Properties	Comment	Real life
Graham W. Conran[40]	1995	Different SS grades	Cr-electroplated and coated (TiN)	Tempering/Hardening Hard chrome plating/ PIII /PVD ion assisted deposition (IAD)/ PVD FADS processes. TiN coating -> FADS	-	PVD and PII operate ≥ 400 °C, the low tempering temperature alloys were not	Lacks information on the properties and life of the dies	YES. Viking dies TiN coated using FADS but no

						taken to the final stages.		additional info
Wilson Lin[41]@	2006	DIN 2550 (steel sheet & dies)	Cr-electroplated @@ DLC	Pre-heated chamber 150 °C Filtered Cathodic Vacuum Arc (FCVA)	Ti interlayer (0.1 µm) DLC (30 min, 0.4 Pa Ar pressure)	Roughness Uncoated: Ra 10 nm Cr-plated: Ra 50 nm DLC: Ra 40 nm Hardness Uncoated: 770 HV Cr-plated: 1100 HV DLC: 3540 HV	Adhesion decrease due to pin holes in substrate	Press lifetime (average strokes) Uncoated: 3000–4500 Cr-plated: 7500–9000 DLC: >30000
Kalincová [57]	2011	Bohler K455	Cr-plated	Heat treatment Chrome-plating	R1: 25min. R2: 12min. R3: unknown	R1: max. 16.89 µm R2: max. 2.53 µm R3: max. 3.62 µm R1 shows cracks	Coining die used as standard struck 450 000 coins, but no comparison was made. R1 shows cracks	NO
S. Ithisoponakul [23]	2014	H-Steel* C-Steel**	*/**CrN-PVD	Tempering/Hardening PVD coating	PVD: 400 °C, 5h-6h	1-3 µm Best: H-steel 58HRC, 3µm	Peel off, no crack	Yes >300k cycles
			*TiN-PVD *TiCN-PVD		250 °C & 400 °C	2-3 µm Best: 400 °C, > thickness.	Excellent adhesion for both TiN and TiCN coating. TiCN adhesive and abrasive wear. TiN only abrasive wear. TiN longer life	Yes >1M
Hideaki Mori [42]	2014	Coinage dies (no info)	DLC	DLC-PVD; DLC with Cr and WC interlayers	Unbalanced magnetron sputtering method	DLC 30% H 1500HV	After 750 coins DLC didn't show wear as opposite to CrN-plated dies. DLC lifetime = 2x Cr-plating	YES 600 up to more than 1000 cycles

Only a few studied tribological properties, in particular pin-on-disc testing, which, despite being a standard testing method, lacks similarity to reality, for applications with cyclical mechanical stresses, such as coin

coining. Thus, to verify the viability of these systems as alternatives to hexavalent chromium in coinage punches, Al and Si were added to CrN coatings and deposited by magnetron sputtering onto stainless steel substrates. To understand the mechanical behavior and the properties of the coatings, multiple impulse testing was performed alongside with complementary analysis to access the structure and morphology and, thus, compared with Böhler K605 steel, one of the most used die materials in minting nowadays [57]. In this thesis we developed an alternative coating to hard chromium with outstanding mechanical properties based on a Cr(Al,Si)N system produced by reactive DC magnetron sputtering. Cr(Al,Si)N coatings are well-known for their excellent hardness, which is one of their key advantages for the application in mind. The combination of mechanical properties makes them ideal for applications requiring wear resistance and durability. The specific mechanical properties of these coatings can be adjusted through control of the composition and deposition conditions.

2.8 Alternatives to electroplated decorative chromium.

Industry and researchers are now focused on finding new surface technologies based on more environmentally friendly processes to substitute chrome plating. Various processes offer themselves as alternatives to chromium plating. Current chrome plating methods have limitations and drawbacks. The automotive, appliances, and decorative industries are seeking alternatives that offer the same appearance and durability without the environmental and cost issues. Chemical vapor deposition (CVD), physical vapor deposition (PVD), which include sputtering techniques and thermal spraying (HVOF) are used to alter the surface of different substrates with different coatings, depending on the application, either valves, decorative surfaces or tools [3], [9], [38], [58]. Magnetron sputtering is one of such techniques which can be used on a wide range of available polymers, it has a reduced environmental impact and it is becoming an increasingly attractive industrial process for polymer metallization, especially for the deposition of chromium nitride (CrN) films. "Chrome-look" processes and coatings for automotive decoration and lighting (in parabolic headlight mirrors) based on PVD have been used for years. As UV-cured paint systems have developed, so has our understanding of the technique and its unique capabilities and applications. [59]–[61].

The most common polymers used in the automobile industry are Acrylonitrile butadiene styrene (ABS), Polycarbonate (PC) and PC/ABS blends. Additionally, there is an interest in Polyamide (PA) fiber-glass reinforced [28]. Typically, PC exhibits a variety of optical and technical applications, and its demand is increasing year by year. It is widely used in optical data storage devices, bulletproof windows, and food packaging. Because of its good properties such as optical transmittance, excellent thermal and flame

resistance, high impact strength and high stability to different environmental conditions, PC is used in a wide range of industrial applications, such as the automotive [29].

Beyond the materials chosen, design, and manufacturing processes, different problems must be addressed in the automotive industry.

The metallization of polymers with a thin metallic layer by magnetron sputtering starts in 1994 by Grimberg *et al.* [62]. Depositing TiN onto ABS the authors, stated that to coat the polymer with TiN two conditions should be met: i) the adhesion must be assured, for that Cu and Ni layers were added by electroplating and ii) that the deposition must be performed at low temperature to avoid polymer degradation. Respecting this last condition, the author kept the deposition temperature around 100-110 °C.

Later P. Sukwisute *et al.* [63] , deposited CrN coatings on the ABS substrates using the reactive DC magnetron to achieve a higher wear resistance of the ABS surface. In the study 3D printed ABS samples were coated with different sputtering powers. The authors reported an increase in hardness when increasing power up to 9.58 GPa despite the occurrence of voids and cracks alongside.

Paulo Pedrosa *et al.* [64] studied the development of an environmentally friendly magnetron sputtering based process for ABS chrome metallization that is able to deposit CrN films (up to 739 nm) with protective and decorative properties comparable to the ones obtained traditionally by electroplating. In his work obtained samples were deposited by varying N_2 flow inside the vacuum chamber as well as deposition time. The authors considered that the CrN sample sputtered with a lower N_2 for 20 min was considered to possess the most appropriate brightness, color, electrochemical stability and interfacial adhesion to fit the end-user requirements without explicitly stating, however, the values demanded by the industry, nor to which specific standards.

Despite the popularity of CrN in the literature, mainly due to the need to eliminate electrodeposited hexavalent chromium from industrial processes, other metallic elements are being studied.

Justin White et al. [24] deposited Cu and Cr onto printed ABS substrates subjected to different activation methods, such as acetone dipping, sanding and plasma etched. Afterwards, samples were metallized with a chromium adhesion layer and a copper film. In the end the authors demonstrated that adhesion of the film is more strongly affected by morphological effects than chemical effects, and that the strong

film adhesion from atmospheric plasma treatment was a result of only morphological effects. The authors achieved aesthetically pleasing surfaces but couldn't combine it with good adhesion.

A major limitation of vacuum processes such as sputtering, is that high deposition rates are associated with thermal load which is incompatible with polycarbonate [65].

Several examples of it can be found in the literature, Martin Andritshky and Kaj Pishow, [66] study the mass production of copper layer onto PC and concludes in that study that is possible to overcome the difficulties of depositing a metal onto plastic parts. However, when selecting deposition parameters the authors find out that it is needed to take in consideration that higher magnetron current, increases plastic peak temperature, affecting coating properties. And, when reducing substrate thickness is desired it may demand adjustments in magnetron current, possibly requiring more magnetrons and allow for cooling to maintain coating quality and thickness.

Drew Evans *et al*. [67] produced chrome zirconium (CrZrx), by co-sputtering onto pre-coated polycarbonate substrates having a glass transition temperature below 150 °C. Because of this, below 100 °C, over time frames of only 1 to 2 min resulting in ultrathin coating of 60 nm for decorative purposes.

Boentoro *et al*. [68] concerning the increasing in PC usage in their time study the field of scratch protecting films to achieve mechanical properties like glass on soft substrates made of PC. Reactive magnetron sputtering was used to deposit silicon oxide onto several commercially available PC at room temperature. They concluded that critical load increases linearly with the increase of the film thickness, but no further conclusions were taken.

Since Polycarbonate substrates are damaged by high temperatures, UV radiation or high energy ion bombardment, a less aggressive deposition technique, running at substrate temperatures well below the glass temperature of the polycarbonate substrates sometimes is needed. For that, T. Schmauder *et al*. [69] used high-rate microwave Plasma CVD on PC substrates, transparent hard coatings were deposited onto PC substrates.

Using another PVD technique, N Laidani *et al*. [70] deposited hard carbon and tetragonal zirconia films by RF magnetron sputtering onto PC to harden the substrate and end up concluding that efforts should be oriented to design films with high cohesion strength and controlled internal stress and to promote the interfacial energy. The authors reported a high level of residual compressive stresses within the coatings.

The adhesion failure mechanism seemed to be cohesive in carbon/PC systems, whereas in zirconia/PC systems, it was attributed to relieving high internal stress. Both types of films were observed to harden the PC substrates, with carbon coatings exhibiting a more pronounced effect.

Alexander Höflich *et al.*[71] assessed the relationship between residual stress, surface morphology and film properties for a defined microstructure, they deposited very thin Cr films with different residual stresses on polycarbonate substrates. Studying 33 ± 2 nm thick Cr produced by magnetron sputtering the authors concluded that high power improves the packing density of the film, enhances the size of the grains and results in a symmetrical more normalized distribution of the surface roughness. In the context of automotive PC parts, this could imply that optimizing the deposition process parameters, such as power settings, could result in Cr coatings with enhanced adhesion, durability, and surface quality, potentially improving the performance and longevity of automotive components.

Literature states that friction in the exterior and interior of automotive as a common cause of damage [72] [73] [74] [75] and often accompanied by corrosion. Corrosion is normally linked to metal oxidation of steels used in automotive bodies due to humidity, being the main cause of corrosion complaints in the industry [76]. Despite its excellent corrosion resistance in coated and uncoated conditions, aluminium, another common material in vehicles, can still develop galvanic, filiform, or crevice corrosion [77], which influences the end user's perception of finishing quality. This aesthetic effect is more noticeable in highly handled pieces such as doorhandles and buttons [9][10][11][12]. In automotive vehicles, corrosion can be due to rain and salt in the exterior whereas in the interior can be due to perspiration.

Human perspiration encounters many everyday objects, leading to unwanted effects such as discoloration, corrosion, and in the worst-case scenario malfunction due to the corrosive nature of sweat [78]. In an early attempt to understand the effects of corrosion on CrN/TiN decorative coatings for heavy human contact applications such as wristbands, Shimpi K. *et al.* [79] exposed coated stainless steel to supersaturated solution of sodium metabisulphite for porosity check and later analyzed samples for corrosion signs. The authors concluded that the CrN/ TiN decorative coating protected the substrate from corrosion but no real attempt to understand perspiration effect on the coatings designed for wristbands was made.

Suo X. *et al.* [80], studied the corrosion properties, of CrN coatings fabricated by magnetron sputtering on aluminium alloy, through electrochemical techniques such as potentiodynamic measurement and salt spray tests concluding that CrN coatings exhibited an excellent corrosion resistance on aluminium alloy

indicating that CrN could be a promising decorative and protective coating for equipment's made of aluminium and exposed to corrosive environments, such as those addressed in the present paper.

More recently Abhijeet Yadav *et al.* [81] studied the correlation between sweat and hearing aid device failure. They found out that corrosive media such as human sweat was the primary cause for corrosion failures in those devices, hearing aid, where a higher corrosion rate was shown in the summertime.

Studies on the effect of artificial sweat on PVD-coated and anodized materials for decorative applications were performed by Fenker et al.[82]. The authors immersed Nb-coated and anodized Ti samples in artificial sweat mimicking the corrosion behavior of heavily touched colored objects such as eyeglass frames, cutlery, and others. They reported that corrosion can be prevented with a PVD coating.

While sputtered coating for decorative automotive parts offers numerous advantages, challenges remain, including adhesion deficiencies, compromised mechanical properties, and inconsistent optical characteristics. Additionally, current research often inadequately simulates real-world conditions, neglecting factors like long-term exposure to corrosion and frequent human contact. This thesis aims to address these shortcomings. We focused on overcoming adhesion issues, maintaining strong mechanical performance, and achieving a wide range of consistent colours and optical properties throughout the product's lifecycle. Furthermore, we employed characterization techniques attempting to closely replicate real-world environmental stresses, including those encountered during everyday use and mandated by OEM testing protocols.

2.9 References

[1] H. H. Lou and Y. Huang, "Electroplating," *Encyclopedia of chemical processing*, vol. 1, pp. 839–848, 1978, doi: 10.1081/E-ECHP-120007747.

[2] Mandich, N. V., & Snyder, D. L. "Electrodeposition of chromium. Modern electroplating", 5, 205-241, 2010.

[3] H. Yasbandha, "Surface Engineering of Coinage Dies", Doctor of Philosophy Thesis, Faculty of Engineering, University of Wollongong (2001), http://ro.uow.edu.au/theses/1838

[4] L. Zhen, L. Wang, J. Fu, Y. Li, N. Zhao, and X. Li, "Hexavalent chromium affects sperm motility by influencing protein tyrosine phosphorylation in the midpiece of boar spermatozoa," *Reproductive Toxicology*, vol. 59, pp. 66–79, 2016, doi: 10.1016/j.reprotox.2015.11.001.

[5] K. K. Dermentzis, A. Christoforidis, and E. Valsamidou, "Removal of nickel, copper, zinc and chromium from synthetic and industrial wastewater by electrocoagulation," *Int J Environ Sci*, vol. 1, no. 5, pp. 697–710, 2011, doi: 10.6088/ijessi.00105020001.

[6] C. Liu, N. Fiol, J. Poch, and I. Villaescusa, "A new technology for the treatment of chromium electroplating wastewater based on biosorption," *Journal of Water Process Engineering*, vol. 11, pp. 143–151, 2016, doi: 10.1016/j.jwpe.2016.05.002.

[7] L. Fedrizzi, S. Rossi, R. Cristel, and P. L. Bonora, "Corrosion and wear behaviour of HVOF cermet coatings used to replace hard chromium," *Electrochim Acta*, vol. 49, no. 17–18, pp. 2803–2814, 2004, doi: 10.1016/j.electacta.2004.01.043.

[8] H. Oliveira, "Chromium as an environmental pollutant: Insights on induced plant toxicity," *J Bot*, vol. 2012, pp. 1–8, 2012, doi: 10.1155/2012/375843.

[9] T. Sahraoui, N. E. Fenineche, G. Montavon, and C. Coddet, "Alternative to chromium: Characteristics and wear behavior of HVOF coatings for gas turbine shafts repair (heavy-duty)," *J Mater Process Technol*, vol. 152, no. 1, pp. 43–55, 2004, doi: 10.1016/j.jmatprotec.2004.02.061.

[10] T. L. DesMarias and M. Costa, "Mechanisms of chromium-induced toxicity," *Current Opinion in Toxicology*, vol. 14. 2019. doi: 10.1016/j.cotox.2019.05.003.

[11] R. Chakraborty *et al.*, "Mechanism of chromium-induced toxicity in lungs, liver, and kidney and their ameliorative agents," *Biomedicine and Pharmacotherapy*, vol. 151. 2022. doi: 10.1016/j.biopha.2022.113119.

[12] R. R. Ray, "Adverse hematological effects of hexavalent chromium: An overview," *Interdisciplinary Toxicology*, vol. 9, no. 2. 2016. doi: 10.1515/intox-2016-0007.

[13] A. Liang, Y. Li, H. Liang, L. Ni, and J. Zhang, "A favorable chromium coating electrodeposited from Cr(III) electrolyte reveals anti-wear performance similar to conventional hard chromium," *Mater Lett*, vol. 189, pp. 221–224, 2017, doi: 10.1016/j.matlet.2016.12.022.

[14] T. Uchimoto *et al.*, "Newly developed surface modification punches treated with alloying techniques reduce sticking during the manufacture of ibuprofen tablets," *Int J Pharm*, vol. 441, no. 1–2, pp. 128–134, 2013, doi: 10.1016/j.ijpharm.2012.12.006.

[15] P. R. Laity, "Effects of punches with embossed features on compaction behaviour," *Powder Technol*, vol. 254, pp. 373–386, 2014, doi: 10.1016/j.powtec.2014.01.042.

[16] V. Mazel, V. Busignies, H. Diarra, I. Reiche, and P. Tchoreloff, "The surface layer of pharmaceutical compacts: The role of the punch surface and its impact on the mechanical properties of the compacts," *Int J Pharm*, vol. 442, no. 1–2, pp. 42–48, 2013, doi: 10.1016/j.ijpharm.2012.08.005.

[17] K. Shimamura, Y. Matsumoto, and T. Matsunaga, "Some applications of amorphous alloy coatings by sputtering," *Surf Coat Technol*, vol. 50, no. 2, pp. 127–133, 1992, doi: 10.1016/0257-8972(92)90053-D.

[18] T. S. McDermott, J. Farrenkopf, A. Hlinak, J. P. Neilly, and D. Sauer, "A material sparing method for quantitatively measuring tablet sticking," *Powder Technol*, vol. 212, no. 1, pp. 240–252, 2011, doi: 10.1016/j.powtec.2011.05.023.

[19] K. Reed, C. Davies, and K. Kelly, "Tablet sticking: Using a 'compression toolbox' to assess multiple tooling coatings options," *Powder Technol*, vol. 285, pp. 103–109, 2015, doi: 10.1016/j.powtec.2015.05.005.

[20] Z. Wang *et al.*, "Measuring the sticking of mefenamic acid powders on stainless steel surface," *Int J Pharm*, vol. 496, no. 2, pp. 407–413, 2015, doi: 10.1016/j.ijpharm.2015.09.067.

[21] S. Paul *et al.*, "Mechanism and Kinetics of Punch Sticking of Pharmaceuticals," *J Pharm Sci*, vol. 305, pp. 1–8, 2016, doi: 10.1016/j.xphs.2016.07.015.

[22] H. Yasbandha, "Surface Engineering of Coinage Dies", Doctor of Philosophy Thesis, Faculty of Engineering, University of Wollongong (2001), http://ro.uow.edu.au/theses/1838

[23] S. Ithisoponakul, T. Wongsamarnmanee, and V. Premanond, "Improvement of an industrial tool life for minting the circulating coins," *Wear*, vol. 320, no. 1, pp. 68–76, 2014, doi: 10.1016/j.wear.2014.08.014.

[24] J. White, C. Tenore, A. Pavich, R. Scherzer, and S. Stagon, "Environmentally benign metallization of material extrusion technology 3D printed acrylonitrile butadiene styrene parts using physical vapor deposition," *Addit Manuf*, vol. 22, no. May, pp. 279–285, 2018, doi: 10.1016/j.addma.2018.05.016.

[25] J. Skelly, "Decorative Hating Processes for Common Plastic Resins Resin," *Metal Finishing*, pp. 61–65, 2008.

[26] P. Pedrosa *et al.*, "Surface & Coatings Technology Properties of CrN thin fi lms deposited in plasma-activated ABS by reactive magnetron sputtering," *Surf Coat Technol*, vol. 349, no. June, pp. 858–866, 2018, doi: 10.1016/j.surfcoat.2018.06.072.

[27] A. D. Gmbh, "ANALYSIS OF ALTERNATIVES non-confidential report". (accessed Feb. 5 2022)

[28] K. Bewilogua *et al.*, "Surface technology for automotive engineering," *CIRP Ann Manuf Technol*, vol. 58, no. 2, pp. 608–627, 2009, doi: 10.1016/j.cirp.2009.09.001.

[29] E. V. Antonakou and D. S. Achilias, "Recent advances in polycarbonate recycling: A review of degradation methods and their mechanisms," *Waste and Biomass Valorization*, vol. 4, no. 1. pp. 9–21, 2013. doi: 10.1007/s12649-012-9159-x.

[30] C. S. Hattori *et al.*, "Microstructure and fatigue properties of extruded aluminum alloys 7046 and 7108 for automotive applications," *Journal of Materials Research and Technology*, vol. 14, pp. 2970–2981, 2021, doi: 10.1016/j.jmrt.2021.08.085.

[31] Y. Ota, T. Masuda, and S. Kimura, "Technical trends in aluminum alloy sheets for automotive body panels," *R and D: Research and Development Kobe Steel Engineering Reports*, vol. 69, no. 1, pp. 15–18, 2019.

[32] J. Hirsch, "Automotive trends in aluminium - The European perspective," *Materials Forum*, vol. 28, no. January 2014, pp. 15–23, 2004.

[33] K. Sivanur, K. V. Umananda, and D. Pai, "Advanced materials used in automotive industry-a review," in *AIP Conference Proceedings*, 2021, p. 020032. doi: 10.1063/5.0036149.

[34] G. Bräuer, B. Szyszka, M. Vergöhl, and R. Bandorf, "Magnetron sputtering – Milestones of 30 years," *Vacuum*, vol. 84, no. 12, pp. 1354–1359, Jun. 2010, doi: 10.1016/j.vacuum.2009.12.014.

[35] P. J. J. Kelly and R. D. D. Arnell, "Magnetron sputtering: a review of recent developments and applications," *Vacuum*, vol. 56, no. 3, pp. 159–172, 2000, doi: 10.1016/S0042-207X(99)00189-X.

[36] K. Wasa, "2 - Sputtering Phenomena," in *Handbook of Sputtering Technology (Second Edition)*, K. Wasa, I. Kanno, and H. Kotera, Eds., Oxford: William Andrew Publishing, 2012, pp. 41–75. doi: https://doi.org/10.1016/B978-1-4377-3483-6.00002-4.

[37] L. Vernhes, M. Azzi, and J. E. Klemberg-Sapieha, "Alternatives for hard chromium plating: Nanostructured coatings for severe-service valves," *Mater Chem Phys*, vol. 140, no. 2–3, pp. 522–528, 2013, doi: 10.1016/j.matchemphys.2013.03.065.

[38] C. Forsich *et al.*, "Potential of thick a-C: H: Si films as substitute for chromium plating," *Surf Coat Technol*, vol. 241, pp. 86–92, 2014, doi: 10.1016/j.surfcoat.2013.11.011.

[39] S. Wang, C. Ma, and F. C. Walsh, "Alternative tribological coatings to electrodeposited hard chromium: a critical review," *Transactions of the IMF*, vol. 98, no. 4, pp. 173–185, Jul. 2020, doi: 10.1080/00202967.2020.1776962.

[40] G. W. Conran, "The evaluation and heat treatment of steels for the manufacture of coining dies and their subsequent surface coating," *Surf Coat Technol*, vol. 71, no. 2, pp. 98–101, 1995, doi: 10.1016/0257-8972(95)80025-5.

[41] W. Lin, M. S. Leu, C. K. Lin, and C. Y. Su, "The failure mechanism of diamond like coatings prepared by the filtered cathodic arc technique for minting application," *Surf Coat Technol*, vol. 201, no. 7 SPEC. ISS., pp. 4430–4435, 2006, doi: 10.1016/j.surfcoat.2006.08.080.

[42] H. Mori, Y. Shibata, S. Araki, T. Imanara, K. Sakamoto, and Y. Yama, "Surface improvement of coining dies with DLC films," *Procedia Eng*, vol. 81, no. October, pp. 1933–1938, 2014, doi: 10.1016/j.proeng.2014.10.259.

[43] W. Lin, M. S. Leu, C. K. Lin, and C. Y. Su, "The failure mechanism of diamond like coatings prepared by the filtered cathodic arc technique for minting application," *Surf Coat Technol*, vol. 201, no. 7 SPEC. ISS., pp. 4430–4435, 2006, doi: 10.1016/j.surfcoat.2006.08.080.

[44] C. Forsich *et al.*, "Potential of thick a-C: H: Si films as substitute for chromium plating," *Surf Coat Technol*, vol. 241, pp. 86–92, 2014, doi: 10.1016/j.surfcoat.2013.11.011.

[45] S. Ithisoponakul, T. Wongsamarnmanee, and V. Premanond, "Improvement of an industrial tool life for minting the circulating coins," *Wear*, vol. 320, no. 1, pp. 68–76, 2014, doi: 10.1016/j.wear.2014.08.014.

[46] L. Major, "Wear mechanisms of multilayer TiN/Ti/a-C:H coatings investigated by transmission electron microscopy technique," *Archives of Civil and Mechanical Engineering*, vol. 14, no. 4, pp. 615–621, 2014, doi: 10.1016/j.acme.2014.01.007.

[47] L. Hongxi, J. Yehua, Z. Rong, and T. Baoyin, "Wear behaviour and rolling contact fatigue life of Ti/TiN/DLC multilayer films fabricated on bearing steel by PIIID," *Vacuum*, vol. 86, no. 7, pp. 848–853, 2012, doi: 10.1016/j.vacuum.2011.02.015.

[48] G. Zhang, T. Wang, and H. Chen, "Microstructure, mechanical and tribological properties of TiN/Mo2N nano-multilayer films deposited by magnetron sputtering," *Surf Coat Technol*, vol. 261, pp. 156–160, 2015, doi: 10.1016/j.surfcoat.2014.11.041.

[49] D. E. Wolfe, B. M. Gabriel, and M. W. Reedy, "Nanolayer (Ti,Cr)N coatings for hard particle erosion resistance," *Surf Coat Technol*, vol. 205, no. 19, pp. 4569–4576, 2011, doi: 10.1016/j.surfcoat.2011.03.121.

[50] H. C. Barshilia, B. Deepthi, K. S. Rajam, K. P. Bhatti, and S. Chaudhary, "Growth and characterization of TiAlN/CrAlN superlattices prepared by reactive direct current magnetron sputtering," *Journal of Vacuum Science & Technology A: Vacuum, Surfaces, and Films*, vol. 27, no. 1, pp. 29–36, Jan. 2009, doi: 10.1116/1.3013858.

[51] H. T. Wang, Y. X. Xu, and L. Chen, "Optimization of Cr-Al-N coating by multilayer architecture with TiSiN insertion layer," *J Alloys Compd*, vol. 728, no. September, pp. 952–958, 2017, doi: 10.1016/j.jallcom.2017.09.096.

[52] Y. Makino and K. Nogi, "Synthesis of pseudobinary Cr-Al-N films with B1 structure by rf-assisted magnetron sputtering method," *Surf Coat Technol*, vol. 98, no. 1–3, pp. 1008–1012, 1998, doi: 10.1016/S0257-8972(97)00391-5.

[53] W. Wu *et al.*, "Design of AlCrSiN multilayers and nanocomposite coating for HSS cutting tools," *Appl Surf Sci*, vol. 351, pp. 803–810, 2015, doi: 10.1016/j.apsusc.2015.05.191.

[54] A. Al-Rjoub *et al.*, "Characterization of magnetron sputtered sub-stoichiometric CrAlSiNx and CrAlSiOyNx coatings," *Surf Coat Technol*, vol. 328, pp. 134–141, 2017, doi: 10.1016/j.surfcoat.2017.08.038.

[55] T. Polcar and A. Cavaleiro, "High-temperature tribological properties of CrAlN, CrAlSiN and AlCrSiN coatings," *Surf Coat Technol*, vol. 206, no. 6, pp. 1244–1251, 2011, doi: 10.1016/j.surfcoat.2011.08.037.

[56] W. Wu *et al.*, "Design of AlCrSiN multilayers and nanocomposite coating for HSS cutting tools," *Appl Surf Sci*, vol. 351, pp. 803–810, 2015, doi: 10.1016/j.apsusc.2015.05.191.

[57] D. Kalincová, O. Barborák, and I. Andrejčák, "Quality of chrome layers of coining dies and its impact on their reliability and lifetime in operation," pp. 457–461, 2011.

[58] L. Vernhes, M. Azzi, and J. E. Klemberg-Sapieha, "Alternatives for hard chromium plating: Nanostructured coatings for severe-service valves," *Mater Chem Phys*, vol. 140, no. 2–3, pp. 522–528, 2013, doi: 10.1016/j.matchemphys.2013.03.065.

[59] A. M. A. Reheem, M. I. A. A. Maksoud, and A. H. Ashour, "Surface modification and metallization of polycarbonate using low energy ion beam," *Radiation Physics and Chemistry*, vol. 125, pp. 171–175, 2016, doi: 10.1016/j.radphyschem.2016.04.010.

[60] S. Olivera, H. B. Muralidhara, K. Venkatesh, K. Gopalakrishna, and C. S. Vivek, "Plating on acrylonitrile–butadiene–styrene (ABS) plastic: a review," *J Mater Sci*, vol. 51, no. 8, pp. 3657–3674, 2016, doi: 10.1007/s10853-015-9668-7.

[61] M. Charbonnier, M. Romand, E. Harry, and M. Alami, "Surface plasma functionalization of polycarbonate: Application to electroless nickel and copper plating," *J Appl Electrochem*, vol. 31, no. 1, pp. 57–63, 2001, doi: 10.1023/A:1004161707536.

[62] I. Grimberg, B. Bouaifi, U. Draugelates, K. Soifer, and B. Z. Weiss, "Microstructure and adhesion mechanisms of TiN coatings on metallized acrylonitrile-butadiene-styrene," *Surf Coat Technol*, vol. 68–69, no. C, pp. 166–175, 1994, doi: 10.1016/0257-8972(94)90155-4.

[63] P. Sukwisute, R. Sakdanuphab, and A. Sakulkalavek, "Hardness and wear resistance improvement of ABS surface by CrN thin film," in *Materials Today: Proceedings*, Elsevier Ltd, 2017, pp. 6553–6561. doi: 10.1016/j.matpr.2017.06.167.

[64] P. Pedrosa *et al.*, "Properties of CrN thin fi lms deposited in plasma-activated ABS by reactive magnetron sputtering," *Surf Coat Technol*, vol. 349, no. June, pp. 858–866, 2018, doi: 10.1016/j.surfcoat.2018.06.072.

[65] D. Katsamberis, K. Browall, C. Iacovangelo, M. Neumann, and H. Morgner, "Highly durable coatings for automotive polycarbonate glazing," vol. 34, pp. 130–134, 1998.

[66] M. Andritschky and K. Pischow, "Mass production of thick copper vacuum metalization on plastic parts," vol. 82, pp. 1269–1273, 2008, doi: 10.1016/j.vacuum.2008.02.007.

[67] D. Evans, K. Zuber, and P. Murphy, "Ultrathin fi lms of co-sputtered CrZr x alloys on polymeric substrates," vol. 206, pp. 3733–3738, 2012, doi: 10.1016/j.surfcoat.2012.03.023.

[68] W. Boentoro, A. P, and B. Szyszka, "Scratch resistance analysis of coatings on glass and polycarbonate," vol. 517, pp. 3121–3125, 2009, doi: 10.1016/j.tsf.2008.11.119.

[69] T. Schmauder, K. Nauenburg, K. Kruse, and G. Ickes, "Hard coatings by plasma CVD on polycarbonate for automotive and optical applications," vol. 502, pp. 270–274, 2006, doi: 10.1016/j.tsf.2005.07.296.

[70] N. Laidani, G. Speranza, A. Nefedov, L. Calliari, and M. Anderle, "Characterization of carbon and zirconia films deposited on polycarbonate for scratch-proof coating applications," vol. 7, pp. 1394–1402, 1998.

[71] A. Hö, N. Bradley, C. Hall, D. Evans, P. Murphy, and E. Charrault, "Packing density / surface morphology relationship in thin sputtered chromium fi lms," vol. 291, pp. 286–291, 2016, doi: 10.1016/j.surfcoat.2016.02.061.

[72] D. J. Mihora and A. C. Ramamurthy, "Friction induced damage: Preliminary numerical analysis of stresses within painted automotive plastics induced by large curvature counterfaces," *Wear*, vol. 203–204, no. 96, pp. 362–374, 1997, doi: 10.1016/S0043-1648(96)07452-2.

[73] A. C. Ramamurthy, W. I. Lorenzen, and S. J. Bless, "Stone impact damage to automotive paint finishes: An introduction to impact physics and impact induced corrosion," *Prog Org Coat*, vol. 25, no. 1, pp. 43–71, 1994, doi: 10.1016/0300-9440(94)00502-8.

[74] R. A. Ryntz, M. Everson, and G. Pollano, "Friction induced paint damage as affected by clearcoat chemistry," *Prog Org Coat*, vol. 31, no. 4, pp. 281–288, 1997, doi: 10.1016/S0300-9440(97)00082-9.

[75] A. C. Ramamurthy, J. A. Charest, M. D. Lilly, D. J. Mihora, and J. W. Freese, "Friction induced paint damage - A novel method for objective assessment of painted engineering plastics," *Wear*, vol. 203–204, pp. 350–361, 1997, doi: 10.1016/S0043-1648(96)07453-4.

[76] A. Chami, R. Benabbou, M. Taleb, Z. Rais, and M. El Haji, "Analysis of survey data on corrosion in the automotive industry," *Mater Today Proc*, vol. 45, pp. 7636–7642, 2021, doi: 10.1016/j.matpr.2021.03.113.

[77] B. LIU, X. rong ZHOU, and X. xin ZHANG, "Filiform corrosion behaviour on machined AA7150 aluminium alloy," *Transactions of Nonferrous Metals Society of China (English Edition)*, vol. 30, no. 8, pp. 2056–2066, 2020, doi: 10.1016/S1003-6326(20)65360-2.

[78] R. J. Rathish *et al.*, "Corrosion Behaviour of Metals in Artificial Sweat," pp. 38–44, 2010.

[79] K. C. Shimpi, K. Ravindranath, A. K. Jani, D. C. Kothari, and C. S. Harindranath, "Decorative coatings produced using combination of reactive arc evaporation and magnetron sputtering," 1997.

[80] X. Suo, C. Guo, D. Kong, and L. Wang, "Corrosion behaviour of TiN and CrN coatings produced by magnetron sputtering process on aluminium alloy," *Int J Electrochem Sci*, vol. 14, no. 1, pp. 826–837, Jan. 2019, doi: 10.20964/2019.01.81.

[81] A. Yadav, K. Kumar, and R. Ambat, "Statistical analysis of corrosion failures in hearing aid devices from tropical regions," vol. 130, no. May, 2021, doi: 10.1016/j.engfailanal.2021.105758.

[82] M. Fenker *et al.*, "Corrosion performance of PVD-coated and anodised materials for the decorative market," *Surf Coat Technol*, vol. 188–189, no. 1-3 SPEC.ISS., pp. 466–472, 2004, doi: 10.1016/j.surfcoat.2004.08.054.

CHAPTER III – Development of alternative coatings to hexavalent chromium for minting applications

The following chapter is partially based on the results published in:

E. Carneiro, José D. Castro, S.M. Marques, A. Cavaleiro, S. Carvalho, "REACH regulation challenge: Development of alternative coatings to hexavalent chromium for minting applications", Surface and Coatings Technology, 2021, Volume 418, 127271, https://doi.org/10.1016/j.surfcoat.2021.127271

3 Introduction

In this chapter, various alternative coatings for coinage punches are investigated as environmentally friendly and effective replacements for hexavalent chromium coatings, which pose health and environmental risks [1–20]. We explored physical vapor deposition (PVD) an alternative coating method, with a focus on gradient-based coating designs to tailor surface properties and enhance mechanical and wear resistance. Alloying elements like Si and Al were incorporated to improve coating properties, offering potential benefits in minting applications [21–38]. The research evaluated the structure of the materials and how it influenced the mechanical behavior of these alternative coatings through multiple impulse testing and comparative analysis with conventional die materials, aiming to enhance the performance and durability of coinage punches.

3.1 Materials and methods

Cr(Si,Al)N coatings, were deposited by reactive DC magnetron sputtering on stainless steel and silicon substrates (monocrystalline silicon wafers (100 P-type/B) after ultrasonic cleaning, at room temperature, in distilled water, acetone and ethanol (for 10 minutes in each solvent). Different targets were used for the deposition, a pure Cr target (99.5%), an Al-Cr target (70-30 at. % in composition and 99.8% purity) and an Al-Si target (65-35 wt. % in composition and 99.99% pure), all with 200 × 100 mm^2, supplied by Testbourne Ltd. Ar and N_2 gas flows were mixed inside the dual magnetron sputtering chamber and the coatings were deposited at a temperature lower than 200°C, with a rotation speed of 7 rpm. The magnetrons are configured in an unbalanced magnetic arrangement, facing each other within the chamber. The base pressure in the chamber was approximately 3×10^{-4} Pa. Working pressures were kept approximately at 8.5×10^{-1} Pa. Before every deposition an etching process was performed, using a pulsed power source with 200 kHz, a pulse width of 1536 ns and 200 mA current. The deposition time was selected in order not to exceed typical thickness of minting dies nitride-based coatings ranging between 1.5-5 μm [39]. The deposition parameters are depicted in table III-1.

To improve adhesion, prior to the coating deposition, a graded CrN_x interlayer was deposited, starting with pure Cr and progressively increasing the nitrogen flux in steps of 1.5 sccm up to 9 sccm. Such gradual transition is seen as a flexible way to optimize the material response through the control of mechanical stress by elimination of either defect-nucleating stress concentrations or abrupt stress jumps typically occurring at sharp interfaces; furthermore, the gradient allows to decrease the local crack driving force,

contributing for the adhesion improvement [40], [41]. A bias voltage of -75 V was applied to the rotating substrate holder during all the depositions.

All chemical compositions were estimated in an EDAX – Pegasus X4M (EDS/EBSD) system coupled to a Nano SEM–FEI Nova 200(FEG/SEM) microscope with an energy of 12 keV.

The crystalline structure of the coatings was analysed by X-ray diffraction in a Bruker AXS Discover D8 operating with Cu Kα radiation (λ= 1.5406 Å at an incidence angle of α = 4° and in a 2θ interval of 20-75°).

Chemical bonds were evaluated by X-ray photoelectron spectroscopy (XPS). The measurements were done in a Kratos AXIS Ultra HSA equipment with an AlKα X-ray source and 15 kV pass energy. Before the XPS measurement, Ar+ etching (4 keV, 600 s) was conducted to clean up the impurities and contaminants. The binding energy was referenced to the C 1 s peak position at 285.0 eV. The XPS spectra analysis and peaks fitting were performed using the CasaXPS software.

The Hardness (H) and reduced Young's modulus (Er) were measured by depth-sensing indentation using a Berkovich diamond pyramid indenter, applying a load (P) of 10 mN to assure not to exceed 10% of coatings thickness and hence, avoid the substrate influence over the measurements. Coating Young's modulus (E) was calculated according to the Oliver and Pharr method [42] and applying the following equation:

$$\frac{1}{Er} = \left(\frac{1-\nu^2}{E}\right) + \left(\frac{1-\nu_i^2}{E_i}\right) \quad (1)$$

Where the sub index *i* indicates values from indenter material. For our measurements, all calculations used 1141 GPa and 0.07 as indenter Young's modulus and Poisson ratio respectively [43]. Also, Poisson ratio's for CrN and CrAlN was used from Wang *et al.* (2016) [44], and CrAlSiN Poisson ratio was extracted from Chang *et al.* (2016) [45].

The plastic index (PI) was calculated using the reversible and the un-reversible work in every indentation. The equation used to calculate this index was [46]:

$$PI = \frac{W_p}{W_p + W_e} \quad (2)$$

Where Wp is the plastic work applied during the loading process in the indentation, and We is the elastic work during the unloading step. An example of an indentation curve is displayed in figure III-1.

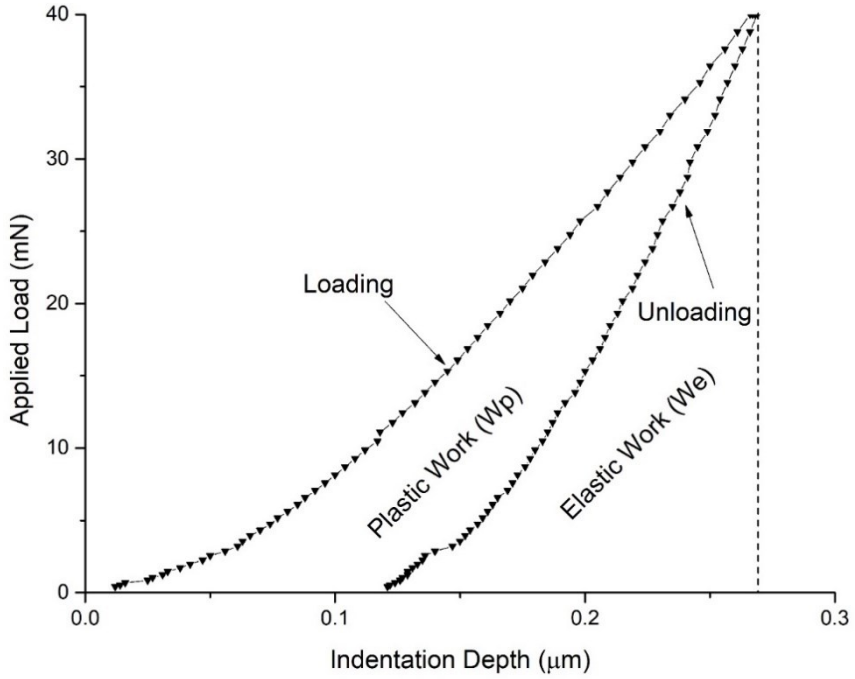

Figure III-1. Schema of a typical indentation curve.

The fracture toughness was carried out after indentations and using the equation used in several studies [44], [47]:

$$K_{Ic} = \alpha \left(\frac{E}{H}\right)^{\frac{1}{2}} \left(\frac{P}{c^{3/2}}\right) \quad (3)$$

Here, α is the geometric constant of the indenter (0.04 for the cube-corner indenter [47]) and c is the mean value by averaging the lengths of 15 radial cracks. These cracks were measured by imaging treatment (ImageJ software) using SEM micrographs obtained with the Nano SEM–FEI Nova 200(FEG/SEM) microscope mentioned before.

Multiple impact tests were conducted using the 'Multiple Impulse' module of a NanoTest system from Micro Materials with 6 different loads, 1, 5, 10, 20, 50 and 100 mN. Multiple impact testing was performed using a NTcube corner indenter. Every measure was executed in 200 s, with time cycles of 1 s ON (loading the programmed force onto the sample surface) and 3 s OFF (unloading process and return of the indenter until the initial position), generating 50 impacts at each location, 5 times for each sample, spaced 100 micrometers between each individual location.

3.2 Results and discussion

3.2.1 Chemical Composition versus Deposition Parameters

Table III-1, discloses the composition, the thickness, and the deposition rate for all coatings.

Table III-1. Experimental details: Current density on each target and gas flow inserted onto the chamber. Samples were named* taking in consideration chemical elements present in the coating. Thickness (h), deposition rate and chemical composition are also presented.

Sample*	Current density (mA/cm^2)			N_2 Partial Pressure (Pa)	Thickness (μm)	Dep. rate (μm/h)	Chemical composition (at.%)				Cr/N
	Cr target	AlSi target	AlCr target				Cr	N	Al	Si	
CrN	10.0	-	-	2.1×10^{-1}	2.7	2.5	52.5	47.5	-	-	1.1
CrAlN	5.0	-	12.5	3.2×10^{-1}	2.9	2.2	34.9	48.7	16.4	-	0.7
CrAlSiN	10.0	12.5	-	3.4×10^{-1}	3.8	3.5	33.3	50.6	10.7	5.4	0.7

The Cr/N ratio closer to 1 suggests formation of CrN phase. For the other samples, the detected elements agree with the deposition conditions; Cr content was kept approximately constant and the (Al+Si) content for the CrAlSiN is similar to the Al content for the CrAlN coating. The silicon content in CrAlSiN is of about 5.4 at. %, trying to meet the literature results. In fact, Wang *et al.* [48] reported that Si contents around 5.9 at. % when compared with lower contents (e. g. 1.8 at. %) could increase the coating hardness while maintaining resistance to crack propagation. Increasing silicon content could even lead to higher hardness value, however it is accompanied by an increase in brittleness. The deposition rates were estimated through SEM cross-sectional (figure III-2) micrographs in silicon substrates; the whole thickness of the coating was taken for the calculation of the total deposition rate. Two main conclusions can be drawn (i) as expected the deposition rate is higher when the samples were deposited with an additional target, keeping the same current density in the other target (case of CrAlSIN samples); (ii) in CrAlN the deposition rate is lower compared to the CrN coatings; it should be noted that for the former the Cr target is also being sputtered, reinforcing the much lower sputtering rate of AlCr target This fact, can be explained by the higher Cr sputtering rate in comparison to Al [49].The reported sputtering yield, for a Ar ion energy of 1000 eV, of Cr is 1.9 against 1.5 for Al [50]. Furthermore, due the higher N_2 partial pressure used in CrAlN deposition and the higher affinity of Al for N than Cr [51] makes possible the partial poisoning of

the CrAl target decreasing the sputtering rate and, therefore, the lower final total deposition rate for the CrAlN coating. The formation of a compound in the target surface changes the target condition, in particular the effective secondary electron emission yield (SEEY). In this case, for a constant current density, a significant variation on the target voltage occurs, promoting a lower sputtering yield in AlCr target [52]. Considering that N is preferentially bonded to Al, the analysis of Table III-1 data allows to conclude that, approximately, the same Cr/N ratio would be expected in CrN and CrAlN, if we would consider that separate CrN and AlN phase would be formed. In fact, assuming that AlN compound is preferentially formed due to the higher affinity of Al for N, a Cr/N ratio of ≈1 is calculated (N = 48.7 – 16.4 at.%). This ratio is the same as the one calculated for the pure CrN coating. If a similar analysis was performed for CrAlSiN, assuming the same premises, the Cr/N would be similar.

3.2.2 Morphology

Representative cross-section SEM micrographs of the samples in BSE mode are presented in figure III-2. The brightness in the micrographs can be related to the chemical composition. Brighter phases contain elements with heavier atomic weight while lighter elements are present as darker zones [39].

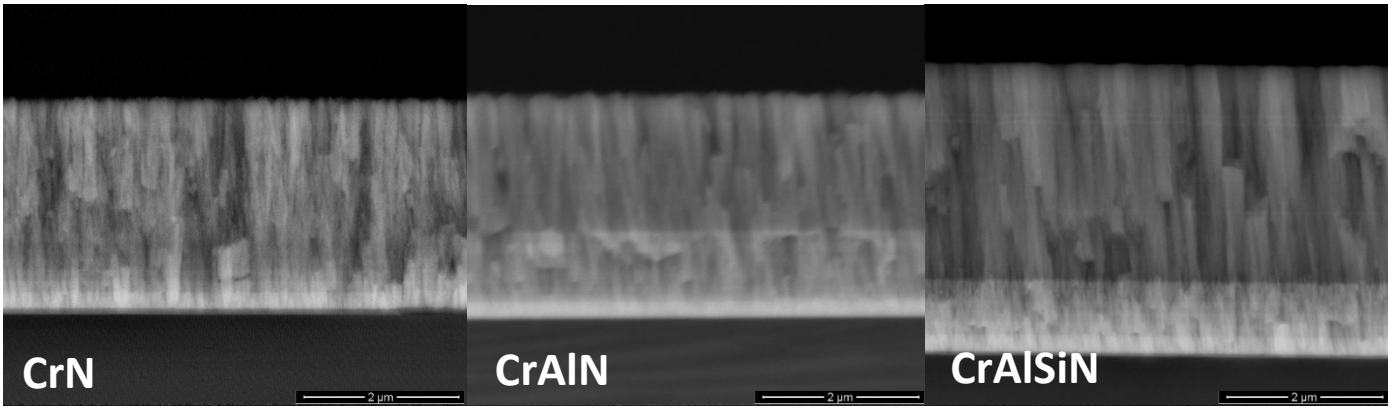

Figure III-2. SEM micrographs of the coatings deposited in Si substrates in BSE mode. From left to right, CrN, CrAlN and CrAlSiN.

Samples present several layers (as expected for the adhesion layer) underneath the topcoat. From the bottom-up, brightness decreases with nitrogen flow increase. Also, the thickness of each layer decreases, an effect similar to that reported by Hao Zhang *et al.* [53], which is directly related with a decrease in the CrN deposition rate with increase of nitrogen flow. The partial poisoning of the target surface and the changes in the electrical characteristics of the target are responsible for a decrease in the deposition sputtering yield as commonly observed for transition metal nitrides deposition.

In all micrographs, the coatings, including the graded adhesion layer, show a well-defined columnar structure. In many cases, the continuity of the columns of the adhesion layer to the top coatings is observed. The influence of the previous layer in the next one inducing a "column-on-column" epitaxial alignment was already documented in the literature [54], [55], being the developed microstruture intrinsically related with the grain growth. This effect can be responsible for the CrN morphology, as well as the Si-containing coatings (figure III. 2), contrasting with the data presented in the literature that reported smoother coatings, without distinct columnar structure, for CrAlSiN when Si is added to CrAlN matrices [56], [57].

3.2.3 Structural Analysis

The structure was evaluated by XRD and the results are shown in figure III-3 for all deposited coatings. XRD diffraction peaks belong to (111), (200) and (220) of a cubic (fcc-B_1) chromium nitride structure (ICDD card 76-2494). For sample CrN a dominant CrN (111) peak is observed, for the reason that to minimize surface energy, atoms tend to be arranged with the maximum compactness planes parallel to the surface. In fcc structures, growth takes place according to (111) plane [58].

The maximum solubility of Al in $Cr_{1-x}Al_xN$ structure is normally located between x = 0.6–0.8 [37] before wurtzite-type AlN is formed. No peaks of wurtzite AlN phase can be observed, pointing towards a CrAlN solid solution [59], which is in agreement with the differences observed on the lattice parameter. The lattice parameter was calculated, using Scherrer equation and interplanar distance of (111), in all coating and the results are presented in table III-2.

From the literature [60], CrN coatings at room temperature have a lattice constant a=4.14 Å, however our samples have a shortfall of nitrogen leading to a substoichiometric regime with lattice parameter of 4.11 Å. In CrAlN sample a shift of the diffraction peaks toward lower angle is exhibited. This is caused by lattice parameter expansion from 4.11 to 4.17 Å when Al atoms (1.43 Å) replace Cr atoms (1.40 Å) in the CrN structure to form (Cr,Al)N phase solid solution [35].

Adding Si to the coatings results in a broadening of XRD peaks, which is related to a reduction in grain size from 11 nm to ≈ 2 nm and/or an increase in micro-stress, as confirmed by the literature [57]. Some authors also state that silicon segregates as amorphous SiN_x along grain boundaries inhibiting the grain growth [37] [57]. When transitioning from CrAlN to CrAlSiN, we notice an increase in deposition rate

leading to an increase in surface mobility that should be enough to allow Si atoms segregation and the formation of an amorphous SiNx phase [61].

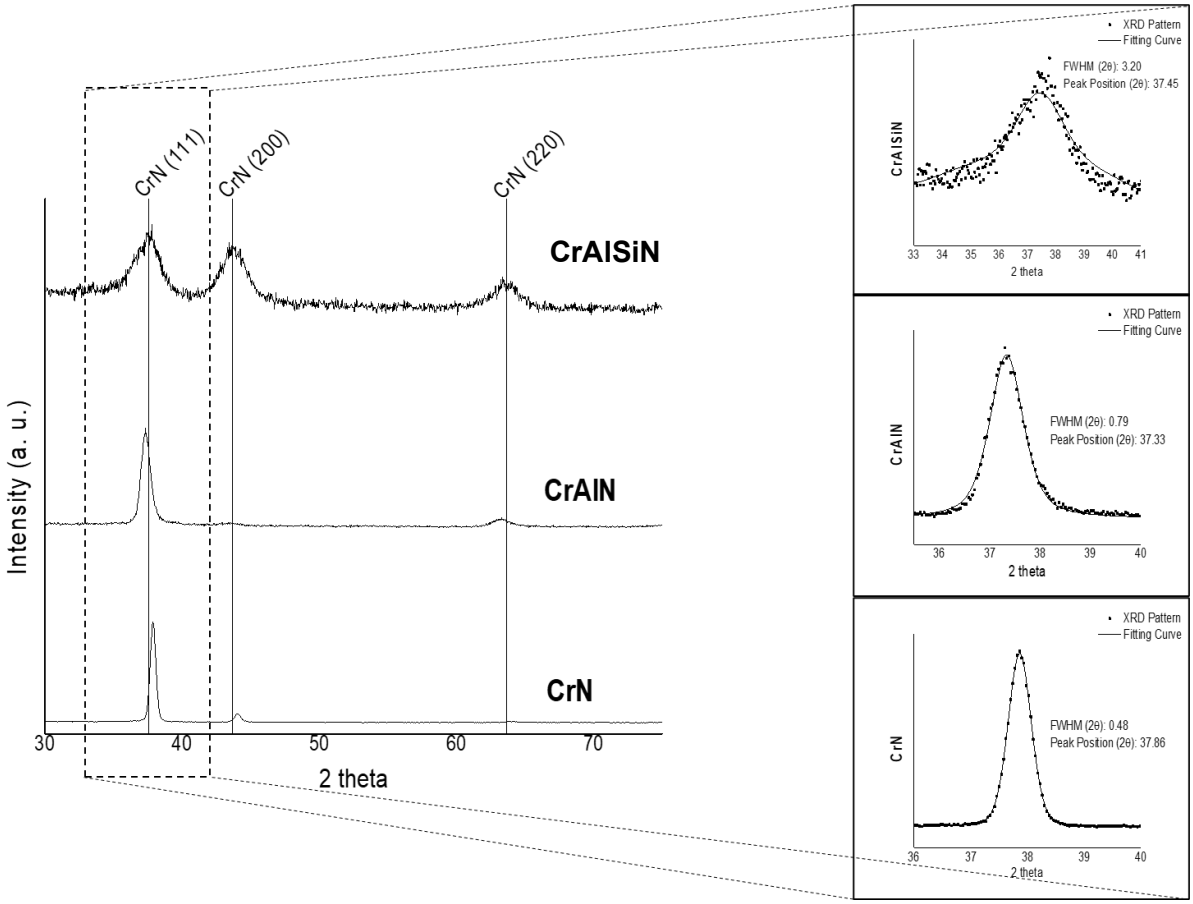

Figure III-3. XRD patterns in grazing incidence ((Cu K α radiation), insets show fitting for crystallite size calculation.

Table III-2. Sample crystalline details

Sample	CrN (111)	Lattice parameter	Crystallite size (nm)
	2θ	(Å)	
CrN	37.86	4.11	18
CrAlN	37.36	4.17	11
CrAlSiN	37.60	4.14	2

3.2.4 X-ray photoelectron spectroscopy

To confirm some of the previous statements, XPS analysis was performed for all the samples.

Electric charge effect was corrected by the reference of the C 1s peak at 285 eV and a Shirley background was used for electron background correction. The area ratios of 1:2 for p core levels was taken into consideration and the same FWMH was forced as well. The individual XPS spectra of the detected elements are displayed in Figures III-4, III-5 ,III-6 and III-7.

The deconvolution of Cr 2p3/2 for CrN sample (Figure III-4, bottom) displayed the correspondent doublet with Cr 2p3/2 at 574.3 eV (Cr 2p1/2 at 583.6 eV), having a spin orbital splitting of 9.3 eV.

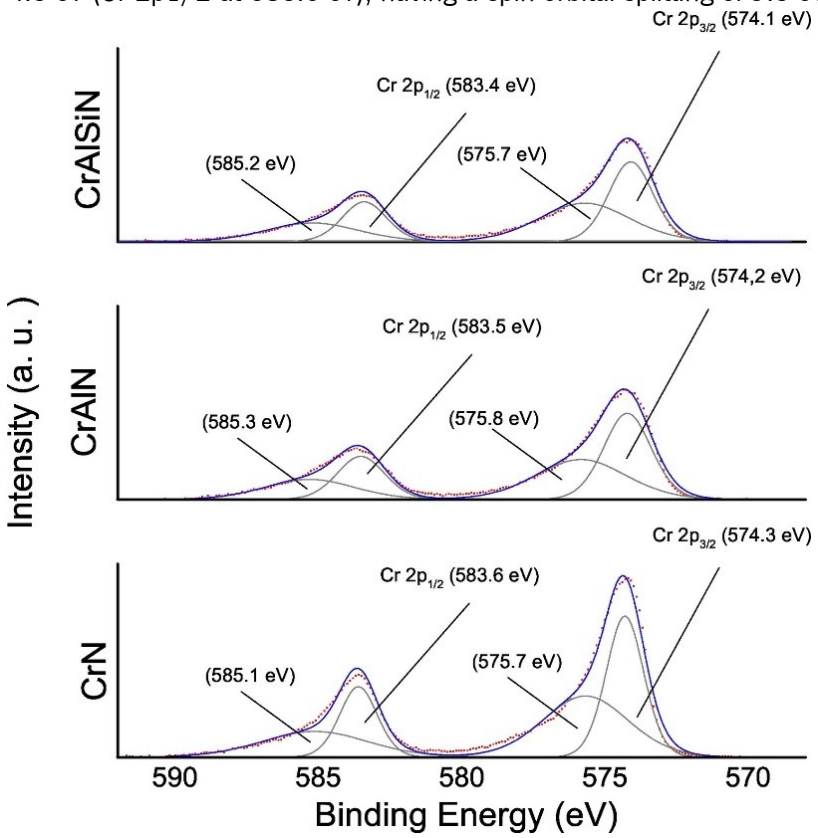

Figure III-4. Cr 2p spectra from all samples

The Cr $2p_{3/2}$ band is composed of two features, the first one at around 574.3 eV (related to Cr-N bonds) and the second one at 575.7 eV (related to Cr-O bonds) while N 1s (figure III-6) is at 397.3 eV. According to literature [62], chemical composition in table III-1 alongside with XRD spectra in figure III-3, they should correspond to a CrN_x phase (with $0.5<x<1$).

When adding Al into the matrix a shift to lower energies, CrAlN, is noted in Cr 2p3/2 (574.2 eV) and Cr 2p1/2 (583.5 eV) (figure III-4) as well as N1s, from 397.3 eV from CrN sample to 396.5 eV in CrAlN bonding energy (figure III-6), indicating Al solubility into CrN matrix (figure III-5).

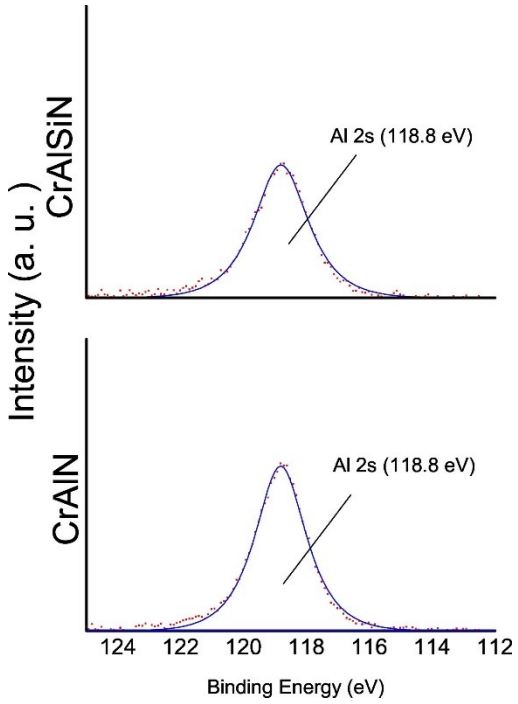

Figure III-5. Al 2s spectra of Al-containing samples.

In sample CrAlSiN a shift to intermediate binging energy, 396.7 eV is observed in N 1s spectra (figure III-6) as well in Cr 2p spectra Cr 2p3/2 (574.1 eV) and Cr 2p1/2 (583.4 eV) ((figure III-4), this phenomenon can be explained by the fact that Si is segregating into grain boundaries and/or to the lower aluminium amount comparing with CrAlN coating which correlates with the results in table III-2. Also, no changes were found in the Al 2s peak positions between CrAlN and CrAlSiN, 118.8 eV (figure III-5).

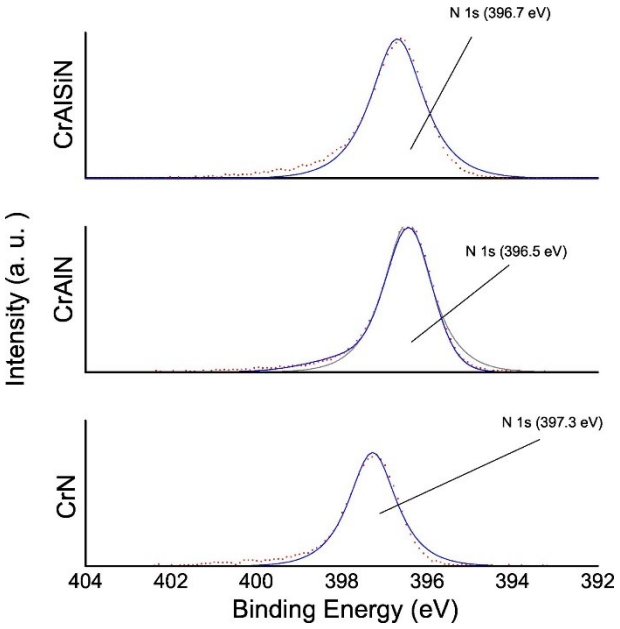

Figure III-6. N 1s spectra of all samples.

Examining the XPS spectra (Figure III-7) of Si 2p two peaks were reveled at 101.8, and 98.8 eV. Published reports attribute this peak at 98.8 position to Si_3N_4, mainly by self-organization upon spinodal phase

segregation [63] or Ka5.5 Al 2s plasmon respectively, [37][64]. However as a consequence of ion beam mixing during ion bombarding to etch the samples the formation of chromium silicide (Si 2p at around 98.8 eV [65]) can also be possible.

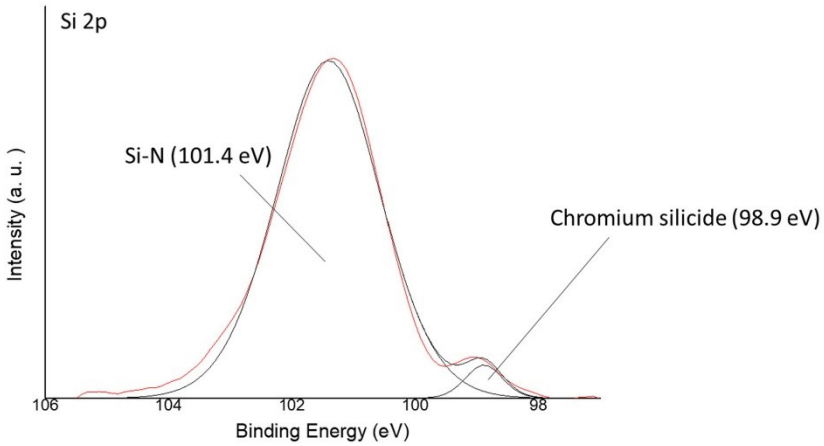

Figure III-7. XPS spectra of Si 2p in CrAlSiN.

3.2.5 Mechanical properties

Table III-3 shows the mechanical properties of the produced coatings, regarding hardness, Young´s modulus, H/E, plasticity index and fracture toughness.

Table III-3. Mechanical properties of the different samples, comparing with the substrate (Böhler K605)

Sample	Hardness [GPa]	E [GPa]	H/E	Plasticity Index	K_{Ic} [kPa*m$^{1/2}$]
Böhler K605	7 ± 1	259	0.027	0.76	-
CrN	8 ± 1	218	0.039	0.68	30.83
CrAlN	13 ± 1	311	0.041	0.65	288.96
CrAlSiN	16 ± 1	285	0.058	0.58	84.07

Hardening process by Al addition and further Si addition, is due to the solid-solution hardening rather than the Hall-Petch effect as reported by other authors [44]. Based on Veprek statements, the Hall-Petch hardening in polycrystalline materials has a lower limit among 10 – 20 nm crystallite size [66]. Nonetheless, according to crystallite size drop reported in table III-2 (from 18 nm at CrN to 2 nm at CrAlSiN) is below to the established by Veprek [66], hence this hardening mechanism is discarded for our films.

Böhler K605, a steel commonly used in minting (chemical composition: 0.55% C, 0.3% Si, 0.4% Mn, 1% Cr, 0.25% Mo and 3% Ni) was evaluated to establish a reference point for our study. Comparing this steel with the obtained coatings, all of them surpass it in hardness value as is expected from ceramic coatings, mainly the CrAl(Si)N coatings

Comparing Young's modulus among obtained coatings, CrAlN presented the highest value (311 GPa). This means that CrAlN sample has a higher elastic zone under load regime and it could support higher load without reaching plastic deformation.

High H/E ratios can be related with improvements in abrasive wear contact, [63]; according to Leyland and Mathews [67], a high H/E ratio in coatings with a sufficiently high hardness and a low elastic modulus can promote a most durable film. Related to the strain-to-break (H/E) parameter, CrAlSiN sample has 0.058 and CrAlN sample presents a value of 0.041, both higher than CrN sample (0.039). It is important to emphasize that not only Young´s modulus should be considered, also H/E ratio is an important parameter related with elastic and plastic zones inside coatings and hence their relationship with fracture events in elastoplastic contacts is probable [68].

In previous works, Rebholtz *et al.* [69] studied mechanical properties of CrN based coatings by reactive magnetron sputtering technique on 316 stainless steel, reaching similar H/E values. Authors named the coatings as Cr(N) when N content was between 10-15 at. % (Metallic) and, with higher contents (higher that 15 at. % N) coating was denominated as CrN (Ceramic). Comparing ceramic nitride (CrN, H = 22.5 GPa, E = 400 GPa, H/E = 0.056) and metallic (Cr(N), H = 15 GPa, E = 280 GPa, H/E = 0.054) coatings, Cr(N) showed better performance to impact wear due to its lower elastic modulus, despite closer values of H/E ratio. Similar behaviour was exhibited by coatings obtained by Wang *et al.* [44], who studied CrN based films by reactive magnetron sputtering, adding Al. According with the report by Wang *et al.*, CrN (H = 14.5 GPa, E = 271 GPa, H/E = 0.054) and CrAlN (H = 17.7 GPa, E = 315 GPa, H/E = 0.056) showed a hardening process due to the Hall-Petch effect and a slight improvement in elastic strain to failure.

Gathering all above-mentioned facts, CrAlN and CrAlSiN coatings would be good candidates for wear applications when compared with CrN samples in this study.

The fracture toughness revealed that the CrN sample had the worst resistance to fracture (30.83 $kPa*m^{1/2}$). On the other hand, CrAlN coating showed the best fracture toughness (288.96 $kPa*m^{1/2}$) and

for CrAlSiN we obtained an intermediate value (84.07 kPa*$m^{1/2}$). This discloses that the CrAlN film could show a better performance in nano-impact test at higher loads as it will be discussed in the next sections.

Another important parameter for fatigue resistance to avoid early failures on coatings is the plasticity index (PI). According to Zhang *et al.* [70], for an elastoplastic contact as indentation, the plasticity index (PI) is a dimensionless ratio between plastic work (Wp) and total work (Wt) during this measurement. PI is related with fatigue (local impact) performance of coating and with H/E ratio. A higher H/E with lower PI is beneficial for many cyclic contact applications. Higher PI can be correlated with higher toughness and fracture resistance in conditions dominated by fatigue wear. For our coatings (see figure III-8), CrN displayed the lowest H/E ratio and PI values, whereas CrAlSiN presented highest H/E ratio and lowest PI.

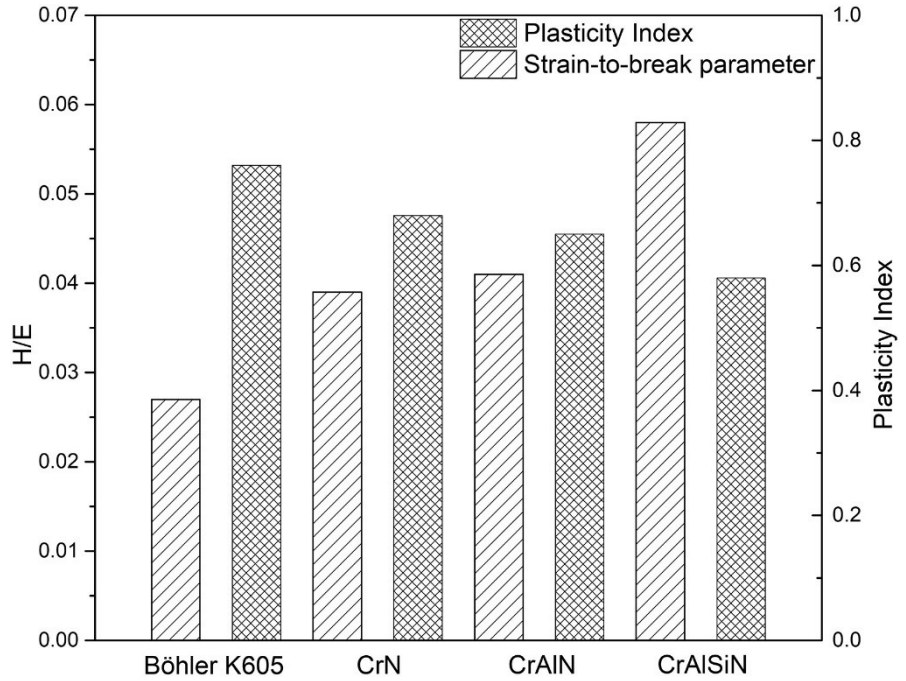

Figure III-8. H/E ratios and Plasticity index in coatings and standard minting steel.

Contrasting with obtained films, the standard steel Böhler K605, as expected presented the lowest H/E and highest PI. Again, both CrAlSiN and CrAlN have coherent properties in achieving a real improvement on typical metallic substrates such as steels in minting applications.

3.2.6 Nano-impact tests

Lacking a proper method to study our coatings in real world conditions, nano-impact test was performed on all systems as a viable approximation. Nano-impact test makes it possible to detect the onset of damage and in many cases, obtain information to understand the local fatigue wear phenomenon in thin films when fracture is a crucial factor [71]. According to Beake *et al.*[72], hard films response in the nano-

impact test can be summarized in four phases: Initial impact, Fatigue, Crack coalescence/fracture and Repetition of the fatigue cycle. For a better understanding of the film response phases present in our coatings, a sample selected randomly was tested, giving the schematic nano-impact test curve exhibited in figure III-9. The initial impact zone can be viewed between the 30th and 35th impacts, wherein practically the initial impact depth is kept, despite increasing impact number.

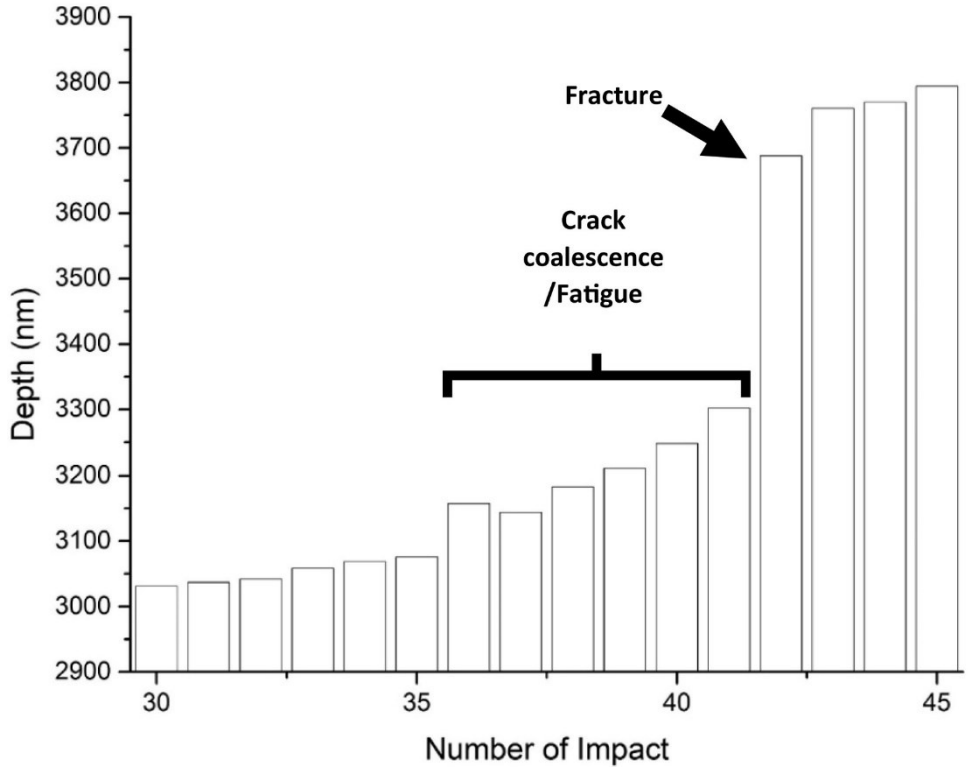

Figure III-9. Schematic nano-impact (local fatigue) test graph representing number of impact vs. indenter depth.

Between the 36th and 41st impacts, there appears the fatigue zone where one may note a slight acceleration of impact depth growth. With a dramatic depth increase, crack coalescence/fracture must be evident in the 42nd impact and finally since the 43rd impact, the fatigue cycle starts again.

Concerning the developed coatings until 10 mN impact test (figure III-10), the behavior depicted in figure III-9 does not quite match, due mainly to a low applied load. However, it gives us indications of the coating's performance. As expected CrN had the worst performance as shown in figure III-10. For initial impact, CrN coating reached 670 nm depth value, showing the worst behavior. Its fatigue process was more evident than any other sample, showing a continuously growing depth along the impact test, almost reaching the substrate. On the other hand, CrAlN and CrAlSiN show better performance, without important fatigue events. It is worth pointing out, CrAlN (showing in fact the lowest final depth) exhibited the highest Young modulus (E), which is fundamental to support higher loads without suffering plastic

deformation. In fact, our results are opposite to the report by several authors [70], [71], [73], that softer coatings with lower elastic modulus resist impacts better in comparison with harder coatings with higher elastic modulus. Due to the nano-impact test nature, the substrate could affect the coating's performance and this topic will be later discussed.

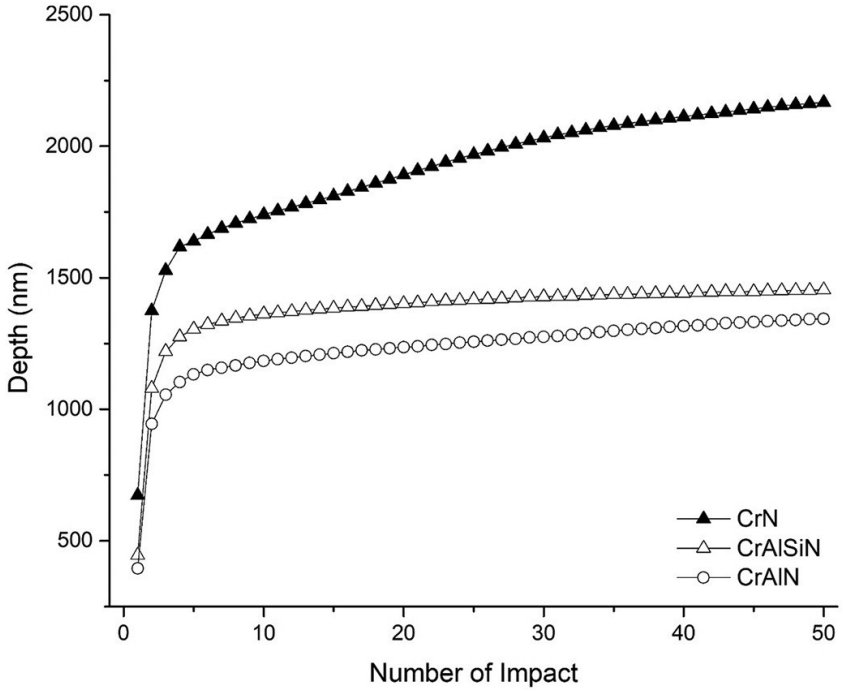

Figure III-10. Nano-impact results for sample, CrN, CrAlN and CrAlSiN at 10 mN load.

Zhang [68] explains that lower depth in nano-impact tests are related with higher toughness and improved performance in time under a fatigue tests. With that in mind, CrAlN system was chosen to be submitted to higher loading (20, 50 and 100 mN) tests to elucidate fatigue behavior compared to Böhler K605. Comparative results are displayed in figure III-11.

For tests performed at 20 mN, the CrAlN coating and the Böhler K605 steel display differences in their behavior (figure III-11). While both were not affected through the running test (no fractures are evident), depth of initial indentation as well as after 50 impacts was significantly lower in CrAlN coating than its K605 steel. The same tendency is visible for all the other loading cycling conditions. Comparing results at higher loads (100 mN), CrAlN had the best performance showing a final depth of 3.3 μm, and the Bohler K605 final depth went up to 6 μm. Assessing number of impacts and reached depth, CrAlN coating did not present a catastrophic failure event according to the fracture stages presented by Beake *et al.*[72], keeping some protection over the substrate in almost all tested loads. Faisal *et al.* [74] proposed two possible failure mechanisms in nano-impact tests on amorphous Nitinol thin films. When the indenter contact depth along impacts is always growing, the film could present a fatigue failure with a forward

depth deviation (typical scenario). On the contrary, a backward depth deviation in the nano-impact test could be displayed when the film delamination provokes a decrease in the indenter contact depth.

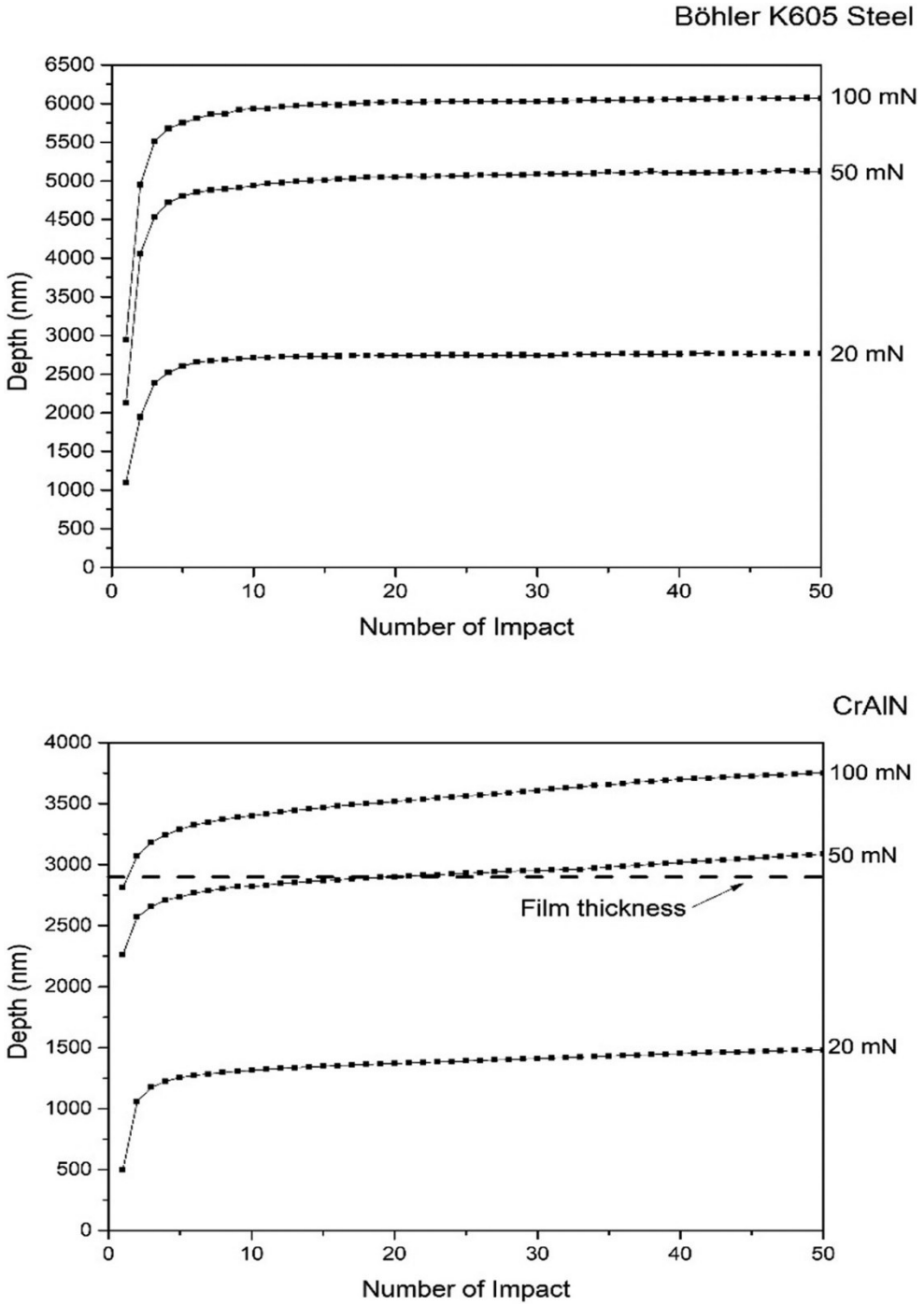

Figure III-11. Nano-impact results in Böhler K605 top) and CrAlN (bottom) coatings with cube-corner indenter.

According to the proposed by Faisal *et al.*, CrAlN exhibited a typical forward depth deviation, hence the coating fatigue. An important point that Faisal *et al.* reported is that the abrupt change in depth during fatigue process might be generally attributed to adhesive failures [74], but the CrAlN coating did not display any event. According to figure III-11, CrAlN revealed a great fracture resistance (H/E = 0.041)

against impacts up to 20 mN without a catastrophic fracture event driven by fatigue and the depth did not reach the film thickness. For higher loads, CrAlN has not exhibited dramatical depth increase or fracture events such as those predicted by Beake *et al.*[72] (figure III-9), but the fatigue process affected the film performance undoubtedly. Indeed, when 50 and 100 mN loads were applied, the penetration depth surpassed film thickness and, induced deformation to the substrate as noted Faisal *et al.*[74]. SEM micrographs were taken after nano-impact tests to verify the proposed scenario (Figure III-12).

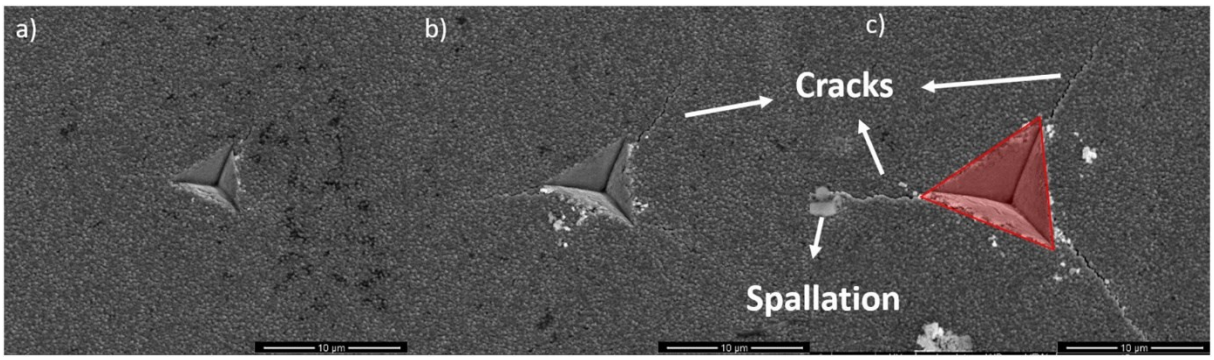

Figure III-12. Representative impact points SEM micrographs of CrAlN after 50 impacts at: a) 20 mN; b) 50 mN; and c) 100 mN. Red triangle corresponds to indentation project area.

According to figure III-12, radial cracks are evident since 50 mN at the edges of indenter print, and with an additional slight film spallation at 100 mN. Those fractures are common in hard brittle coatings when are tested with sharp indenters [68], [75]. Despite figure III-11 exhibits that CrAlN displayed a depth growing trend along nano-impact test suggesting the film fatigue, the fracture mechanism is not clear. In fact, it could be related with the indentation print observed in the 20 mN nano-impact test. At higher loads nano-impact tests (50 and 100 mN), Li *et al.* [75] proposed that the radial cracks appear with film delamination and buckling (figure III-13). Also, high enough indentation load could provoke film spallation such as it was proposed by Chen and Bull [76] based on the model proposed by Li *et al* [75]. Those phenomena were exhibited by CrAlN in figure III-12 for higher load. Thus, figure III-12 shows features close to the ones proposed by Chen and Bull [76]. In fact, the fracture events exhibited by CrAlN coating are close to the ones proposed by this model. On the other hand, this phenomenon is displayed when substrate hardness and elastic modulus are very different compared with coatings. Brittle substrates (as ceramics) with higher H/E ratio are only capable to resist loads up to a certain point. This point on ceramics is driven by the elastic limit and toughness. Above this value, contacts can result in fractures, dramatic delamination and uncontrolled wear [71]. Comparing results of present study with some authors [67], [71], [77], fatigue resistance loss is coherent with abovementioned concepts H/E ratio and their "compatibility" with the substrate are crucial to explain fracture resistance to impact. If one takes into account mechanical properties such as plasticity index and H/E ratio "compatibility" obtained by coatings

in the present study, it could mean a better performance on wear applications according to Zhang *et al.* [70] (high H/E ratio and low PI). In particular, CrAlN sample could show an enhanced performance on metallic substrates in many contact situations to higher loads driven by impact such as those imposed by punches. In fact, reported contact pressures during a typical coining process, vary between 0.5 to 1.4 GPa, [78] and in our study applied loads of 20 mN, 50 mN and 100 mN, correspond respectively to contact pressures of 1.5 GPa, 1.8 GPa and 2.4 GPa. Such pressures are slightly above or higher than the ones found during minting, meaning that our CrAlN coating could withstand such process without failing.

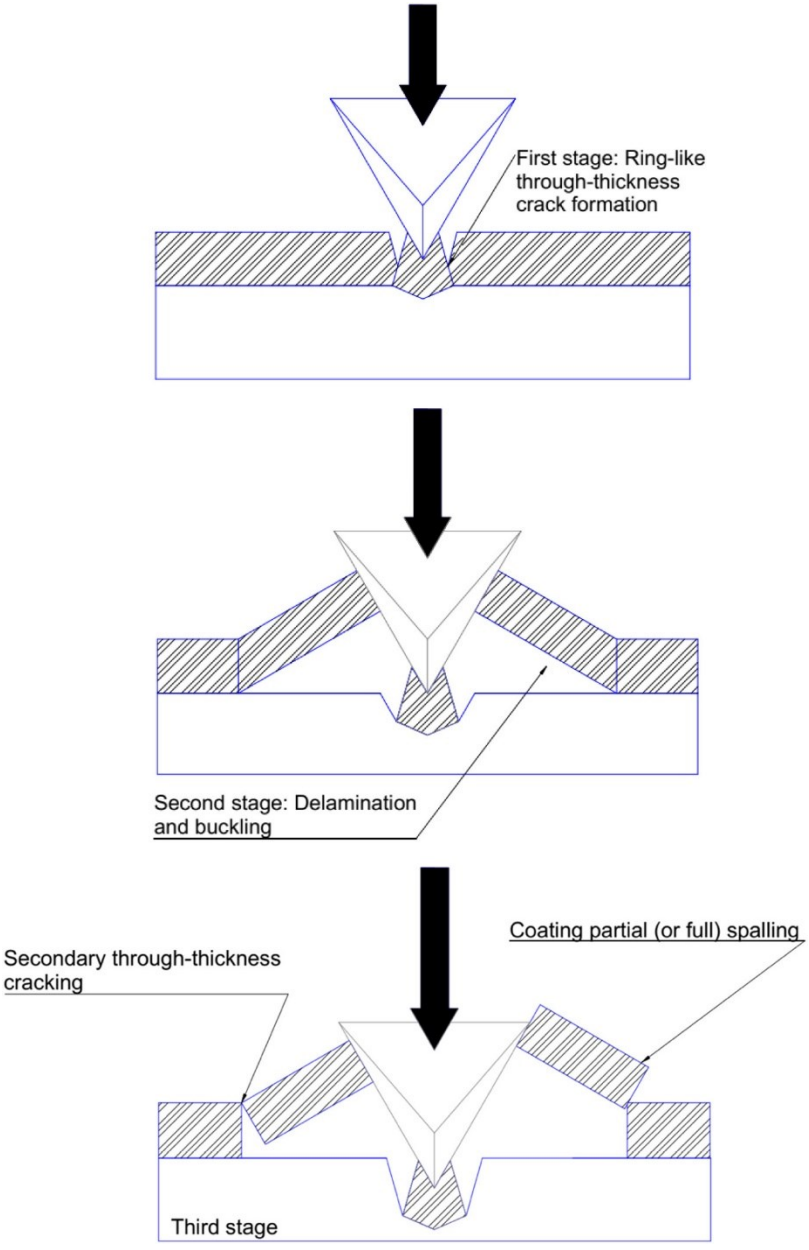

Figure III-13. Schematic fracture mechanism of radial cracking in hard coatings under indentation proposed by Li et al. [75] and modified by Chen and Bull [76].

3.3 Partial conclusions

Cr(Al,Si)N coatings were deposited by reactive magnetron sputtering. The XRD results shows a (Cr,Al)N phase solid solution for the CrAlN coating. Adding Si to the coatings results in a broadening of XRD peaks, due a decrease on the grain size promoted by the segregation of an amorphous Si_3N_4 phase.

CrAlN sample had a better overall mechanical performance when compared to other coatings, with CrAlSiN sample close by. In nano-impact tests, these coatings show a similar behavior at lower loads (10mN) but from 20 mN up, CrAlN sample had the best performance, even reaching contact pressure up to 1.5 GPa. The lower final depth achieved by CrAlN coatings can be related with higher toughness and durability in applications when fracture can be determinant. Another important factor was the mechanical compatibility among coating-substrate translated in H/E value. Resistance to wear driven by impacts on CrAlN coating demonstrates that higher hardness is not a definitive factor in wear applications when impact or fatigue are involved. Indeed, considering the usual contact pressure values involved in minting (1.4 GPa), in this study we infer that CrAlN and CrAlSiN coatings are a good option for electroplated functional hard chrome, with tremendous potential to be used in applications where high impact loads are present such as dies, some drilling operations or punching dies.

3.4 References

[1] H. H. Lou and Y. Huang, “Electroplating,” Encyclopedia of chemical processing, vol. 2. Taylor & Francis, New York, pp. 839–848, 2006.

[2] Nenad V. Mandich and Donald L. Snyder, “Electrodeposition of chromium,” in Modern Electroplating, Fifth Edit., Mordechay Schlesinger and Milan Paunovic, Ed. New Jersey: John Wiley & Sons, Inc, 2010, pp. 205–248.

[3] T. Uchimoto et al., “Newly developed surface modification punches treated with alloying techniques reduce sticking during the manufacture of ibuprofen tablets,” Int. J. Pharm., vol. 441, no. 1–2, pp. 128–134, 2013.

[4] P. R. Laity, “Effects of punches with embossed features on compaction behaviour,” Powder Technol., vol. 254, pp. 373–386, 2014.

[5] V. Mazel, V. Busignies, H. Diarra, I. Reiche, and P. Tchoreloff, “The surface layer of pharmaceutical compacts: The role of the punch surface and its impact on the mechanical properties of the compacts,” Int. J. Pharm., vol. 442, no. 1–2, pp. 42–48, 2013.

[6] K. Shimamura, Y. Matsumoto, and T. Matsunaga, “Some applications of amorphous alloy coatings by sputtering,” Surf. Coatings Technol., vol. 50, no. 2, pp. 127–133, 1992.

[7] T. S. McDermott, J. Farrenkopf, A. Hlinak, J. P. Neilly, and D. Sauer, “A material sparing method for quantitatively measuring tablet sticking,” Powder Technol., vol. 212, no. 1, pp. 240–252, 2011.

[8] K. Reed, C. Davies, and K. Kelly, “Tablet sticking: Using a ‘compression toolbox’ to assess multiple tooling coatings options,” Powder Technol., vol. 285, pp. 103–109, 2015.

[9] Z. Wang et al., “Measuring the sticking of mefenamic acid powders on stainless steel surface,” Int. J. Pharm., vol. 496, no. 2, pp. 407–413, 2015.

[10] S. Paul et al., “Mechanism and Kinetics of Punch Sticking of Pharmaceuticals,” J. Pharm. Sci., vol. 106, no. 1, pp. 151–158, 2017.

[11] Yasbandha, H., "Surface engineering of coinage dies", Doctor of Philosophy thesis, Faculty of Engineering, University of Wollongong, 2001. http://ro.uow.edu.au/theses/1838.”.

[12] S. Ithisoponakul, T. Wongsamarnmanee, and V. Premanond, “Improvement of an industrial tool life for minting the circulating coins,” Wear, vol. 320, no. 1, pp. 68–76, 2014.

[13] European Chemicals Agency, “Understanding REACH,” 2016. [Online]. Available: https://echa.europa.eu/regulations/reach/understanding-reach. [Accessed: 01-Feb-2017].

[14] EUROPEAN PARLIAMENT, REGULATION (EC) No 1907/2006 OF THE EUROPEAN PARLIAMENT AND OF THE COUNCIL. EUROPEAN PARLIAMENT, 2006.

[15] L. Zhen, L. Wang, J. Fu, Y. Li, N. Zhao, and X. Li, “Hexavalent chromium affects sperm motility by influencing protein tyrosine phosphorylation in the midpiece of boar spermatozoa,” Reprod. Toxicol., vol. 59, pp. 66–79, 2016.

[16] D. Konstantinos, C. Achilleas, and V. Evgenia, "Removal of nickel, copper, zinc and chromium from synthetic and industrial wastewater by electrocoagulation," Int. J. Environ. Sci., vol. 1, no. 5, pp. 697–710, 2011.

[17] C. Liu, N. Fiol, J. Poch, and I. Villaescusa, "A new technology for the treatment of chromium electroplating wastewater based on biosorption," J. Water Process Eng., vol. 11, pp. 143–151, 2016.

[18] L. Fedrizzi, S. Rossi, R. Cristel, and P. L. Bonora, "Corrosion and wear behaviour of HVOF cermet coatings used to replace hard chromium," Electrochim. Acta, vol. 49, no. 17–18, pp. 2803–2814, 2004.

[19] H. Oliveira, "Chromium as an environmental pollutant: Insights on induced plant toxicity," J. Bot., vol. 2012, pp. 1–8, 2012.

[20] T. Sahraoui, N. E. Fenineche, G. Montavon, and C. Coddet, "Alternative to chromium: Characteristics and wear behavior of HVOF coatings for gas turbine shafts repair (heavy-duty)," J. Mater. Process. Technol., vol. 152, no. 1, pp. 43–55, 2004.

[21] A. Liang, Y. Li, H. Liang, L. Ni, and J. Zhang, "A favorable chromium coating electrodeposited from Cr(III) electrolyte reveals anti-wear performance similar to conventional hard chromium," Mater. Lett., vol. 189, pp. 221–224, 2017.

[22] L. Vernhes, M. Azzi, and J. E. Klemberg-Sapieha, "Alternatives for hard chromium plating: Nanostructured coatings for severe-service valves," Mater. Chem. Phys., vol. 140, no. 2–3, pp. 522–528, 2013.

[23] C. Forsich et al., "Potential of thick a-C: H: Si films as substitute for chromium plating," Surf. Coatings Technol., vol. 241, pp. 86–92, 2014.

[24] S. Wang, C. Ma, and F. C. Walsh, "Alternative tribological coatings to electrodeposited hard chromium: a critical review," Trans. IMF, vol. 98, no. 4, pp. 173–185, Jul. 2020.

[25] G. W. Conran, "The evaluation and heat treatment of steels for the manufacture of coining dies and their subsequent surface coating," Surf. Coatings Technol., vol. 71, no. 2, pp. 98–101, 1995.

[26] W. Lin, M. S. Leu, C. K. Lin, and C. Y. Su, "The failure mechanism of diamond like coatings prepared by the filtered cathodic arc technique for minting application," Surf. Coatings Technol., vol. 201, no. 7 SPEC. ISS., pp. 4430–4435, 2006.

[27] H. Mori, Y. Shibata, S. Araki, T. Imanara, K. Sakamoto, and Y. Yama, "Surface improvement of coining dies with DLC films," Procedia Eng., vol. 81, no. October, pp. 1933–1938, 2014.

[28] L. Major, "Wear mechanisms of multilayer TiN/Ti/a-C:H coatings investigated by transmission electron microscopy technique," Arch. Civ. Mech. Eng., vol. 14, no. 4, pp. 615–621, 2014.

[29] L. Hongxi, J. Yehua, Z. Rong, and T. Baoyin, "Wear behaviour and rolling contact fatigue life of Ti/TiN/DLC multilayer films fabricated on bearing steel by PIIID," Vacuum, vol. 86, no. 7, pp. 848–853, 2012.

[30] G. Zhang, T. Wang, and H. Chen, "Microstructure, mechanical and tribological properties of TiN/Mo2N nano-multilayer films deposited by magnetron sputtering," Surf. Coatings Technol., vol. 261, pp. 156–160, 2015.

[31] D. E. Wolfe, B. M. Gabriel, and M. W. Reedy, "Nanolayer (Ti,Cr)N coatings for hard particle erosion resistance," Surf. Coatings Technol., vol. 205, no. 19, pp. 4569–4576, 2011.

[32] H. C. Barshilia, B. Deepthi, K. S. Rajam, K. P. Bhatti, and S. Chaudhary, "Growth and characterization of TiAlN/CrAlN superlattices prepared by reactive direct current magnetron sputtering," J. Vac. Sci. Technol. A Vacuum, Surfaces, Film., vol. 27, no. 1, p. 29, 2009.

[33] H. T. Wang, Y. X. Xu, and L. Chen, "Optimization of Cr-Al-N coating by multilayer architecture with TiSiN insertion layer," J. Alloys Compd., vol. 728, no. September, pp. 952–958, 2017.

[34] Y. Makino and K. Nogi, "Synthesis of pseudobinary Cr-Al-N films with B1 structure by rf-assisted magnetron sputtering method," Surf. Coatings Technol., vol. 98, no. 1–3, pp. 1008–1012, 1998.

[35] W. Wu et al., "Design of AlCrSiN multilayers and nanocomposite coating for HSS cutting tools," Appl. Surf. Sci., vol. 351, pp. 803–810, 2015.

[36] A. Al-Rjoub et al., "Characterization of magnetron sputtered sub-stoichiometric CrAlSiNx and CrAlSiOyNx coatings," Surf. Coatings Technol., vol. 328, pp. 134–141, 2017.

[37] T. Polcar and A. Cavaleiro, "High-temperature tribological properties of CrAlN, CrAlSiN and AlCrSiN coatings," Surf. Coatings Technol., vol. 206, no. 6, pp. 1244–1251, 2011.

[38] D. Kalincová, O. Barborák, and I. Andrejčák, "Quality of chrome layers of coining dies and its impact on their reliability and lifetime in operation," pp. 457–461, 2011.

[39] T. Hanes, P. Hvizdoš, M. Ťavodová, D. Kalincová, J. Hricová, and P. Beňo, "Coating surface roughness measurement made on coining dies," Manuf. Technol., vol. 14, no. 3, pp. 309–317, 2014.

[40] A. Prasad, M. Dao, and S. Suresh, "Steady-state frictional sliding contact on surfaces of plastically graded materials," Acta Mater., vol. 57, no. 2, pp. 511–524, 2009.

[41] A. Sola, D. Bellucci, and V. Cannillo, "Functionally graded materials for orthopedic applications – an update on design and manufacturing," Biotechnol. Adv., vol. 34, no. 5, pp. 504–531, 2016.

[42] W. C. Oliver and G. M. Pharr, "Measurement of hardness and elastic modulus by instrumented indentation: Advances in understanding and refinements to methodology," J. Mater. Res., vol. 19, no. 1, pp. 3–20, Jan. 2004.

[43] D. MA, O. C. Wo, J. Liu, and J. HE, "Determination of Young's modulus by nanoindentation," Sci. China Ser. E Technol. Sci., vol. 47, pp. 398–408, 2004.

[44] Q. Wang, F. Zhou, and J. Yan, "Evaluating mechanical properties and crack resistance of CrN, CrTiN, CrAlN and CrTiAlN coatings by nanoindentation and scratch tests," Surf. Coatings Technol., vol. 285, pp. 203–213, 2016.

[45] Y. Y. Chang, W. T. Chiu, and J. P. Hung, "Mechanical properties and high temperature oxidation of CrAlSiN/TiVN hard coatings synthesized by cathodic arc evaporation," Surf. Coatings Technol., vol. 303, pp. 18–24, 2016.

[46] Y. T. Cheng and C. M. Cheng, "Scaling, dimensional analysis, and indentation measurements," Mater. Sci. Eng. R Reports, vol. 44, no. 4–5, pp. 91–149, 2004.

[47] G. M. Pharr, "Measurement of mechanical properties by ultra-low load indentation," Mater. Sci. Eng. A, vol. 253, no. 1–2, pp. 151–159, 1998.

[48] Y. X. Wang, S. Zhang, J. W. Lee, W. S. Lew, D. Sun, and B. Li, "Toward hard yet tough CrAlSiN coatings via compositional grading," Surf. Coatings Technol., vol. 231, pp. 346–352, 2013.

[49] C. Nouveau, B. Tlili, H. Aknouche, Y. Benlatreche, and B. Patel, "Comparison of CrAlN layers obtained with one (CrAl) or two targets (Cr and Al) by magnetron sputtering," Thin Solid Films, vol. 520, no. 7, pp. 2932–2937, 2012.

[50] S. Rossnagel, "8 - Sputtering and Sputter Deposition," in Handbook of Thin Film Deposition Processes and Techniques (Second Edition), Second Edi., K. Seshan, Ed. Norwich, NY: William Andrew Publishing, 2001, pp. 319–348.

[51] P. H. Mayrhofer, H. Willmann, and A. E. Reiter, "Structure and phase evolution of Cr – Al – N coatings during annealing," Surf. Coat. Technol., vol. 202, pp. 4935–4938, 2008.

[52] D. Carter, H. Walde, G. Mcdonough, and G. Roche, "Parameter Optimization in Pulsed DC Reactive Sputter Deposition of Aluminum Oxide," in 45th Annual Technical Conference Proceedings, 2002, vol. 505, no. Society of Vacuum Coaters 505/856-7188, pp. 570–577.

[53] H. Zhang, S. W. Duo, X. M. Xu, and T. Z. Liu, "Effect of N2 Flow Rate on Structure and Mechanical Properties of CrN Coatings Prepared by Closed Field Unbalanced Magnetron Sputtering," Key Eng. Mater., vol. 591, pp. 95–98, 2013.

[54] D. F. Arias, A. Gómez, R. M. Souza, and J. M. Vélez, "Residual stress gradient of Cr and CrN thin fi lms," Mater. Chem. Phys., vol. 204, pp. 269–276, 2018.

[55] R. Daniel, K. J. Martinschitz, J. Keckes, and C. Mitterer, "The origin of stresses in magnetron-sputtered thin films with zone T structures," Acta Mater., vol. 58, no. 7, pp. 2621–2633, 2010.

[56] A. Drnovšek et al., "Correlating high temperature mechanical and tribological properties of CrAlN and CrAlSiN hard coatings," Surf. Coat. Technol., vol. 372, pp. 361–368, 2019.

[57] C. B. Liu, W. Pei, F. Huang, and L. Chen, "Improved mechanical and thermal properties of CrAlN coatings by Si solid solution," Vacuum, vol. 125, pp. 180–184, 2016.

[58] H. N. Shah and R. Jayaganthan, "Influence of Al contents on the microstructure, mechanical, and wear properties of magnetron sputtered CrAlN coatings," J. Mater. Eng. Perform., vol. 21, no. 9, pp. 2002–2009, 2012.

[59] Y. X. Wang, S. Zhang, J. W. Lee, W. S. Lew, and B. Li, "Influence of bias voltage on the hardness and toughness of CrAlN coatings via magnetron sputtering," Surf. Coatings Technol., vol. 206, no. 24, pp. 5103–5107, 2012.

[60] F. Rivadulla et al., "Reduction of the bulk modulus at high pressure in CrN," Nat. Mater., vol. 8, no. December, pp. 947–951, 2009.

[61] S. Carvalho, L. Rebouta, A. Cavaleiro, L. A. Rocha, J. Gomes, and E. Alves, "Microstructure and mechanical properties of nanocomposite (Ti, Si, Al)N coatings," Thin Solid Films, vol. 398–399, pp. 391–396, 2001.

[62] C. Palacio, A. Arranz, and D. Díaz, "Chemical bonding of nitrogen in low-energy implanted chromium," Thin Solid Films, vol. 513, no. 1–2, pp. 175–181, 2006.

[63] S. Veprek, M. G. J. Veprek-Heijman, P. Karvankova, and J. Prochazka, "Different approaches to superhard coatings and nanocomposites," Thin Solid Films, vol. 476, no. 1, pp. 1–29, 2005.

[64] D. Chaliampalias et al., "Compositionally gradient PVD CrAlSiN films: structural examination and oxidation resistance," Surf. Eng., vol. 33, no. 8, pp. 612–618, 2017.

[65] C. Palacio and A. Arranz, "Chromium silicide formation by argon irradiation of Cr/Si bilayers," J. Phys. D. Appl. Phys., vol. 41, no. 3, 2008.

[66] S. Vepřek, "New development in superhard coatings: The superhard nanocrystalline-amorphous composites," Thin Solid Films, vol. 317, no. 1–2, pp. 449–454, 1998.

[67] A. Leyland and A. Matthews, "On the significance of the H/E ratio in wear control: A nanocomposite coating approach to optimised tribological behaviour," Wear, vol. 246, no. 1–2, pp. 1–11, 2000.

[68] S. Zhang, Ed., Thin Films and Coatings: Toughening and Toughness Characterization. Boca Raton: CRC Press, 2016.

[69] C. Rebholz, H. Ziegele, A. Leyland, and A. Matthews, "Structure, mechanical and tribological properties of nitrogen-containing chromium coatings prepared by reactive magnetron sputtering," Surf. Coatings Technol., vol. 115, no. 2–3, pp. 222–229, 1999.

[70] S. Zhang, Nanostructured Thin Films and Coatings: Mechanical Properties. Boca Raton: CRC Press, 2010.

[71] B. D. Beake, S. R. Goodes, J. F. Smith, N. J. Pickford, and G. A. Bell, "Improved nanomechanical test techniques for surface engineered materials," Surf. Eng., vol. 26, no. 1–2, pp. 37–49, 2009.

[72] B. D. Beake, G. A. Bell, S. R. Goodes, N. J. Pickford, and J. F. Smith, "Evaluating the fracture properties and fatigue wear of tetrahedral amorphous carbon films on silicon by nano-impact testing," Surf. Coatings Technol., vol. 26, no. 1–2, pp. 37–49, 2004.

[73] B. D. Beake and J. F. Smith, "Nano-impact testing - An effective tool for assessing the resistance of advanced wear-resistant coatings to fatigue failure and delamination," Surf. Coatings Technol., vol. 188–189, no. 1-3 SPEC.ISS., pp. 594–598, 2004.

[74] N. H. Faisal, R. Ahmed, and R. Fu, "Nano-Impact (Fatigue) Characterization of As-Deposited Amorphous Nitinol Thin Film," Coatings, vol. 2, no. 3, pp. 195–209, Aug. 2012.

[75] X. Li, D. Diao, and B. Bhushan, "Fracture mechanisms of thin amorphous carbon films in nanoindentation," Acta Mater., vol. 45, no. 11, pp. 4453–4461, 1997.

[76] J. Chen and S. J. Bull, "Approaches to investigate delamination and interfacial toughness in coated systems: An overview," J. Phys. D. Appl. Phys., vol. 44, no. 3, 2011.

[77] A. Cavaleiro and J. T. M. De Hosson, Eds., Nanostructured Coatings. New York, NY: Springer New York, 2006.

[78] P. Alexandrino, P. J. Leitão, L. M. Alves, and P. A. F. Martins, "Numerical and experimental analysis of coin minting," vol. 233, no. 5, pp. 842–849, 2019.

CHAPTER IV - Cr-Based Sputtered Decorative Coatings for Automotive Industry

The following chapter is partially based on the results published in:

Carneiro, E.; Parreira, N.M.G.; Vuchkov, T.; Cavaleiro, A.; Ferreira, J.; Andritschky, M.; Carvalho, S; "Cr-Based Sputtered Decorative Coatings for Automotive Industry", Materials, 2021, 14, 5527. https://doi.org/10.3390/ma14195527

4 Introduction

This chapter focused on investigating the use of reactive magnetron sputtering to deposit hexavalent chromium free coatings onto PC substrates for use in decorative parts in the automobile industry. To meet customer demand for different shades of metallic gray, the coatings were deposited from a chromium target using nitrogen (N_2) and oxygen (O_2) as reactive gases. Different types of coatings are produced, including pure chromium, monolithic and graded chromium nitride (CrN), and chromium oxynitrides. The main goal is to achieve the same properties (decorative and mechanical) of electroplated metal-coated plastic parts which are increasingly popular in the automobile and decorative industries. On one hand the polymer substrate offers a combination of low density, flexibility, design versatility, and low production cost, while the coating allows to maintain the shiny finish, high reflectivity, and conductivity of metals [1–20]. Achieving thick coatings, free of pin-hole defects and with good adhesion in a wide range of colors on polymeric substrates remains a challenge. Sputtering deposition of coatings on polymers faces challenges due to polymer limitations, including temperature restrictions to prevent plastic deformation, polymer degassing, and adhesion issues. This research addressed these limitations, aiming to create high-performance coatings with diverse color options for various applications. We studied the impact of using an interlayer and graded composition to improve adhesion and the use of multilayers to achieve better mechanical properties (such as resistance to abrasion) while having a wider range of decorative appearances.

4.1 Materials and methods

The coatings were deposited by DC reactive magnetron sputtering using a home-made vacuum chamber onto monocrystalline silicon wafers (100 P-type) supplied by SIEGERT WAFER GmbH (Germany), and Polycarbonate, PC, (LEXAN ™) samples supplied by SABIC (Saudi Arabia). The PC substrates were coated with an UV cured basecoat prior to the metallization to improve both adhesion and decorative appearance of the coating.

The samples were cleaned with isopropanol and then loaded into the deposition chamber. During the sputtering process, a single Cr target (99.5% purity) was used, Ar gas as sputtering agent and reactive gases N_2, O_2 or a gas mix N_2+O_2 (85% N_2 and 15% O_2) were added at different flow rates as indicated in the Table 1. During the depositions, no external heating was used to keep the deposition temperature as low as possible and a 3.5 rpm rotation was applied to the substrates. The base pressure in the chamber was approximately 1×10^{-3} Pa and the working pressure was kept approximately at 1 Pa. This is a relatively

high pressure for reactive magnetron sputtering and was selected to reduce the energy of the species which bombard the substrates and therefore reducing the temperature increase during deposition. Before every deposition, an etching process was performed, using a pulsed power source with 200 kHz, a pulse width of 1536 ns and 400 mA current during 15 min. A chromium interlayer was deposited prior coating during 50 s to enhance the adhesion. The deposition time of each sample is also presented on Table IV-1. In essence, the total deposition time was 360 s, except for the multilayer coatings that was 480 s. The multilayer coatings were deposited with similar conditions as indicated with each layer being deposited during 60s. The last layer of CrN/CrO is CrxOy and for CrN/CrON is CrxOyNz. No bias voltage was applied during deposition to protect the substrates.

The thickness and morphology of the coatings was analysed using a NanoSEM FEI Nova 200, equipped with a Pegasus X4M for the EDS Chemical composition analysis. The structure of the coatings was analysed by X-ray diffraction in a X'Pert Pro MPD diffractometer operating with Cu K α radiation (λ = 1.5406 Å at a grazing incidence angle of $\alpha = 3^{\circ}$ and in a 2 θ interval of 30-80). Peak deconvolution was performed in Origin(Pro)9 (OriginLab Corporation, USA) using a Pseudo-Voigt function.

The hardness (H) and reduced Young`s modulus (Er) were measured by nanoindentation (Micro Materials Nano Test platform), with a Berkovich diamond pyramid indenter, applying a load of 3 mN to assure that indentation depth was less than 10% of the coating thickness. A total of 16 indentations were performed and the average was calculated.

The adhesion of the coatings on PC substrates was tested using the cross-cut test following the ISO 2409 standard. Two sets of 11 cuts with spacing of 1 mm were made perpendicular to each other, thus making a grid of 100 small blocks. Then a standardized tape (Tesa® 4657) was applied on the crosscut and pulled off with a constant force. The number of blocks removed is an indication of the adhesion following the standard classification between 0 to 5, being 0 a perfect adhesion coating where the edges of the cuts are completely smooth and none of the squares of the lattice is detached and a classification of 5 corresponding to a coating that flaked along the edges of the cuts in large ribbons and/or squares that detached partly or wholly in a proportion higher than 65% of the tested area.

Dry sliding reciprocating tests were performed using the RTEC MFT-5000 platform. Al_2O_3 balls with diameter of 10 mm were used as counterparts. The normal load was set to 1 N, resulting in an initial contact stress of 37 MPa. The stroke was set to 2.2 mm. The reciprocating frequency was 5 Hz. The test duration was limited to 1 min, resulting in a total sliding distance of 1.21 m. For assessing the wear rate,

Alicona 3D optical profilometer was used. The specific wear rates (K_i) were obtained by Equation 1 where ΔV_i is wear volume, F_N is the normal load and L the sliding distance, [21][22]:

$$K_i = \frac{\Delta V_i}{F_N \times L} \quad (1)$$

The color and reflectance of the coatings were measured using a Minolta CM-2600d portable spectrophotometer equipped with a 52 mm diameter integrating sphere and 3 pulsed xenon lamps and a wavelength range of 400–700 nm. The color coordinates were measured in the CIELab-1976 color space at a viewing angle of 10° and using the primary illuminant D65 (specular component included – SCI).

Table IV-1. Deposition conditions of the coatings (gas flow and deposition times), deposition rate and chemical composition of the deposited coatings. Samples were named taking in consideration chemical elements present in the coating.

Coating	Gas Flow (sccm)				Deposition time (s)		Thickness	Deposition rate	Chemical composition (at. %)		
	Ar	N_2	O_2	N_2+O_2	Interlayer	Coating	(nm)	(nm/s)	Cr	O	N
Cr	100					360	603	1.7	92	8	-
gCrN	70	5→25				360	629	1.8	66	6	28
CrN	70	25			50	310	638	1.8	60	8	32
CrO	100		15		50	310	862	2.4	69	31	-
CrON	70			40	50	310	497	1.4	46	21	33
CrN/CrO	70	25	15		50	480	1020	1.9	63	25	12
CrN/CrON	70	25		40	50	480	858	1.6	49	18	33

4.2 Results and discussion

4.2.1 Functional Characterization: Colour and Adhesion

As previously defined these coatings are to be used as decorative in automobile industry in which color and adhesion are important and critical factors.

The color coordinates and reflectance of the films were measured to check if and which of the deposited coatings complied with end-user specifications. It is important to mention that the color is not only dependent of material composition, but also related to surface roughness.

The color coordinates of the deposited coatings in CIE L*a*b* system is shown in Figure IV-1. Note that L* is the brightness where 0 = Black and 100 = White; a* represent the Red and Green on positive and negative axis, respectively and b* represent the Yellow and Blue on positive and negative axis, respectively [23].

Typically, with the increase of non-metallic elements, N or O, the brightness (L* coordinate) of the samples suffer a decrease [24]. Within our samples, having up to 40 at. % of non-metallic elements, coatings Cr, gCrN, CrN and CrO, (see Table IV-1 for composition reference) showed similar brightness: close to 70. The color appearance is determined by the a* and b* coordinates, in special the b* coordinate that increase from 0.5 on Cr to 8 on CrO coating giving it a yellow tonality.

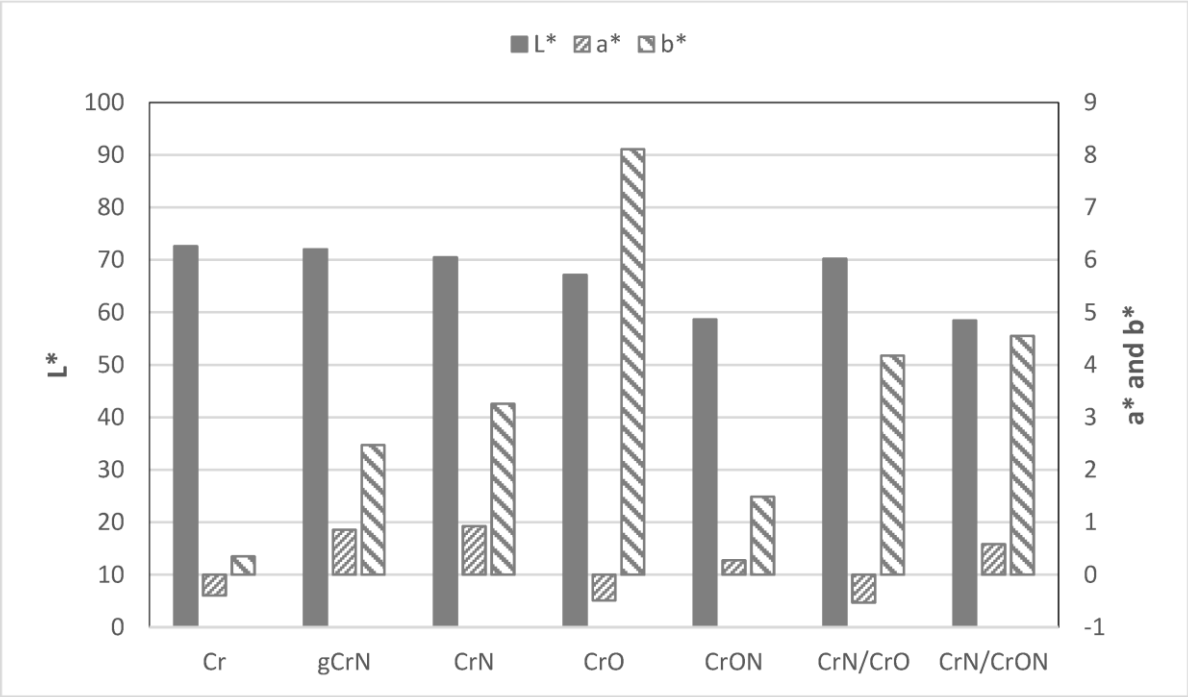

Figure IV-1. CIELAB color coordinates of the sputtered coatings onto PC substrates.

The coating CrON is the one that shown a darker appearance, displaying a tonality of dark grey. Note that this coating has the higher non-metallic element composition (> 50 at.%).

The multilayer coatings, CrN/CrO and CrN/CrON, do not exhibit major differences in color in comparison with the monolithic coatings. These coatings present a tonality and color coordinates, in special L*, ruled by coating's top layer that is CrO for CrN/CrO coating and CrON for CrN/CrON coating.

The reflectance behavior, Figure IV-2, is consistent with the results presented by the brightness, in fact Cr, gCrN, CrN, CrO and CrN/CrO shown similar reflectance with a value between 35 and 50% on the range of 400 to 700 nm and CrON and CrN/CrON present similar reflectance and lower than previous group with a reflectance value between 20 to 30% on the define range.

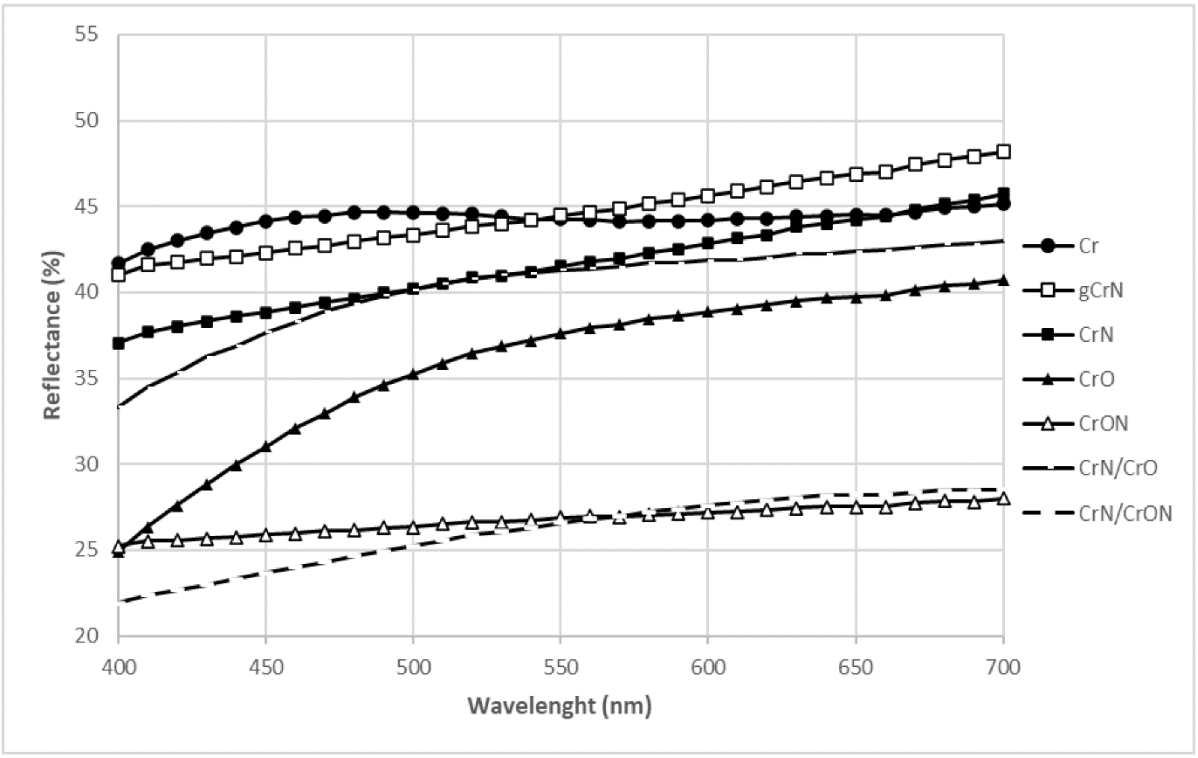

Figure IV-2. Reflectance evolution of the sputtered coatings deposited onto PC substrates.

Other important end-user specification in the development of coatings onto polymers is to have good adhesion to the substrate. Therefore, the adhesion of the coatings was tested using the cross-cut tape test and the results are presented in Figure IV-3.

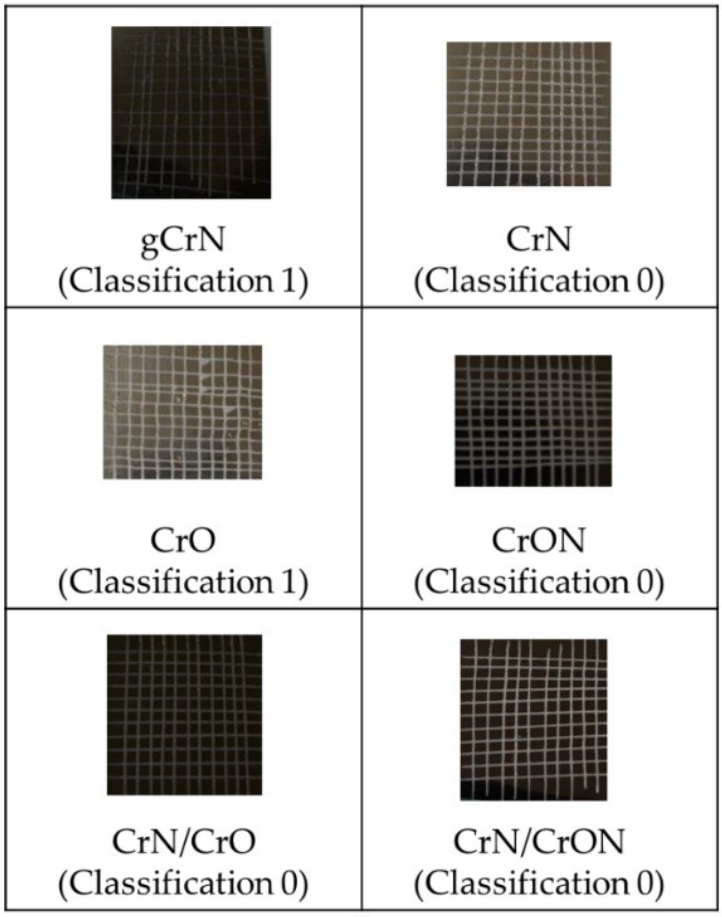

Figure IV-3. Adhesion behaviour assessment of coatings deposited onto PC substrates.

According to the scale defined by the standard, the adhesion of the deposited coatings was rated between 0 (perfect adhesion, since the edges of the cut are completely smooth and none of the squares of the grid were detached after removal of the tape) and 1. A special mention should be given to the gradient coating gCrN that shown a detachment of small flakes of the coatings at the intersection of the cuts on an area smaller than 5%. Based on these results, further investigation into gradient CrN coatings appears to hold limited potential. CrO coating, also present a poor adhesion when compared to the other coatings. The chosen color also plays a role. If the end-user prefers a specific composition/color combination, adhesion optimization might be necessary. Our results in Figure IV-3 suggest that a multilayer configuration could be a promising approach for achieving this.

4.3 Deposition conditions and basic characterization

4.3.1 Chemical composition

The chemical composition for coatings deposited on Si wafer substrates, shown in Table IV-1, was measured by WDS.

We observed a high amount of oxygen in of our all samples, even in the pure Cr coating. This can be explained by the fact that the deposition of the coatings occurs at a relative high pressure, around 1 Pa, and at these working pressures residual oxygen from the chamber can be incorporated in the films. It is also likely that the oxygen presence came from the degasification of the plastic substrates or from the epoxy layer that act as pre-coating.

It is worthy to mention that in the chemical composition results presented for graded and multilayered growth the stated composition is the combination of several different layers composition, in depth, and not individual layers.

The individual results reveal that:

1) gCrN and CrN coatings: for graded CrN coatings, gCrN, deposited with increasing nitrogen flux presents lower N content in comparison with CrN coating. The 33 at.% of N introduced in the CrN coating on a N_2/Ar flow-rate ratio of 0.35 is in line with previous works by Mayhofer *et al.* [25].

2) CrO coating: by adding O_2 as reactive gas inside the deposition chamber it is possible to incorporate a significate oxygen amount (30 at. % of O), even with a much lower gas flow than for N_2-presence coatings, which is explained by the higher reactivity of oxygen to Cr [26];

3) CrON coating: when the gas mixture of 85% N_2 + 15% O_2 was added to the atmosphere, CrON coating, the number of reactive species inside the deposition chamber became higher and this leads to the highest non-metallic elements amount added in the coatings on the present study (~21 at.% of O and ~33 at.% of N). Note that proportionally the amount of O in the coating is higher than the amount of O_2 on the gas mixture (85% N_2 and 15% O_2) which is explained by the higher affinity of O to Cr than N to Cr, as is indicated by the standard molar enthalpy of formation of Cr_2O_3 and CrN: $\Delta_f H^o(Cr_2O_3)$ = - 1139.7 kJ/mol and $\Delta_f H^o$(CrN) = -117.2 kJ/mol [26] also observed in previous studies on oxynitrides coatings [27];

4) CrN/CrO and CrN/CrON coatings: in the case of multilayered coatings CrN/CrO and CrN/CrON, the chemical composition measure shown a value similar to the average of the chemical composition of

individual layers (CrN and CrO or CrON), which indicate that the analytical method had influences from several layers in depth.

The thickness of the coatings was measured by cross-section analysis from SEM micrographs on silicon and after deposition rate was calculated. Those results are shown in Table IV-1 and Figure IV-4 as a function of the deposition conditions.

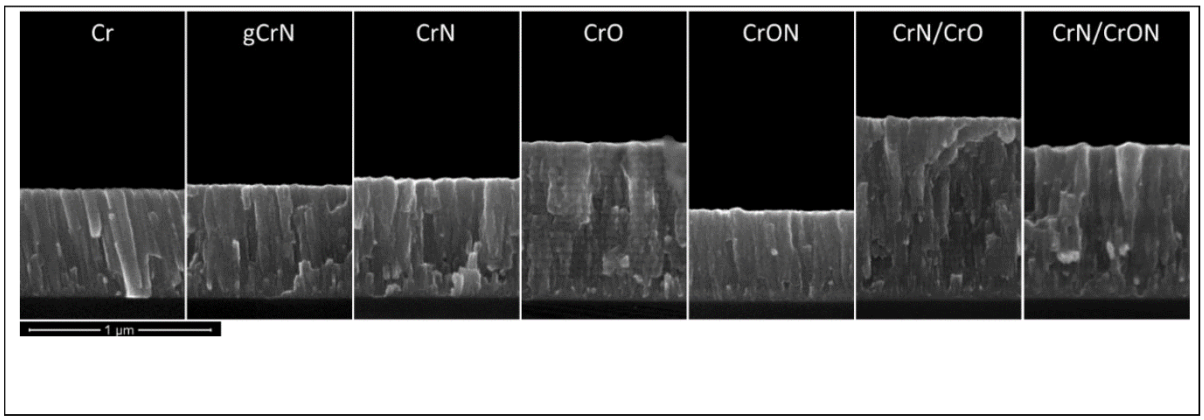

Figure IV-4. Scanning electron cross-section micrographs of the coatings deposited on silicon.

The coating thickness ranged between 500 nm up to 1020 nm and the deposition rate varies between 1.4 up to 2.4 nm/s depending on deposition conditions. Under the defined conditions the deposition rate of pure Cr coatings was close to 1.7 nm/s and for gCrN and CrN coatings showed a value of 1.8 nm/s. This clear shows that the deposition is done in metallic mode, even up to a 33 at. % addition of N. Combining the deposition rate value and the chemical composition, is clearly shown that the deposition is still far from the full poisoning of the target and so the stoichiometric composition of CrN was not reached [28]. For samples deposited with oxygen as reactive gas (CrO coating), the thickness increases, and the deposition rate reaches 2.4 nm/s. This is a typical behavior of the Cr-O coatings when the deposition conditions remain on metallic mode and it is a consequence of the incorporation of O atoms in the Cr lattice that leads to a structural change with the formation of new phases having different atomic arrangement, which give rise to a lower specific molecular weight and consequently to an increase in the coating volume and final coating thickness. This behaviour has been confirmed by Rothhaar *et al.* [29] and observed as well on Mo-O [30] and W-O systems [31].

Multilayer coating CrN/CrO and CrN/CrON showed a deposition ratio very close to the average of the deposition ratio of CrN and CrO or CrON, respectively. In fact, as it will be presented on the morphology discussion, these multilayer coatings showed two clear visible layers, see Figure IV-4: the CrN and CrO or CrON, respectively.

4.3.2 Morphology

The scanning electron cross-section morphology of the deposited coatings is shown in Figure IV-4.

Cr coatings shown a well-defined columnar structure, the same is observed for the gCrN and CrN coatings. In fact, this is a typical behavior for coatings deposited up to 1 Pa (high pressure) and without external heating (low deposition temperature) [32][33]. For CrON coating, still a columnar structure is observed, but less pronounced.

The obtained CrO coating observed in SEM micrograph shown an interesting phenomenon that is a multilayer growth (Figure IV-5). This multilayer morphology can be explained by the deposition conditions, namely the depositions were carried out using only one Cr target in a non-poisoned mode (transition zone) and the substrate holder was rotating at 3.5 rpm. Therefore, the formation of a differentiated plasma surrounding the substrate holder can be expected. When the samples are facing the Cr target, a fresh metallic Cr layer is deposited, and the amount of oxygen is reduced due to the high flux of Cr atoms coming from the target. On the remaining time, when the samples are turning around, the oxidative plasma environment ($Ar + O_2$) promotes the oxidation and the adsorption of the oxygen by the films, which results in an increase of oxygen in the surface of the Cr layer. This phenomenon is clear in Figure IV-5 where charged (brighter) and uncharged (darker) layers are visible, which correspond to O-rich and O-

deficient layers, respectively. This behavior was also found in other similar systems on previous studies on oxided systems deposited on the same chamber [34].

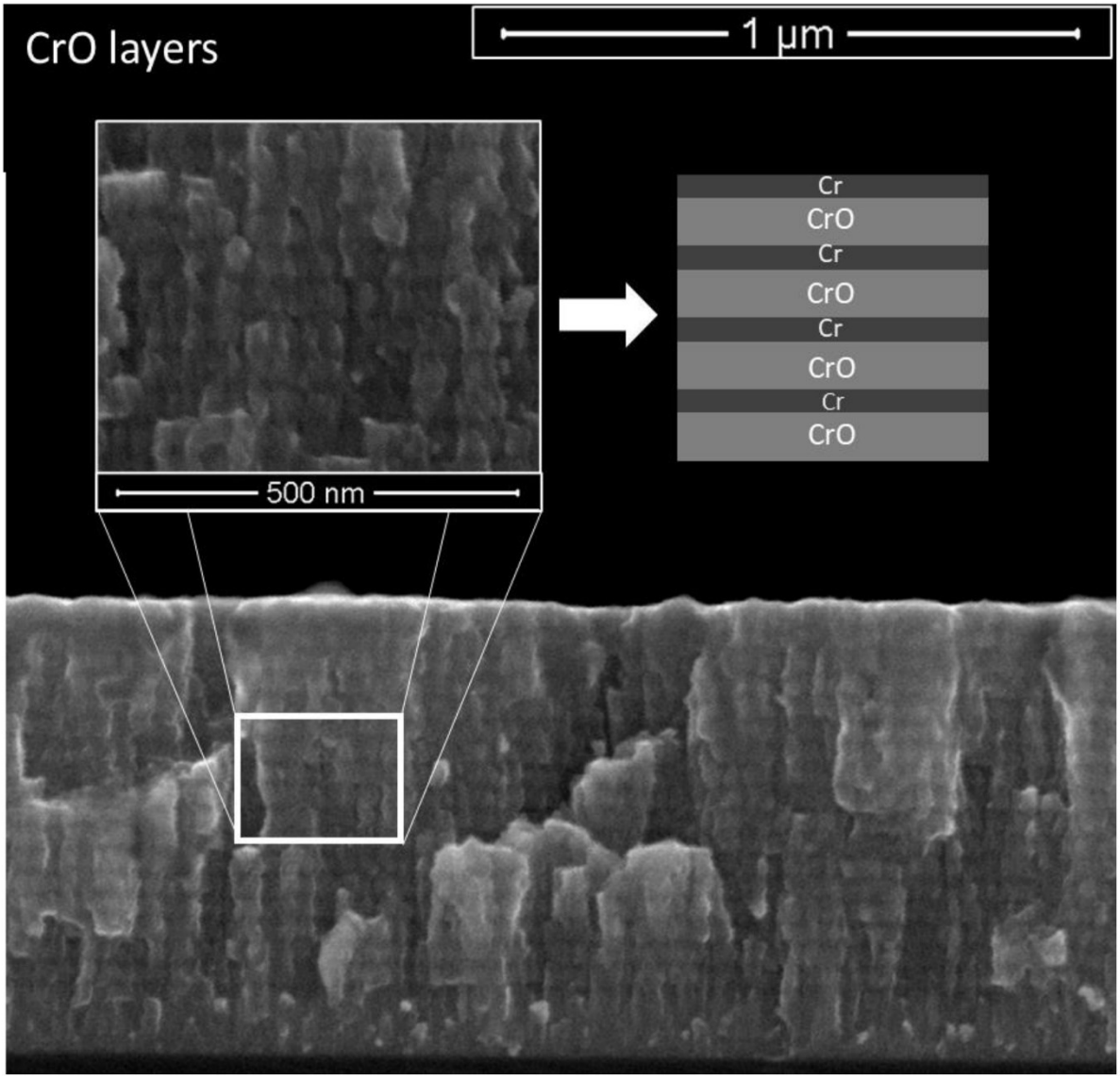

Figure IV-5. Cross-section SEM micrograph of the CrO coatings. We observed a multilayer-like structure with charged and uncharged layers, corresponding to layers deficient and rich in O, respectively.

The cross-section SEM images of the multilayer coatings in secondary electron (SE) and backscattered electron (BSED) modes are shown in Figure IV-6. CrN/CrO coating, Figure IV-6a, shows in SE mode, bands like CrO interrupted by a darker "solid" band. This is even more evident in BSE mode, where brighter and darker areas are more contrasting. In BSED mode, lighter areas correspond to heavier elements or metallic ones [35], meaning that from bottom-up one can see a Cr interlayer, CrN layer and an layer Cr-O that in fact are four bilayers of Cr/CrO due to the phenomenon described earlier for CrO coatings. This is repeated four times, which corresponds to the deposition during 60 seconds of each layer in a total time of 480 s as per Table IV-1.

Regarding CrN/CrON coatings, a similar but not so evident behavior is observed. On the left of Figure IV-6b) using BSED mode (right) a Cr interlayer is present on the bottom and after those 4 bilayers of CrN/CrON are observed, as expected.

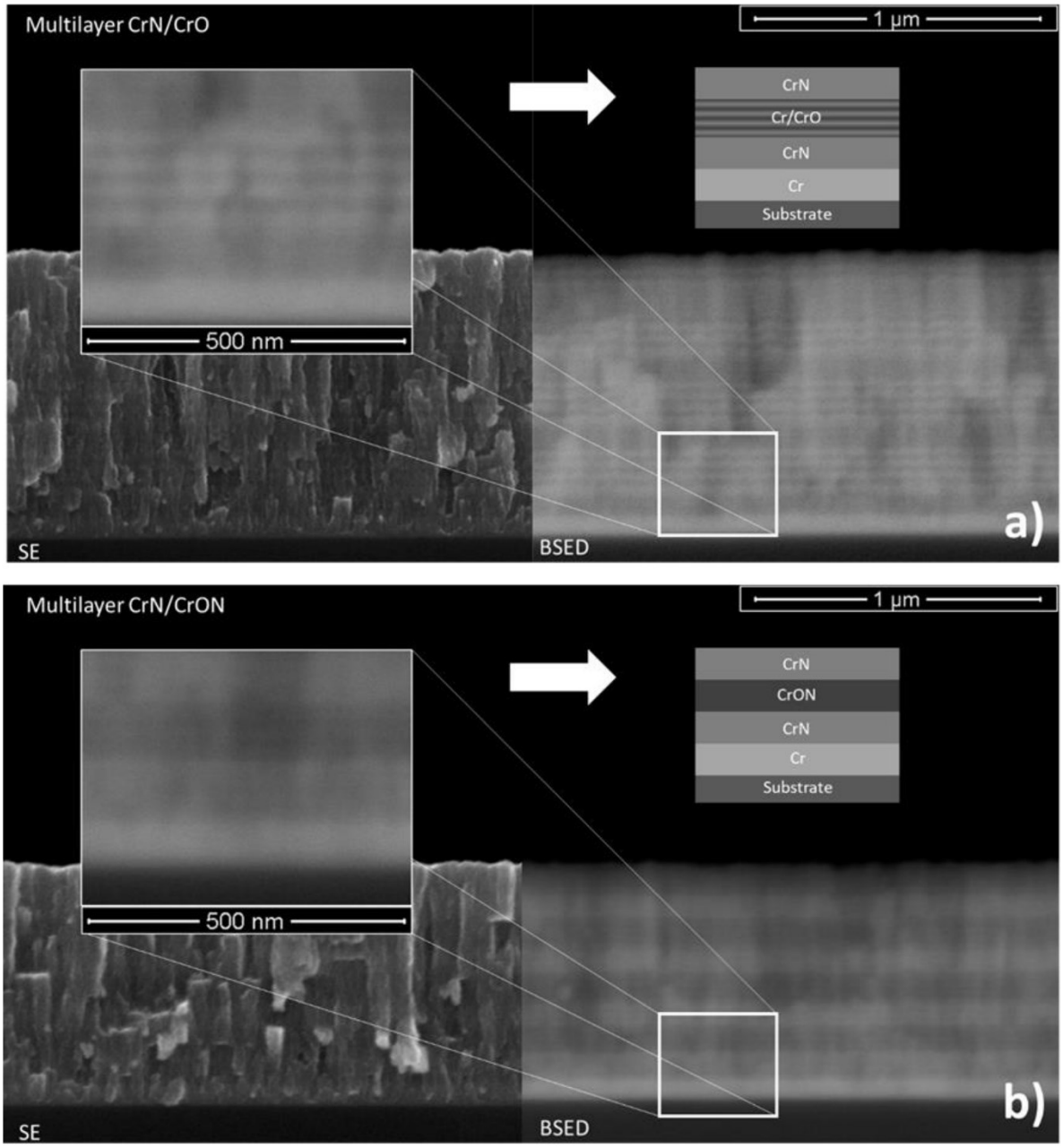

Figure IV-6. Cross-section SEM micrography in secondary electron (left) and backscattered electron modes (right) for (a) CrN/CrO and (b) CrN/CrON multilayer coatings.

4.3.3 Structural characterization

The crystallographic structure was evaluated by X- Ray Diffraction (XRD) and results are shown in Figure IV-7a for all deposited coatings.

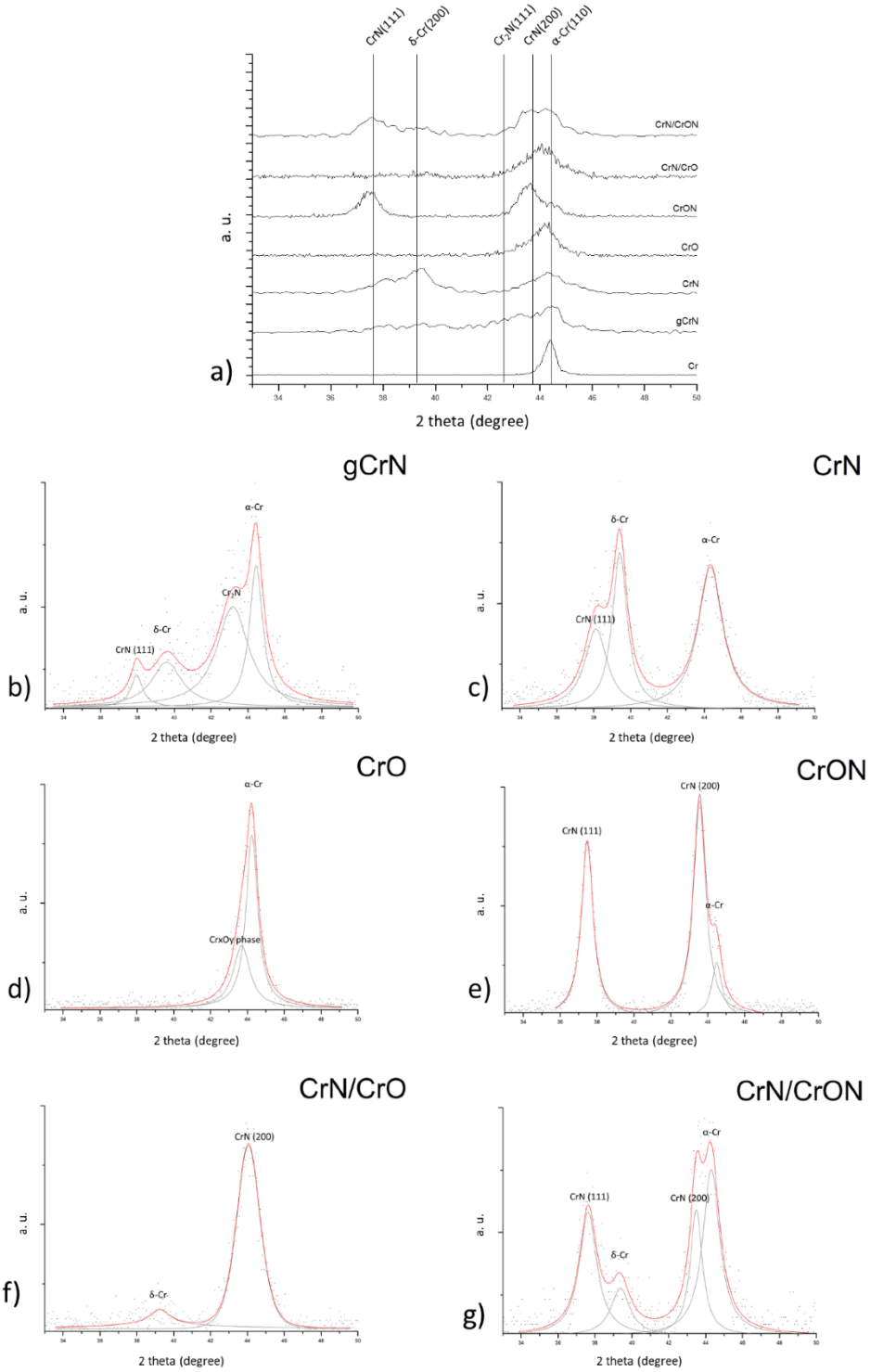

Figure IV-7. XRD patterns of the deposited coatings, (a) plot of all XRD specta for comparison purposes. Individual detailed analysis of the XRD spectra of the different coatings: (b) gCrN; (c) CrN; (d) CrO; (e) CrON; (f) CrN/CrO and (g) CrN/CrON.

Starting from the monolayer metallic chromium coating, Cr, it was observed an intense reflection close to $2\theta = 44.4°$ corresponding to the (110) plane for the b.c.c α-Cr according ICCD card nr. 01-085-1335.

For CrN coating, deposited with a constant nitrogen partial pressure, we observed the (111) peak from CrN phase according to ICCD card nr. 01-076-2494. Close to $2\theta \approx 39.4°$ is visible a strong peak which does not correspond to any known phase of the binary Cr-N system but can correspond to the reflection of the (200) plane of the metastable Cr phase, δ-Cr, according to ICDD card nr. 00-019-0323. This phase is a A15 crystallographic structure, and it may occur in thin films, and it is stabilized by impurities like oxygen or nitrogen [36]–[39]. The presence of the δ-Cr is also presented in previous multilayer Cr/Cr-N studies [40][41]. To complete the phase composition of the CrN diffractogram, is not possible to exclude the presence of b.c.c α-Cr phase close to $2\theta \approx 44.3°$, since these coatings presented a sub-stoichiometric composition (see Table IV-1) and oxygen is present as an impurity, hence a wider peak. The complete analysis of the XRD pattern of CrN (Figure IV-5b) shows that the coating is composed by a mixture of α-Cr, δ-Cr and CrN phases.

gCrN coating, was produced with a gradual increasing of nitrogen flow during the deposition, generating a coating with richer Cr content from the bottom of the coating, starting from pure Cr to a CrN composition on top. By XRD results it is possible to identify a broad peak in the range between 42° up to 44.5 °, which can be assigned to a mixture of different phases, ranging from Cr to CrN in agreement with the graded composition. It is observed the b.c.c α-Cr and reflection close to $2\theta \approx 43.2°$ that correspond to the (-1 -1 1) plane from the hexagonal Cr_2N phase according ICDD card nr° 01-079-2159. We observed as well the CrN crystallographic phases. By applying deconvolution of the gCrN XRD pattern (Figure IV-5b) is possible to observe also broad peaks with low intensity corresponding to CrN close to $2\theta \approx 37.6°$ and a the δ-Cr peak at to $2\theta \approx 39.4°$. So, the crystallographic phases present on the gCrN coating are primarily α-Cr (from the initial phase of coating deposition) and hexagonal Cr_2N in the bulk of the coating and traces similar to the CrN coating phases which are present on the top of the coating with lower XRD intensity.

CrO coating XRD pattern shown one major diffraction peak between $2\theta \approx 42°$ and 47°. By peak deconvolution, see Figure IV-5d, the observed peak is composed by a main peak attributed to α-Cr and a broad superposed peak that can be attributed to chromium oxide phases. From ICDD database on Cr-O system, this peak a $2\theta \approx 43.6°$ can be attributed to Cr_3O phase (ICDD card nr. 01-072-0528) or $CrO_{0.87}$

phase (ICDD card nr. 01-078-0722) both cubic structures. Note that the described δ-Cr, A15 structure is an isomorphic structure with Cr_3O and with (210) preferential orientation. As mentioned in the morphological analysis section, this CrO coating exhibits a multilayer structure with Cr rich zones and O containing zones, so is possible to have these structures together in a nano-arrangement. We also notice a small peak shift to the left (higher diffraction angles) indicating compressive stresses in the coating and when compared to pure Cr coatings, the crystallite size went from 16.8 nm to 7.9 nm on CrO coating, calculated by Scherrer's equation [42].

The XRD pattern of the coating deposited with the mixture of O_2+N_2 gas flow, coating CrON, see Figure IV-5e, exhibit both (111) and (200) reflections of the CrN cubic structure. Close to $2\theta \approx 44.5°$, there is a superimposed peak that can be attributed to α-Cr or δ-Cr with preferential orientation (210) or to a rich oxygen phase like Cr_3O or $CrO_{0.87}$. Even with this combination of phases, there is excess of oxygen in the coating composition. It is possible to have some oxygen in solid solution, but the solubility of oxygen in CrN is very limited [43] and most probably the stoichiometric combination is achieved by having in the coating structure the presence of amorphous Cr_2O_3 which is the most stable phase of the Cr-O system, and even if it is not visible by XRD, anyhow contributes to the mechanical properties of the coatings (to discuss in next section). From the literature, limited works are known on CrON system by reactive magnetron sputtering. In the work by Collard *et al.* [43], that was focused on adding N starting from a Cr_2O_3 structure or adding O to a CrN structure allowing the study of solubility of N and O on oxides and nitrides, respectively, by replacement of the other non-metallic atoms or in interstitial position. In Collard study there are no information concerning the chemical composition, only the flow rates are presented and it is shown that above a ratio of 5 sccm oxygen to 15 sccm nitrogen the coating only shows XRD reflections from oxide, mainly Cr_2O_3-eskolaite. The gas mixture used on the present study, 85% N_2 and 15% O_2 by volume, has a lower ratio of oxygen that in the Collard study, so a simple model of the phase mixture of this coating can be a combination of CrN(O) nanocrystalline phases on a matrix of amorphous Cr_2O_3 and α-Cr or (210) δ-Cr or Cr_3O.

Concerning the multilayer coatings, CrN/CrO and CrN/CrON, the X-ray penetrates and gives information from several layers of the coatings. What is observed from the XRD pattern of these coatings (Figure IV-5f,g, respectively) is a mixture of the individual single phase, CrN, CrO or CrON. Looking in detail for CrN/CrON coating, the XRD pattern shows a mixture of α-Cr (110) plan, δ-Cr, in special (200) reflection and CrN (111) and (200) plane all these phases present in the CrN layer and superimposed by the CrN

reflections are also present in the CrON layer. This multilayer arrangement will have an impact on the mechanical properties of the coatings.

4.4 Mechanical and tribological characterization

4.4.1 Mechanical characterization

Having good mechanical properties is crucial for the potential automotive application of the coatings, as metallized polymer parts encounter various mechanical stresses resulting in scratches, due to small stones, and impacts from other objects. In Figure IV-8, Hardness, H, and Young's Modulus, Er, as measured by nanoindentation are presented.

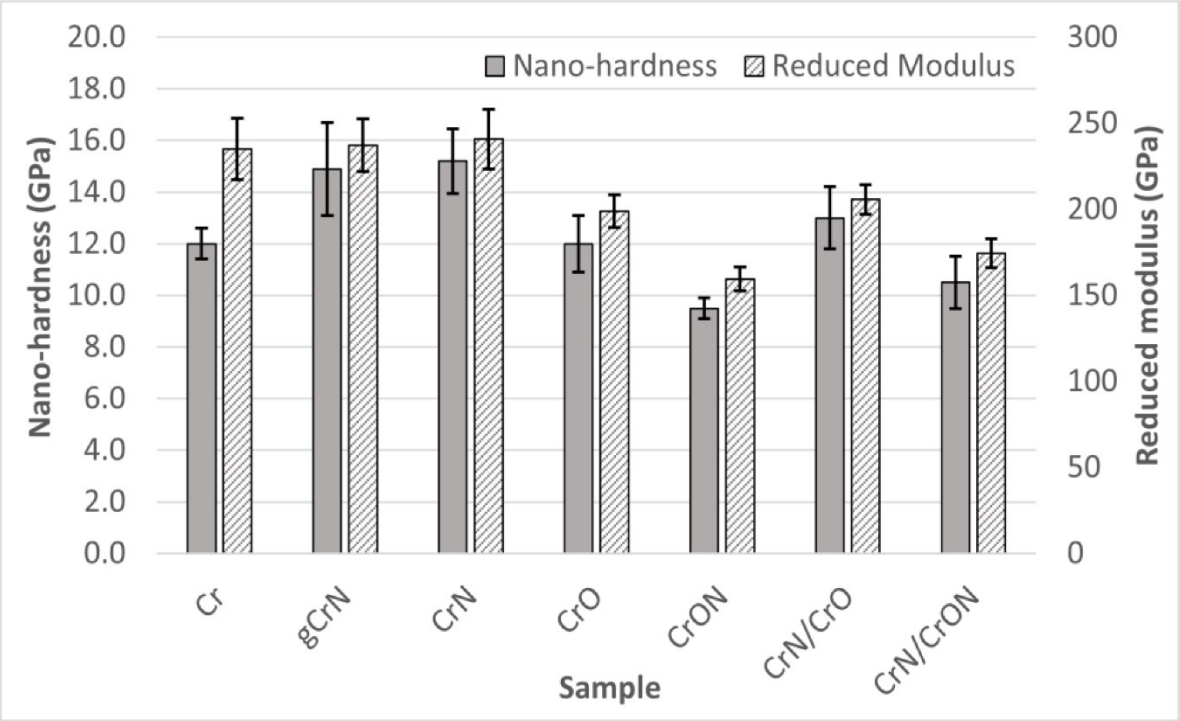

Figure IV-8. Nano-hardness and Young's modulus of the coatings deposited onto Si.

Cr coating has a hardness value of 12 GPa and a Young's Modulus of 235 GPa, being values relatively similar to those reported in the literature [25][44], which shown values close to 10 GPa and 240 GPa for H and Er, respectively. The relative higher hardness is even more notorious having in consideration the columnar structure of the coatings, as viewed in SEM micrographies, Figure IV-1. Although not presented in this study, we noticed that Cr coating present relatively high compressive residual stress which can explain the higher hardness. In studies where negative bias was applied, for example by Forniés *et al.* [45], was also observed a hardness of 12 GPa.

For the gCrN and CrN coatings, as explained in the chemical composition discussion, both have similar N content (~35 at.%) on the top of the coating, the structure of the films is composed by similar phases, and so the hardness and Young's modulus show similar values at ~15 GPa and ~240 GPa, respectively. This hardness value is in line with previous works [46], showing that Cr_2N + CrN or pure CrN structures have a hardness close to 15 GPa. A *Er* value of 240 GPa was also reported by Elangovan [47] in past studies.

The deposited CrO coating exhibits a hardness value of 12 GPa and a Young's Modulus of 199 GPa. These values are in the range of values presented by the works of Pang [48] and Fernandes [49] in particular when deposition happens in metallic mode, having a sub-stoichiometric composition and an amorphous structure. When associating the chemical composition, X-ray diffraction and hardness results of our CrO coating with the work of Barshilia [50], in which a bigger range of Cr-O composition was studied, it reinforces the explanation that our coating is far from a stoichiometric Cr_2O_3 coating which has a reported hardness of 7 GPa.

The CrON coating exhibits the lower hardness results in this series with 9.5 GPa. Note that this is the coatings with more pronounced CrN crystalline structure, despite the relative high amount of oxygen (18~22 at.%), see Figure IV-7.e. So, the presence of oxygen stabilizes the formation of the CrN crystal phase being the oxygen atoms in interstitial positions broadening the crystallographic peaks and/or replacing some nitrogen atoms in that CrN structure. Also, it could be possible that some Cr-O amorphous phases exist and thus creating a nanocomposite of CrN nanograins in a Cr-O amorphous matrix (CrN@Cr-O). Some of the pioneer works on the Cr-O-N system from Collard *et al.* [43], showed a limited incorporation of oxygen into a CrN structure. In fact, according to Collard *et al.* when incorporating oxygen into CrN, a nanocrystalline structure together with an amorphous fraction evolves gradually into a Cr_2O_3 type structure. In a previous author's work on a W-O-N system [39], the rule of mixture could be used to predict the hardness of the coatings. Assuming a nanocomposite model CrN @ Cr-O matrix, the hardness of these coatings could be calculated based on the rule of mixture using the hardness of CrN as 15 GPa (from this work) and the hardness of Cr_2O_3 of 7 GPa [50], the calculated hardness was 12 GPa, estimating 70% of CrN and 30% of Cr_2O_3, but also taking in consideration the material density, the volume of the CrN phase is 62% and Cr_2O_3 is 38%. These calculated values are clearly above the experimental data. Other works on Cr-O-N system by cathodic arc evaporation found a higher hardness, close to 14 GPa [44], attributing that value to the limit of the existence of microstrains in the crystal structure resulting in high compressive residual stress [51], however by arc evaporation method the Cr_2O_3 hardness is higher since

the coatings shown a much higher crystallinity than the films with similar composition produced by magnetron sputtering.

Concerning the mechanical properties of the multilayer coatings, CrN/CrO and CrN/CrON, it is important to mention that these multilayers have a relative long period, Λ, between 140 to 250 nm, so it is not expected an enhancement of mechanical properties due to interfaces influence (Hall and Petch [52] and Lehoczky's [53] theories) yet a behavior close to the rule of mixture is predictable. The hardness value of CrN/CrO was 13 GPa, if taken in consideration the rule of mixture from the hardness of CrN and CrO it should result in 13.6 GPa. Using the same approach, for the coating CrN/CrON, that showed a hardness of 10.5 GPa when calculated by the rule of mixture the average between the CrN and CrON was 12.3 GPa. We always observed a lower hardness value than the average of the individual layer, even if recalculated based on layer volume, as observed in Figure IV-5, for CrO, with bigger layers and lower hardness. If volume weight average was used the hardness value should be lower but still higher than the real measured value. As far as we know, there are no studies in the literature concerning CrN/CrO nor CrN/CrON systems. There are some Cr/CrN studies, even with long multilayer periods, in which some similarities can be found, and we can extrapolate assuming Cr as the softer layer and the CrN as the hard layer. Marulanda *et al.* [54] observed a softening of the coating as the layer period thickness increases, but there is a lack of information to the reference of the monolithic coatings under the same deposition conditions, Kot *et al.* [55] mention that coatings with 1000 nm period show a hardness and modulus values close to pure Cr, so near to the softer layer, whereas the coatings with layer period of 250 and 500 nm had hardness and modulus similar to the harder layer, CrN, and attribute this to Hall-Petch. In Kot's work they found that hardness of multilayer increases when layer period decreases, although this study was done for laser cladding and we did not observe a similarity on our study. Other study from Arias *et al.* [56] also explains the higher hardness of their multilayers with long period (between 200 to 500 nm) resorting to Hall-Petch effect, concluding that a Cr/CrN with long period multilayers have a hardness higher than CrN. Ultimately, different behaviors can be observed. Previous investigations, on a different multilayer system with long layer period, W/W-O [57], and on that case W layers were harder and W-O were the softer layers and overall hardness of the coatings also did not follow the rule of mixture, but tended to be closer to the hardness of the soft layer W-O.

4.4.2 Tribological characterization by dry sliding reciprocating tests

In automotive industry some parts in which decorative coatings are applied, are either under heavy human contact (doorhandles and knobs) or suffer some sort of abrasive aggression from the surrounding

environment. To find out how these coatings behave, the samples were tested by dry sliding reciprocating test against Al_2O_3 ball which the authors consider a good testing counterpart to represent the sand/stones or other environmental debris that can damage the surfaces.

The dry sliding reciprocating tests of the coatings are presented in Figure IV-9. The results showed similar specific wear rate for most of the coatings around $1x10^{-4}$ mm^3/Nm, with exception of gCrN, CrO and CrN/CrON. It is important to mention that the tested coatings were deposited onto polycarbonate, a polymeric substrate, and a limited number of cycles and load were applied, since our goal was to assess durability of the coatings.

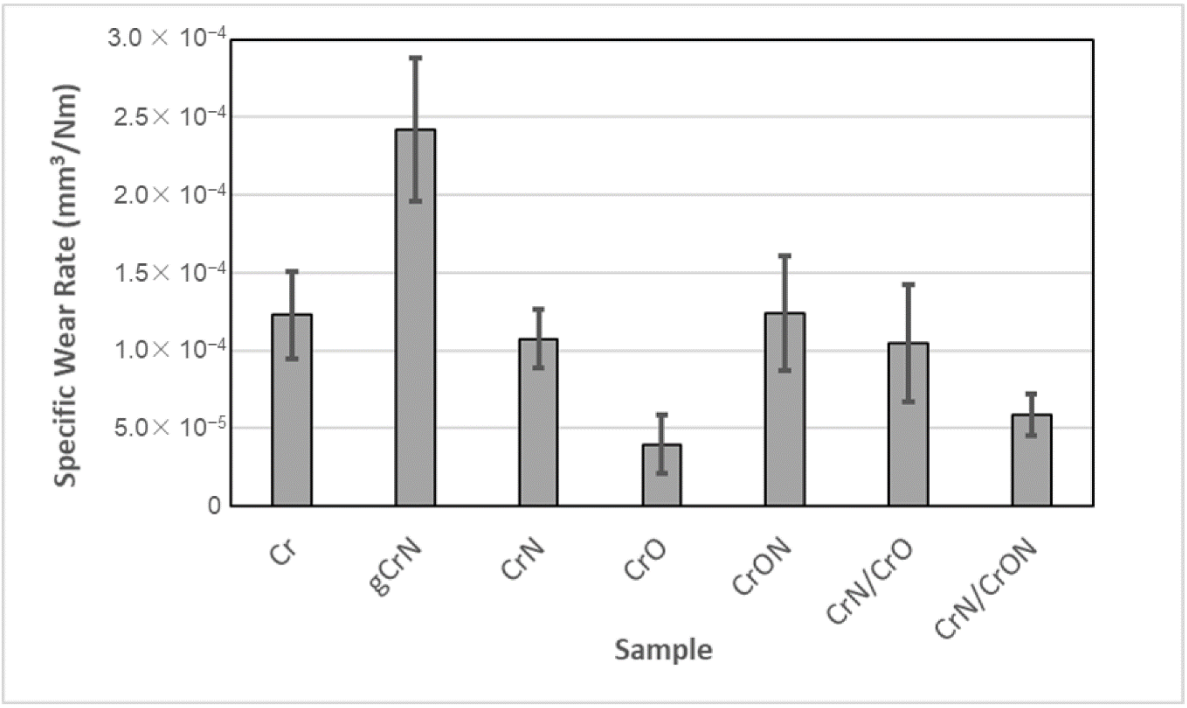

Figure IV-9. Specific wear rate of the coatings tested using dry sliding reciprocating tests.

As shown, under these test conditions, the coatings Cr and CrN present similar wear rate which is different from other tribological studies. A comprehensive literature review revealed no published studies on tribological characterization of Cr and CrN coatings by dry sliding reciprocating tests, only tribological studies carrier by pin-on-disc, on those cases the authors showed a correlation between hardness and the tribological behaviour with CrN coatings exhibiting lower wear rate than Cr coating as an example in the work of He *et al.* [58]. A coating with relative high hardness is the gCrN one, which presents the worst behaviour in this series, and that can be attributed to the lower adhesion of the gCrN coating as shown in Figure IV-3.

CrO coating is highlighted in this study due to having the best tribological behaviour in spite of its relative lower hardness and a classification of 1 in the adhesion test. This result is in line with a previous study from Urgen *et al.* [59], showing that a CrO coating presents lower wear in comparison with CrN or CrON coatings. The multilayer coatings CrN/CrO and CrN/CrON, specially the latter, presents a good wear resistance in dry sliding test, which is an expected result, consistent with the literature where the multilayer coatings present a better wear resistance behaviour than the individual layers [56].

Most of the coatings presented in this study are good candidates for metallization coatings onto plastic, with exception of the gCrN coating that exhibits a high wear rate limiting its use for the intended applications of this study.

4.5 Partial conclusions

The results presented in this work are part of a study to develop environmentally friendly decorative Cr-based coatings for metallization of automotive parts to replace hexavalent chromium plated solutions.

Coatings were deposited by DC reactive magnetron sputtering from a single pure Cr target in reactive atmosphere (N_2 or O_2 or a mixture of the 2 gases). In the defined conditions was possible to incorporate up to 32 at.% of oxygen (in the case of "pure" CrO coating) and 36 at.% of N in the case of CrN coating. The deposition rate varies between 1.4 nm/s for the CrON coating to 2.4 nm/s in the case of the CrO, it is worth mention that CrO coating exhibited higher deposition rate than nitrogen-containing ones.

The morphology of the coating is columnar for the Cr and CrN coatings, type T according to Thornton model for the CrON coating and CrO present a multilayer effect due to the high deposition rate of the oxide phase and the fact that the deposition was done under slow rotation. Concerning the structure, the coating depending of the composition have a b.c.c α-Cr, δ-Cr (a metastable A15 cubic structure), the hexagonal β-Cr_2N and cubic CrN. Note that there was not possible to directly detect oxide phases, but once the Cr_3O and $CrO_{0.87}$ are phases with reflection places superimposed in (110) plane of α-Cr, is not possible to exclude by XRD the presence of these phases. We did not observe an oxide phase by XRD on the CrON coating even with 22 at.% of O and only the reflection of CrN was observed, leading us towards the idea that the coating was a nanocomposite with small CrN grains and with some oxygen in solution in a oxide amorphous phase.

The mechanical properties of the coatings measure by nanoindentation showed a range of hardness between 9.4 GPa and 15.2 GPa for CrON and CrN coating respectively.

The adhesion of the coatings onto PC substrates was measured by cross-cut tape test (using ISO 2409 standard) and all coatings present excellent adhesion. Exception made for just the gradient coating gCrN and CrO coating which showed detachment of small flakes in the intersection of the cuts in an area lower than 5%.

In dry sliding test all coatings, with exception of gCrN, were proven to be good candidates for automotive applications showing wear rates compatible with the industry standards.

The color and reflectance of the coatings was measured by spectrophotometry and all coatings exhibit a grey tonality. Different brightness of the coatings was obtained by changing chemical composition allowing the exploration of a range of grey tones highly desired in the automotive industry.

Focusing our study on Cr-O-N system to be use as decorative coatings we already define some limits in chemical compositions of coatings designed to enhance the performance of decorative coatings. Further studies concerning corrosion behaviour for future industrialization of sputtered Cr based coatings on automotive industries will be discussed in the next chapter.

4.6 References

[1] A. M. A. Reheem, M. I. A. A. Maksoud, and A. H. Ashour, “Surface modification and metallization of polycarbonate using low energy ion beam,” Radiat. Phys. Chem., vol. 125, pp. 171–175, 2016, doi: 10.1016/j.radphyschem.2016.04.010.

[2] S. Olivera, H. B. Muralidhara, K. Venkatesh, K. Gopalakrishna, and C. S. Vivek, “Plating on acrylonitrile–butadiene–styrene (ABS) plastic: a review,” J. Mater. Sci., vol. 51, no. 8, pp. 3657–3674, 2016, doi: 10.1007/s10853-015-9668-7.

[3] M. Charbonnier, M. Romand, E. Harry, and M. Alami, “Surface plasma functionalization of polycarbonate: Application to electroless nickel and copper plating,” J. Appl. Electrochem., vol. 31, no. 1, pp. 57–63, 2001, doi: 10.1023/A:1004161707536.

[4] J. White, C. Tenore, A. Pavich, R. Scherzer, and S. Stagon, “Environmentally benign metallization of material extrusion technology 3D printed acrylonitrile butadiene styrene parts using physical vapor deposition,” Addit. Manuf., vol. 22, no. June 2017, pp. 279–285, 2018, doi: 10.1016/j.addma.2018.05.016.

[5] X. Tang, J. Wang, C. Wang, and B. Shen, “A novel surface activation method for Ni/Au electroless plating of acrylonitrile-butadiene-styrene,” Surf. Coatings Technol., vol. 206, no. 6, pp. 1382–1388, 2011, doi: 10.1016/j.surfcoat.2011.08.064.

[6] A. Garcia et al., “ABS polymer electroless plating through a one-step poly(acrylic acid) covalent grafting,” ACS Appl. Mater. Interfaces, vol. 2, no. 4, pp. 1177–1183, 2010, doi: 10.1021/am1000163.

[7] European Parliament, “DIRECTIVE 2005/90/EC OF THE EUROPEAN PARLIAMENT AND OF THE COUNCIL.” 2006.

[8] L. Vernhes, M. Azzi, and J. E. Klemberg-Sapieha, “Alternatives for hard chromium plating: Nanostructured coatings for severe-service valves,” Mater. Chem. Phys., vol. 140, no. 2–3, pp. 522–528, 2013, doi: 10.1016/j.matchemphys.2013.03.065.

[9] T. Sahraoui, N. E. Fenineche, G. Montavon, and C. Coddet, “Alternative to chromium: Characteristics and wear behavior of HVOF coatings for gas turbine shafts repair (heavy-duty),” J. Mater. Process. Technol., vol. 152, no. 1, pp. 43–55, 2004, doi: 10.1016/j.jmatprotec.2004.02.061.

[10] C. Forsich et al., “Potential of thick a-C: H: Si films as substitute for chromium plating,” Surf. Coatings Technol., vol. 241, pp. 86–92, 2014, doi: 10.1016/j.surfcoat.2013.11.011.

[11] Yasbandha, H., "Surface engineering of coinage dies", Doctor of Philosophy thesis, Faculty of Engineering, University of Wollongong, 2001. http://ro.uow.edu.au/theses/1838.

[12] K. Bewilogua et al., “Surface technology for automotive engineering,” CIRP Ann. - Manuf. Technol., vol. 58, no. 2, pp. 608–627, 2009, doi: 10.1016/j.cirp.2009.09.001.

[13] E. V. Antonakou and D. S. Achilias, “Recent advances in polycarbonate recycling: A review of degradation methods and their mechanisms,” Waste and Biomass Valorization, vol. 4, no. 1. pp. 9–21, 2013, doi: 10.1007/s12649-012-9159-x.

[14] I. Grimberg, B. Bouaifi, U. Draugelates, K. Soifer, and B. Z. Weiss, “Microstructure and adhesion mechanisms of TiN coatings on metallized acrylonitrile-butadiene-styrene,” Surf. Coatings Technol., vol. 68–69, no. C, pp. 166–175, 1994, doi: 10.1016/0257-8972(94)90155-4.

[15] P. Sukwisute, R. Sakdanuphab, and A. Sakulkalavek, "Hardness and wear resistance improvement of ABS surface by CrN thin film," Mater. Today Proc., vol. 4, no. 5, pp. 6553–6561, 2017, doi: 10.1016/j.matpr.2017.06.167.

[16] P. Pedrosa et al., "Properties of CrN thin fi lms deposited in plasma-activated ABS by reactive magnetron sputtering," Surf. Coat. Technol., vol. 349, no. June, pp. 858–866, 2018, doi: 10.1016/j.surfcoat.2018.06.072.

[17] E. Carneiro, J. D. Castro, S. M. Marques, A. Cavaleiro, and S. Carvalho, "REACH regulation challenge: Development of alternative coatings to hexavalent chromium for minting applications," Surf. Coatings Technol., p. 127271, 2021, doi: https://doi.org/10.1016/j.surfcoat.2021.127271.

[18] B. Subramanian and M. Jayachandran, "Preparation of chromium oxynitride and chromium nitride films by DC reactive magnetron sputtering and their material properties," Corros. Eng. Sci. Technol., vol. 46, no. 4, pp. 554–561, 2011, doi: 10.1179/147842209X12579401586807.

[19] Y. Yuan et al., "Structure and optical properties of CrOxNy films with composition modulation," Surf. Eng., vol. 36, no. 4, pp. 411–417, 2020, doi: 10.1080/02670844.2019.1656356.

[20] R. Mientus, R. Grötschel, and K. Ellmer, "Optical and electronic properties of CrOxNy films, deposited by reactive DC magnetron sputtering in Ar/N2 /O2(N2O) atmospheres," Surf. Coatings Technol., vol. 200, no. 1-4 SPEC. ISS., pp. 341–345, 2005, doi: 10.1016/j.surfcoat.2005.02.181.

[21] K. Kato, "Friction and wear of passive metals and coatings," Tribocorrosion Passiv. Met. Coatings, pp. 65–99, 2011, doi: 10.1533/9780857093738.1.65.

[22] D. A. Colombo, M. D. Echeverria, S. Laino, R. C. Dommarco, and J. M. Massone, "Sliding wear behavior of PVD CrN and TiN coated austempered ductile iron," ISIJ Int., vol. 54, no. 12, pp. 2860–2867, 2014, doi: 10.2355/isijinternational.54.2860.

[23] U. Beck, G. Reiners, U. Kopacz, and H. A. Jehn, "Decorative hard coatings: interdependence of optical, stoichiometric and structural properties," Surf. Coatings Technol., vol. 60, no. 1–3, pp. 389–395, 1993, doi: 10.1016/0257-8972(93)90119-9.

[24] E. Budke, J. Krempel-Hesse, H. Maidhof, and H. Schüssler, "Decorative hard coatings with improved corrosion resistance," Surf. Coatings Technol., vol. 112, no. 1–3, pp. 108–113, 1999, doi: 10.1016/S0257-8972(98)00791-9.

[25] P. H. Mayrhofer, G. Tischler, and C. Mitterer, "Microstructure and mechanical/thermal properties of Cr-N coatings deposited by reactive unbalanced magnetron sputtering," Surf. Coatings Technol., vol. 142–144, pp. 78–84, 2001, doi: 10.1016/S0257-8972(01)01090-8.

[26] "Handbook of chemistry and physics," Journal of the Franklin Institute, vol. 209, no. 6. p. 847, 1930, doi: 10.1016/s0016-0032(30)91499-8.

[27] N. M. G. Parreira, T. Polcar, N. Martin, O. Banakh, and A. Cavaleiro, "Optical and electrical properties of W-O-N coatings deposited by DC reactive sputtering," Plasma Process. Polym., vol. 4, no. SUPPL.1, pp. 69–75, 2007, doi: 10.1002/ppap.200730405.

[28] J. Xu, H. Umehara, and I. Kojima, "Effect of deposition parameters on composition, structures, density and topography of CrN films deposited by r.f. magnetron sputtering," Appl. Surf. Sci., vol. 201, no. 1–4, pp. 208–218, 2002, doi: 10.1016/S0169-4332(02)00942-X.

[29] U. Rothhaar and H. Oechsner, "R.f. magnetron sputter deposition of Cr2O3 layers on ceramic Al2O3 substrates," Surf. Coatings Technol., vol. 59, no. 1–3, pp. 183–186, 1993, doi: 10.1016/0257-8972(93)90080-8.

[30] M. Kharrazi, A. Azens, L. Kullman, and C. G. Granqvist, "High-rate dual-target d.c. magnetron sputter deposition of electrochromic MoO3 films," Thin Solid Films, vol. 295, no. 1–2, pp. 117–121, 1997, doi: 10.1016/S0040-6090(96)09306-6.

[31] N. M. G. Parreira, N. J. M. Carvalho, and A. Cavaleiro, "Synthesis, structural and mechanical characterization of sputtered tungsten oxide coatings," Thin Solid Films, vol. 510, no. 1–2, pp. 191–196, 2006, doi: 10.1016/j.tsf.2005.12.299.

[32] R. Daniel, K. J. Martinschitz, J. Keckes, and C. Mitterer, "The origin of stresses in magnetron-sputtered thin films with zone T structures," Acta Mater., vol. 58, no. 7, pp. 2621–2633, 2010, doi: 10.1016/j.actamat.2009.12.048.

[33] D. F. Arias, A. Gómez, R. M. Souza, and J. M. Vélez, "Residual stress gradient of Cr and CrN thin fi lms," Mater. Chem. Phys., vol. 204, pp. 269–276, 2018, doi: 10.1016/j.matchemphys.2017.10.053.

[34] C. F. A. Alves et al., "An experimental and theoretical study on the crystal structure and elastic properties of Ta 1–x O x coatings," Surf. Coatings Technol., vol. 364, no. March 2018, pp. 289–297, 2019, doi: 10.1016/j.surfcoat.2019.02.054.

[35] T. Kowoll et al., "Contrast of Backscattered Electron SEM Images of Nanoparticles on Substrates with Complex Structure," vol. 2017, 2017.

[36] K. Kimoto and I. Nishida, "An electron diffraction study on the crystal structure of a new modification of chromium," J. Phys. Soc. Japan, vol. 22, no. 3, pp. 744–756, Mar. 1967, doi: 10.1143/JPSJ.22.744.

[37] J. Peralta, J. Esteve, and A. Lousa, " δ -A15 and bcc phases coexist in sputtered chromium coatings with moderate oxygen contents," Thin Solid Films, vol. 693, no. June 2019, p. 137676, 2020, doi: 10.1016/j.tsf.2019.137676.

[38] N. M. G. Parreira, N. J. M. Carvalho, and A. Cavaleiro, "On the structural evaluation of unbiased W-O-N sputtered coatings," Mater. Sci. Forum, vol. 514–516, no. PART 1, pp. 825–830, 2006, doi: 10.4028/www.scientific.net/msf.514-516.825.

[39] N. M. G. Parreira, N. J. M. Carvalho, F. Vaz, and A. Cavaleiro, "Mechanical evaluation of unbiased W-O-N coatings deposited by d.c. reactive magnetron sputtering," Surf. Coatings Technol., vol. 200, no. 22-23 SPEC. ISS., pp. 6511–6516, 2006, doi: 10.1016/j.surfcoat.2005.11.020.

[40] H. J. Song and Q. Yan, "The characteristics of CrNx coatings with different interlayer," Adv. Mater. Res., vol. 204–210, pp. 938–941, 2011, doi: 10.4028/www.scientific.net/AMR.204-210.938.

[41] D. M. Marulanda, A. Lousa, L. Martinez-De-Olcoz, and J. J. Olaya, "Microstructure characterization of nano-structured Cr/Cr2N multilayer films produced through radio frequency magnetron sputtering," Thin Solid Films, vol. 550, pp. 272–277, 2014, doi: 10.1016/j.tsf.2013.11.016.

[42] C. Suryanarayana, M. G. Norton, "X-Ray Diffraction A Practical Approach," Plenum Press, New York, 1998..

[43] S. Collard, H. Kupfer, G. Hecht, W. Hoyer, and H. Moussaoui, "The reactive magnetron deposition of CrNxOy films: First results of property investigations," Surf. Coatings Technol., vol. 112, no. 1–3, pp. 181–184, 1999, doi: 10.1016/S0257-8972(98)00752-X.

[44] P. Hones, M. Diserens, and F. Lévy, "Characterization of sputter-deposited chromium oxide thin films," Surf. Coatings Technol., vol. 120–121, pp. 277–283, 1999, doi: 10.1016/S0257-8972(99)00384-9.

[45] E. Forniés, R. Escobar Galindo, O. Sánchez, and J. M. Albella, "Growth of CrNx films by DC reactive magnetron sputtering at constant N2/Ar gas flow," Surf. Coatings Technol., vol. 200, no. 20–21, pp. 6047–6053, 2006, doi: 10.1016/j.surfcoat.2005.09.020.

[46] P. Hones, R. Sanjines, and F. Lévy, "Characterization of sputter-deposited chromium nitride thin films for hard coatings," Surf. Coatings Technol., vol. 94–95, pp. 398–402, 1997, doi: 10.1016/S0257-8972(97)00443-X.

[47] T. Elangovan, P. Kuppusami, R. Thirumurugesan, V. Ganesan, E. Mohandas, and D. Mangalaraj, "Nanostructured CrN thin films prepared by reactive pulsed DC magnetron sputtering," Mater. Sci. Eng. B Solid-State Mater. Adv. Technol., vol. 167, no. 1, pp. 17–25, 2010, doi: 10.1016/j.mseb.2010.01.021.

[48] X. Pang, K. Gao, and A. A. Volinsky, "Microstructure and mechanical properties of chromium oxide coatings," J. Mater. Res., vol. 22, no. 12, pp. 3531–3537, 2007, doi: 10.1557/jmr.2007.0445.

[49] F. Fernandes, T. B. Yaqub, and A. Cavaleiro, "Influence of Ag additions on the structure, mechanical properties and oxidation behaviour of Cr-O coatings deposited by HiPIMS," Surf. Coatings Technol., vol. 339, no. November 2017, pp. 167–180, 2018, doi: 10.1016/j.surfcoat.2018.02.025.

[50] H. C. Barshilia and K. S. Rajam, "Growth and characterization of chromium oxide coatings prepared by pulsed-direct current reactive unbalanced magnetron sputtering," Appl. Surf. Sci., vol. 255, no. 5 PART 2, pp. 2925–2931, 2008, doi: 10.1016/j.apsusc.2008.08.057.

[51] L. Castaldi, D. Kurapov, A. Reiter, V. Shklover, P. Schwaller, and J. Patscheider, "Effect of the oxygen content on the structure, morphology and oxidation resistance of Cr-O-N coatings," Surf. Coatings Technol., vol. 203, no. 5–7, pp. 545–549, 2008, doi: 10.1016/j.surfcoat.2008.05.018.

[52] E. O. Hall, “The deformation and ageing of mild steel: III Discussion of results,” Proc. Phys. Soc. Sect. B, vol. 64, no. 9, pp. 747–753, 1951, doi: 10.1088/0370-1301/64/9/303.

[53] S. L. Lehoczky, " Retardation of Dislocation Generation and Motion in Thin-Layered Metal Laminates", Phys. Rev. Lett. vol. 41, pp. 1814, 1978, doi: 10.1103/PhysRevLett.41.1814.

[54] D. M. Marulanda, J. J. Olaya, U. Piratoba, A. Mariño, and E. Camps, “The effect of bilayer period and degree of unbalancing on magnetron sputtered Cr/CrN nano-multilayer wear and corrosion,” Thin Solid Films, vol. 519, no. 6, pp. 1886–1893, 2011, doi: 10.1016/j.tsf.2010.10.010.

[55] M. Kot, W. A. Rakowski, Major, R. Major, and J. Morgiel, “Effect of bilayer period on properties of Cr/CrN multilayer coatings produced by laser ablation,” Surf. Coatings Technol., vol. 202, no. 15, pp. 3501–3506, 2008, doi: 10.1016/j.surfcoat.2007.12.036.

[56] D. F. Arias, A. Gómez, J. M. Vélez, R. M. Souza, and J. J. Olaya, “A mechanical and tribological study of Cr/CrN multilayer coatings,” Mater. Chem. Phys., vol. 160, pp. 131–140, 2015, doi: 10.1016/j.matchemphys.2015.04.015.

[57] N. M. G. Parreira, T. Polcar, and A. Cavaleiro, “Characterization of W-O coatings deposited by magnetron sputtering with reactive gas pulsing,” Surf. Coatings Technol., vol. 201, no. 9-11 SPEC. ISS., pp. 5481–5486, 2007, doi: 10.1016/j.surfcoat.2006.07.017.

[58] X.-M. He, N. Baker, B. A. Kehler, K. C. Walter, M. Nastasi, and Y. Nakamura, “Structure, hardness, and tribological properties of reactive magnetron sputtered chromium nitride films,” J. Vac. Sci. Technol. A Vacuum, Surfaces, Film., vol. 18, no. 1, pp. 30–36, 2000, doi: 10.1116/1.582154.

[59] M. Urgen, V. Ezirmik, E. Senel, Z. Kahraman, and K. Kazmanli, “The effect of oxygen content on the temperature dependent tribological behavior of Cr-O-N coatings,” Surf. Coatings Technol., vol. 203, no. 16, pp. 2272–2277, 2009, doi: 10.1016/j.surfcoat.2009.02.027.

CHAPTER V - Corrosion Resistance in Artificial Perspiration of Cr-Based Decorative Coatings

The following chapter is partially based on the results published in:

Carneiro, E.; Castro, J.D.; Lima, M.J.; Ferreira, J.; Carvalho, S., "Corrosion Resistance in Artificial Perspiration of Cr-Based Decorative Coatings. Nanomaterials", 2023, 13, 2346. https://doi.org/10.3390/nano13162346

5 Introduction

Our goal is to investigates the transition to more environmentally friendly magnetron-sputtered coatings in the automotive industry for decorative finishes on various components not only plastic parts but also more structural ones. As previously discussed, thermoplastics have gained popularity due to their lower density and cost advantages over metallic materials, however, aluminium-based components are also in use, offering high-strength alloys and ease of manufacturing. The present chapter follows the finding of chapter IV and explores the use of the sputtered coating onto aluminium substrates that are also used in the automotive industry. Furthermore, the chapter explores the corrosion effects of human perspiration on decorative coatings, particularly focusing on the application of hexavalent chromium-free coatings on aluminium substrates in automotive parts and consumer products such as external casing of appliances and small equipment's, utilizing reactive magnetron sputtering and assessing their corrosion resistance against artificial sweat, ultimately addressing the need for sustainable and durable coatings in the industry. Here, we present the results for similar coatings deposited on aluminium substrates. This chapter delves directly into the evaluation of corrosion resistance for aluminium-based sputtered coatings since the fundamental characterization was already discussed in section 4.3 of chapter IV.

5.1 Materials and methods

Coatings were deposited by DC reactive magnetron sputtering in a home-made vacuum chamber onto monocrystalline silicon wafers (100 P-type) and polished Al plates (alloy AA 5052) samples. Aluminium substrates were protected with a transparent UV-cured basecoat (based on acrylate resins) before the metallization to improve both the adhesion and decorative appearance of the coating.

Despite employing similar deposition procedures for both PC and aluminium, the deposition times varied and are presented in the Table V-1 alongside with a summarization of deposition parameters and characterization of the coatings produced. The multilayer coating (CrN/CrO) was deposited with similar conditions of monolithic coatings with each layer being deposited for 60s. For graded CrN coatings (gCrN), depositions were carried out with increasing nitrogen flow up to 25 sccm to match CrN conditions in the outermost portion of the coating.

Table V-1. Deposition conditions of the coatings (gas flow and deposition times), deposition rate, and chemical composition characterization of the deposited coatings.

Coating	Gas Flow (sccm)			Deposition Time (s)		Thickness	Deposition Rate	Chemical Composition (at. %)		
	Ar	N_2	O_2	Interlayer	Coating	(nm)	(nm/s)	Cr	O	N
Cr	100				720	1390	1.9	91	9	-
gCrN	70	5⟶25			720	1180	1.6	66	6	28
CrN	70	25		50	670	1110	1.5	60	8	32
CrO	100		15	50	670	1660	2.3	69	31	-
CrN/CrO	70	25	15	50	720	1420	1.8	63	25	12

Surface roughness of the as-deposited coatings, and after 96 h of exposure to artificial sweat was assessed using atomic force microscopy (Icon Dimension, Bruker, Billerica, Massachusetts, United States) at room temperature with a conductive Si cantilever in contact mode. Three measurements were performed to evaluate average surface roughness (S_a) and root-mean-square roughness (S_q) in all samples according to the ISO 25178 standard and holding a 2.5 × 2.5 μm^2 area.

The wettability studies were carried out using optical contact angle (CA) measurements (DataPhysics Instruments GmbH, Filderstadt, Germany, OCA20 equipment) with artificial sweat described above. Drop volume was maintained at < 10 μL for each measure to avoid possible interferences in the contact angle measurements from the drop weight.

To evaluate the effect of sweat exposure on the coating's surface, artificial sweat was made according to the industry standard TL 226 from the Volkswagen group. Ammonia, mass percentage $w_{(NH3)}$ = 0.036%, and sodium chloride, $w_{(NaCl)}$ = 0.5%, were added to water. In detail, 1 g of NH_3 solution (25%, for analysis purposes) with 690.72 g of distilled water (in practice: 691 g) were used, and 3.47 g NaCl was added.

Corrosion behaviour was induced via potentiodynamic polarization and electrochemical impedance spectroscopy (EIS) techniques, using artificial sweat to simulate long exposure to human touch for 96 h. All measurements were acquired in a Gamry 600 potentiostat connected to an electrochemical cell with a three-electrode configuration with the sample as working electrode (exposed area = 0.35 cm^2), a platinum sheet as the counter electrode, and a saturated calomel electrode (SCE) as the reference electrode. The potentiodynamic polarization measurements were performed between −1500 mV and 1500 mV vs. E_{ref} with a 1 mV/s scan rate. EIS measurements were acquired at 10 points/decade, applying 10 mV rms, between 100 kHz and 0.01 Hz. All the samples were exposed for 3600 s to achieve

stabilization before measurements. Three replicas of electrochemical tests were performed (for every coating in all exposure times). To fit the data from the potentiodynamic polarization test and calculate the corrosion rates, the ASTM G102-89 standard was followed.

5.2 Results and discussion

5.2.1 Chemical Composition

The chemical composition (shown in Table V-1) of coatings deposited onto Si wafer substrates was measured with EDS. The high deposition pressure used (1 Pa) led to significant oxygen incorporation in all coatings, even the pure chromium one similar to their polymeric substrate counterparts. Nitrogen content varied between 28% and 32% for the nitride coatings, with the constant nitrogen flow leading to a higher amount in the CrN sample. The oxygen-rich atmosphere and high reactivity of chromium to oxygen resulted in a chromium oxide coating rich in oxygen. For the graded and multilayered samples, the reported composition represents an average of the individual layers.

5.2.2 Structural Characterization

The crystallographic structure was evaluated using X-ray diffraction (XRD), and the results are shown in Figure V-1 for all deposited coatings.

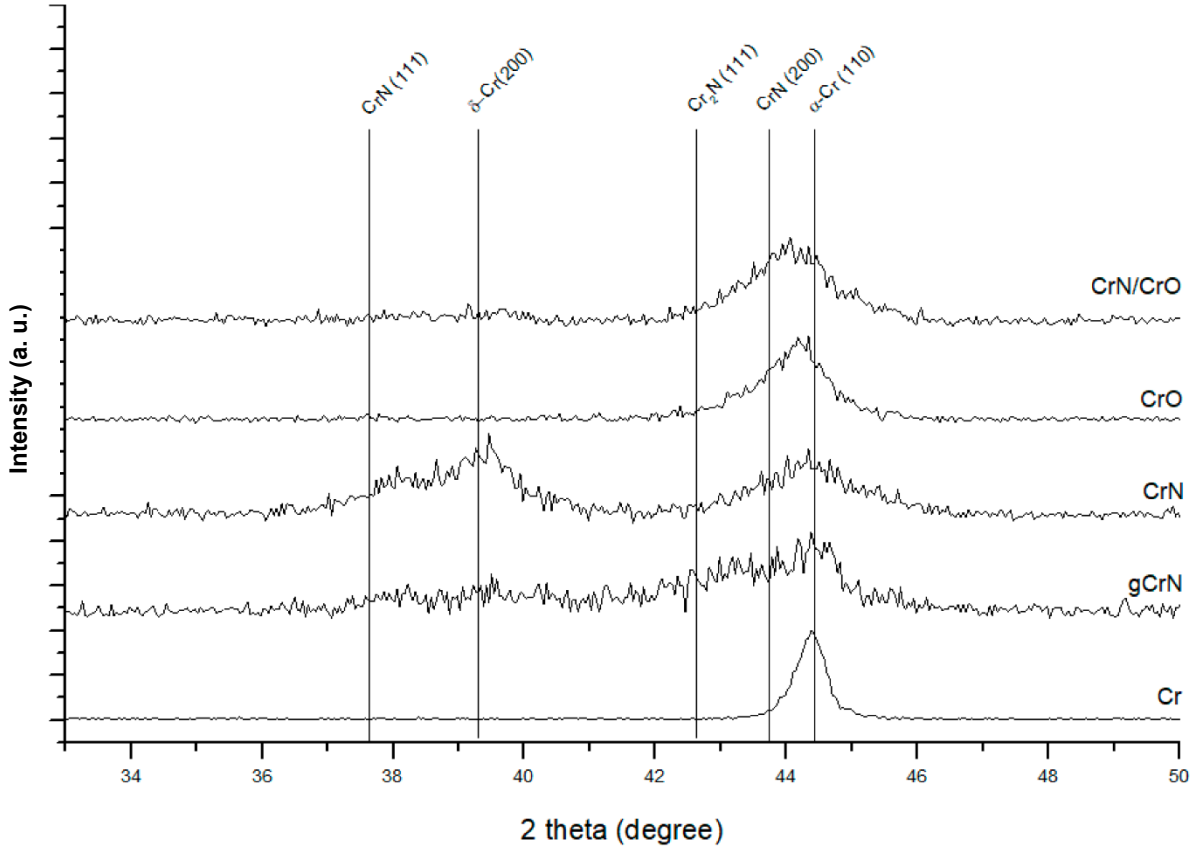

Figure V-1. XRD patterns of the deposited coatings.

In Chapter IV, we conducted a comprehensive and detailed analysis of similar samples on polymer substrates. In the current chapter, we provide a concise summary of the key observations.

XRD analysis confirmed the expected phases for each coating: α-Cr for pure Cr, a mix of Cr, CrN, and Cr_2N for graded CrN, dominant CrN with some metastable Cr for constant-flow CrN, and a combination of α-Cr and chromium oxide for CrO (possibly with stress-induced peak shift). The multilayer coating reflected a mix of the individual CrN and CrO phases.

5.2.3 Morphology

The thickness of the coatings was obtained by cross-section analysis from SEM micrographs on silicon substrate. Those results are shown in Table V-1 and Figure V-2. Surface morphology was also obtained from SEM micrographs.

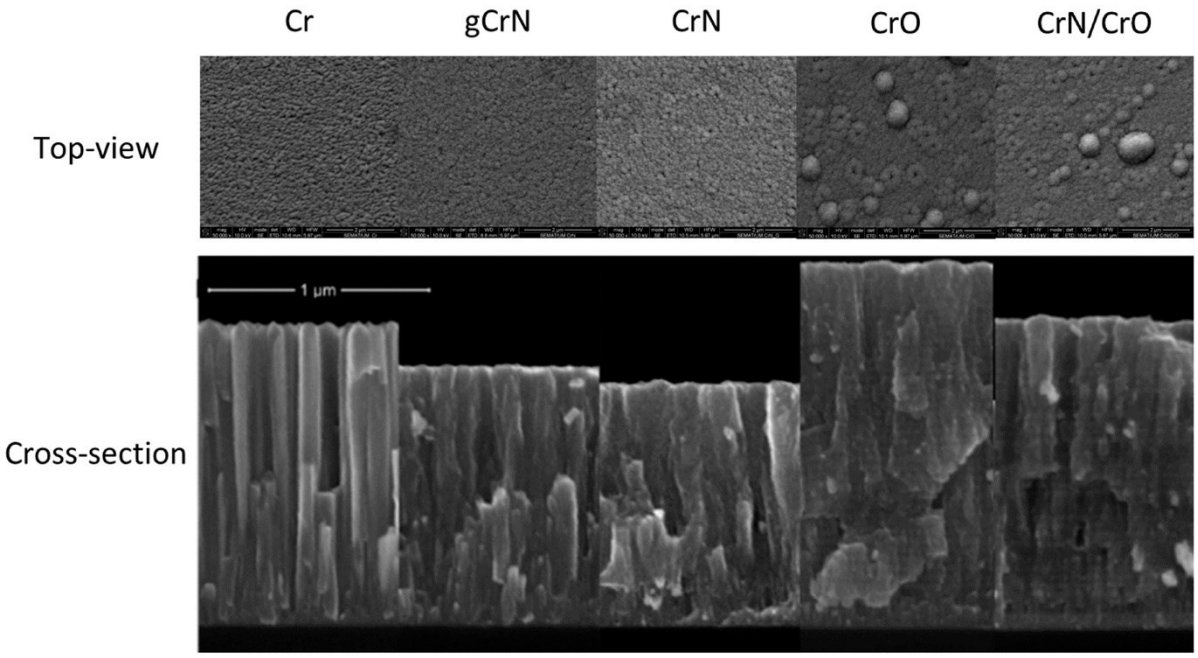

Figure V-2. Scanning electron top-view and cross-section micrographs of the coatings deposited on silicon.

Top-view SEM micrographs showed an increase in surface defects with the increase in nitrogen content, Figure V-2. The introduction of oxygen as reactive gas for sample CrO and multilayer CrN/CrO promoted the appearance of large boulders on the surface. Since this morphology can be closely related to corrosion, a deeper analysis of morphology was conducted in correlation with corrosion behavior in Sections 5.2.5 and 5.2.6.

Coating thickness ranged between 1100 nm and 1660 nm for CrN and CrO, respectively, and the deposition rate varied between 1.5 and 2.3 nm/s.

The deposition rate of Cr coating was 1.9 nm/s, and gCrN and CrN coatings showed a value of 1.6 and 1.5 nm/s. With the increase in the N_2 flow ratio, the deposition rate decreased, which correlates with the consecutively lower thickness observed on samples Cr, gCrN, and CrN in Figure V-2. When the partial pressure of the reactive gas increased inside the vacuum chamber, film growth behavior changed from a columnar-like type—usual in metallic sputtered Cr—to an increasingly denser columnar-like CrN coating, which indicates a lower deposition rate, as observed and reported by others [23].

The thickness increased for samples deposited with oxygen as reactive gas (CrO coating), and the deposition ratio reached 2.3 nm/s. This is a normal behaviour of the sub-stoichiometric Cr-O system [24].

For coating CrN/CrO, the deposition rate is the average of the deposition ratio of CrN and CrO.

The CrO micrograph showed the presence of consecutive layers either deficient or rich in O. The same behavior was observed on the CrN/CrO multilayer coating. This phenomenon was explained by deposition conditions and discussed in chapter IV.

5.2.4 Adhesion

Adhesion of the coatings deposited on aluminium was tested using the cross-cut tape test, and the results are presented in Figure V-3.

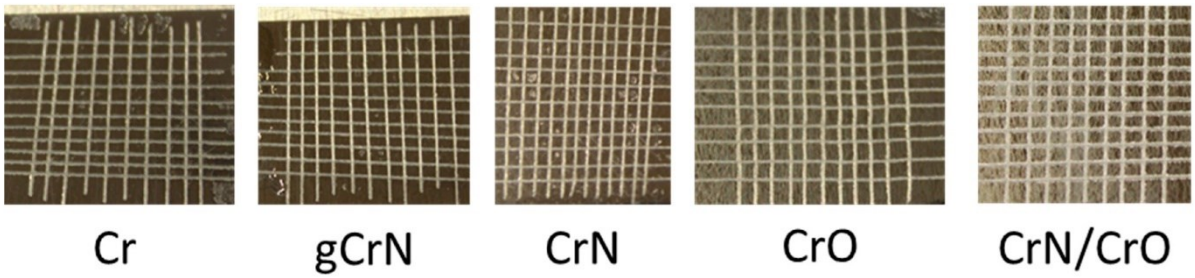

Figure V-3. Adhesion behavior assessment of coatings deposited onto aluminium substrates.

According to the standard, the adhesion of the deposited coatings was rated 0 according to the ISO 2409 standard, meaning perfect adhesion. All coatings had perfect adhesion (Figure V-3), where the edges of the cut were completely smooth, and none of the small squares that made up the grid were detached after removing the tape. The good adhesion behavior is also exponentiated by the acrylate layer between the coating and the substrate even for the CrN/CrO coating, whose surface seems cracked due to residual stress caused by the difference in coefficients of thermal expansion of the two materials in contact [26,27], but ultimately the adhesion of the coating was not affected.

5.2.5 Roughness and Wettability

The roughness of the coatings was measured as deposited and after corrosion test conditions to assess the damage caused by the artificial sweat over the films. Table V-2 and Figure V-4 summarize the results obtained from AFM measurements.

Table V-2. Roughness and contact angles (measured with artificial sweat on as-deposited films) from obtained coatings.

Sample	As Deposited			After Corrosion Tests			Contact Angle (°)
	S_q (nm)	S_{sk}	S_{ku}	S_q (nm)	S_{sk}	S_{ku}	
Cr	14.4 ± 0.1	−0.7	0.4	27.0 ± 0.3	−1.2	2.3	122.6 ± 1
gCrN	9.5 ± 0.2	0.1	2.1	93.7 ± 4.2	−1.1	2.3	105.2 ± 1
CrN	8.6 ± 0.1	−0.6	1.9	92.8 ± 3.8	−1.1	1.5	94.6 ± 1
CrO	8.3 ± 0.1	0.2	0.1	8.4 ± 0.2	0.7	1.4	108.5 ± 2
CrN/CrO	9.8 ± 0.1	0.2	1.0	12.9 ± 0.5	0.1	−0.2	108.1 ± 4

Concerning the films, Cr exhibited a negative skewness with low kurtosis, which means some low bumpy holes in the analysed area (see Figure V-4). After corrosion tests, this surface showed some spiky mounds maintaining the presence of holes. Its increase in S_{ku} (from 0.4 to 2.3) and decrease in S_{sk} (from −0.7 to −1.2) indicate the increase in valleys in the film after sweat interaction but with fewer height differences as demonstrated by the height bar in Figure V-4 (Cr after corrosion tests). Some particles over the film surface were noted after corrosion tests in this sample, which could be related to a possible oxidation process. It was quite surprising to note that Cr film did not exhibit important harm after the corrosion test.

Apparently, the variations in areal roughness were strongly influenced by the electrolyte in nitride films (gCrN and CrN), exhibiting ~10 times higher S_q values, skewness (S_{sk})—which denotes the spikes (positive values) or valleys (negative values) present on the analysed area [28]—and kurtosis (S_{ku})—which qualifies the width of the height distribution [29] or the sharpness of the height profile [28,30]. According to these definitions, the decrease in S_{sk} could be related to the presence of pitting in the sample surfaces after corrosion tests (see Figure V-5).

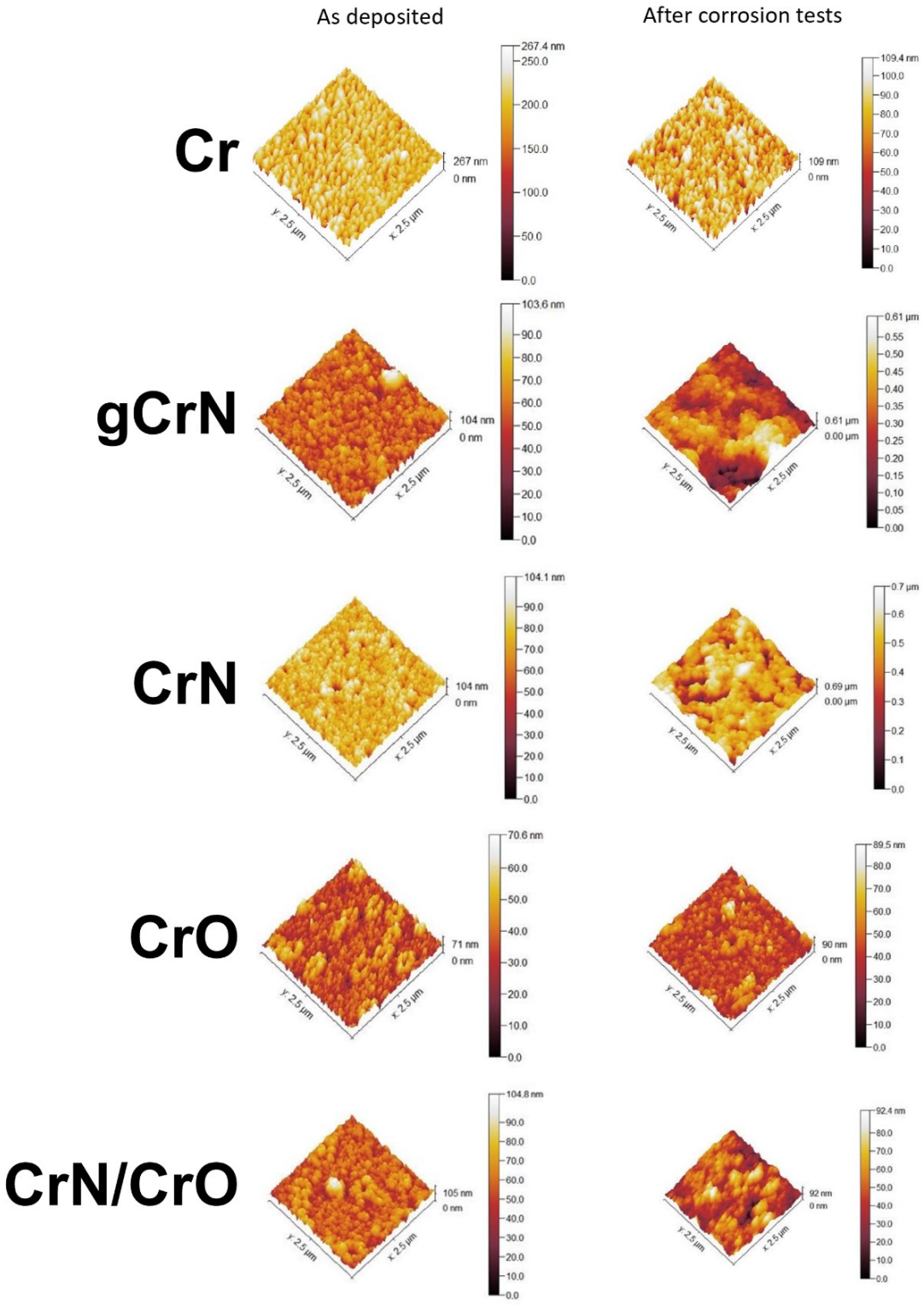

Figure V-4. AFM measurements from obtained coatings in as-deposited conditions and after corrosion test (96 h of artificial sweat exposure).

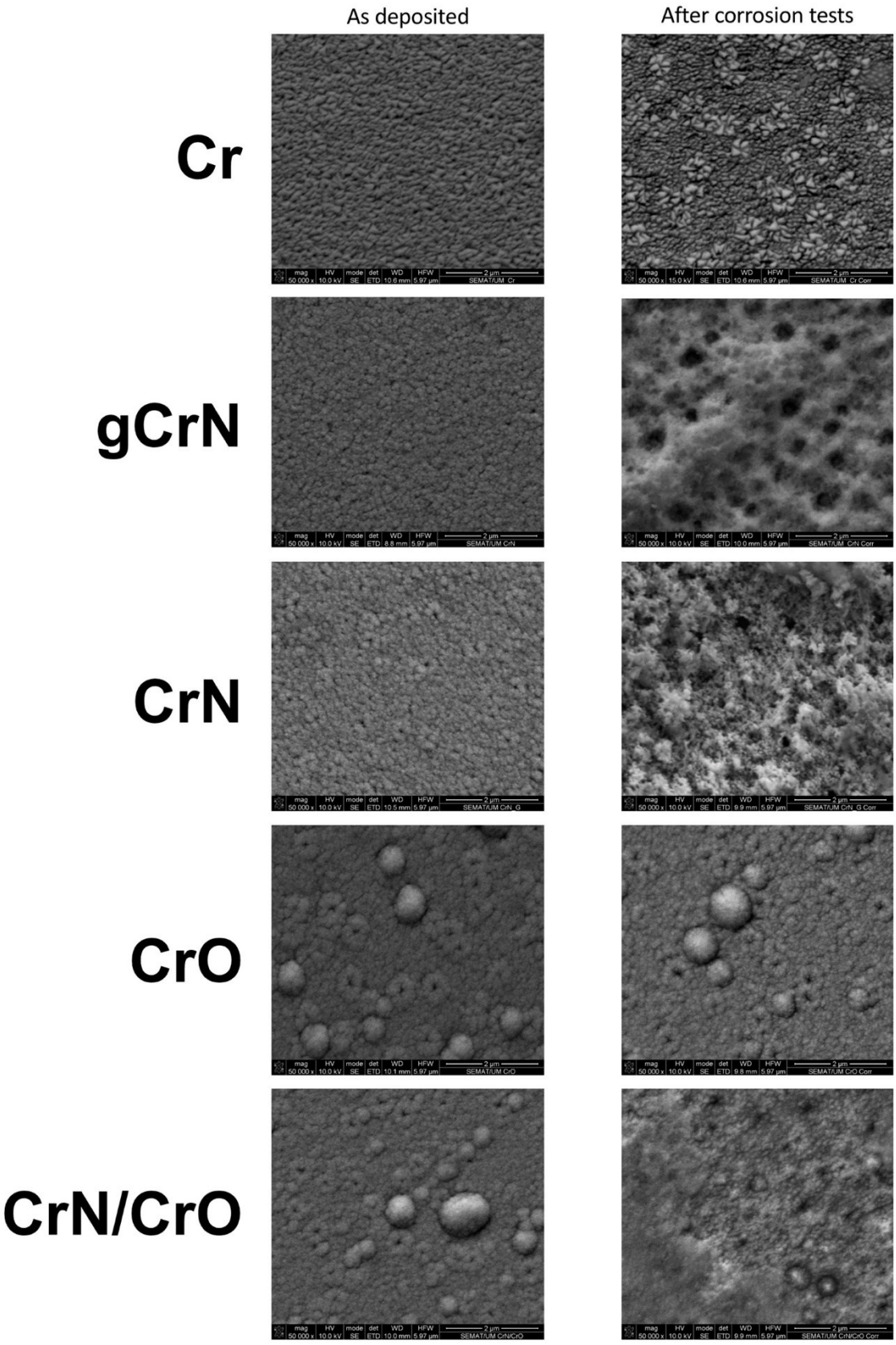

Figure V-5. SEM micrographs from coatings in as-deposited condition and after corrosion test (96 h of artificial sweat exposure).

Furthermore, the nitride films (gCrN and CrN samples) displayed a strong variation of skewness, achieving more negative values after corrosion tests. Figure V-5 exhibits that nitride films suffer an aggressive pitting process, which could be considered the corrosion mechanism in these samples. This behavior could be promoted by defects in the film (i.e., holes), which could facilitate the electrolyte penetration, and corroding during the exposure time (96 h), like the findings of Chipatecua et al. [31] in CrN/Cr multilayers. Indeed, the nitride films displayed the highest increase in roughness (S_a and S_q) after corrosion tests.

CrO was not apparently affected by the artificial sweat after 96 h (see figures V4 and V5). This sample shows a slight increase in S_{ku} and S_{sk} (from 0.1 to 1.4 and 0.2 to 0.7, respectively), but this did not influence the film integrity.

On the other hand, CrN/CrO displayed a S_{ku} decrease (from 1.0 to −0.2), denoting that the "defects" in the film surface are blunter, (see Figure V-5), hence suggesting a uniform corrosion action.

The nitride samples (CrN and gCrN) seem to show the most corroded surfaces when exposed to artificial sweat. Based on AFM results, film defects have a determinant role in triggering the penetration of the electrolyte througth the film, prompting its posterior detachment. Nonetheless, this action was more controlled in the multilayered CrO film because the oxide layer acted as a "barrier" against the chemical action of the electrolyte, demonstrating immunity just like the CrO film.

Wettability measurements with artificial sweat were performed to assess the capacity of the film to allow the electrolyte penetration. According to the values exhibited in Table V-2, nitride films (mainly the CrN sample) displayed less hydrophobic behavior than oxides films. This behavior was influenced by the nature of the film surface as aforementioned. Remarkably, Cr film showed the highest contact angle value with artificial sweat, which helps to explain its relative stability, displaying fewer changes in roughness and morphology after corrosion tests, despite being a high-purity metallic film. The obtained films could be coherent with the Cassie–Baxter model [32]. Some studies have demonstrated that hydrophobicity is a critical surface characteristic to avoid corrosion, as mentioned by Jin et al. [33]. Other authors related the density and absence of superficial defects on films to avoiding corrosion events [34,35]. According to our findings, the phase composition (Cr + CrN), the nanocrystalline structure, and the less hydrophobicity displayed for nitride films played the main role in explaining the film degradation. Furthermore, a chemical reaction between CrN and the electrolyte could also affect the film performance as shown by Ibrahim et al. [36], who measured the corrosion resistance of CrN films against 0.5 M NaCl and borate buffer (pH 9.0) solutions. The CrN film exhibited worse anticorrosive properties whilst exposed to the borate solution.

The authors explained this action as the consequence of two combined factors: the solution capacity to dissolve the film and the corrosion process through pinholes in the film morphology.

5.2.6 Corrosion Resistance against Artificial Sweat

Figure V-6 exhibits the potentiodynamic curves of all samples and the substrate with base coat. According to the potentiodynamic polarization tests, all coatings displayed a nobler behaviour than the substrate. All the sputtered coatings showed lower corrosion current densities than the substrate. As a first insight, all the samples showed two regions of passivation with their perspective breakdown zones. Just Cr showed a quick passivation, and afterwards the current density always increased constantly, which suggests that the anodic reaction did not come close to stopping at any time. On the other hand, gCrN exhibited a passivation of the surface and its respective breakdown with the increase in potential. In fact, gCrN displayed several current fluctuations in the second passivation zone (above +0.5 mV vs. E_{ref}), which indicates the presence of pitting events during the tests and confirms the pits exhibited in Figure V-5, as discussed before. After the second passivation, the transpassive zone always appeared, showing stable behaviour in terms of current densities.

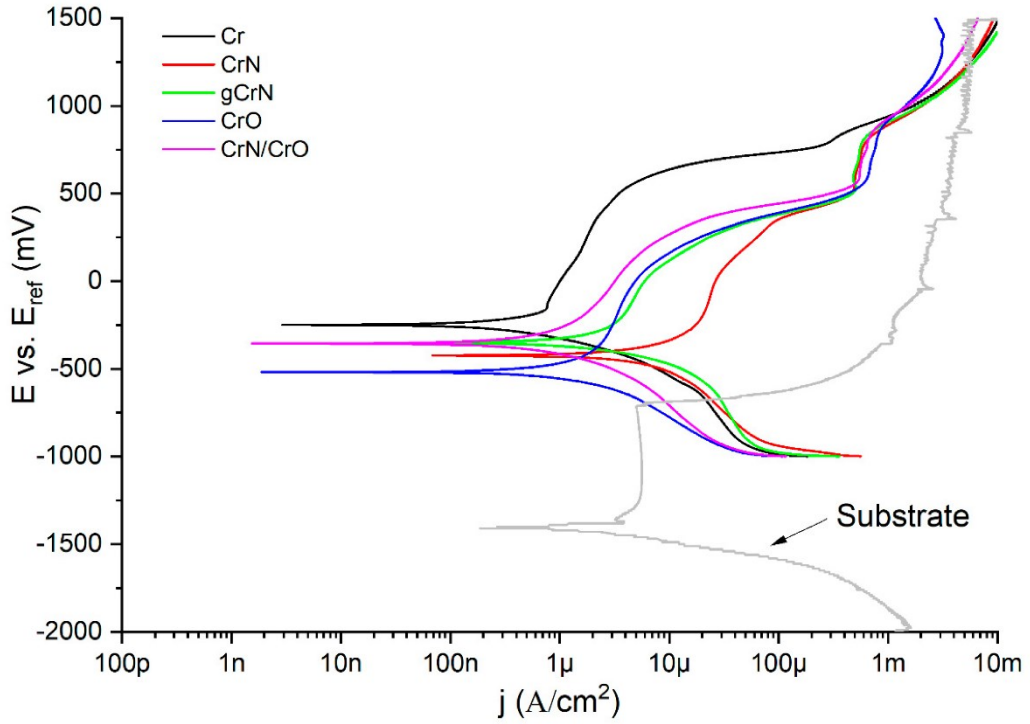

Figure V-6. Tafel plots from obtained films and substrate.

Current densities measured by Tafel extrapolations are strongly associated with the polarization resistance (R_p). According to the ASTM G3 standard, R_p could be calculated from [37]:

$$R_p = \frac{\beta_a * \beta_c}{2.303 * (\beta_a + \beta_c) * j_{corr}} \quad (1)$$

where β_a and β_c are the anodic and cathodic Tafel slopes, respectively, and j_{corr} is the corrosion current density. The fit parameters as well as every calculated R_p is displayed by Table V-3. R_p values demonstrated that nitride films displayed the worst anticorrosive behavior against artificial sweat. The presence of nanocrystalline structure and the phase composition compromise the corrosion behavior. This approach also justifies the behavior of the multilayer system. In fact, the nitride phase affects the corrosion performance of multi-layered CrN/CrO film, which shows closer values of J_{corr} to CrN film and exhibits uniform corrosion (see Figure V-5). The CrO film showed the highest polarization resistance, indicating higher corrosion resistance against artificial sweat. Our results are coherent according to the description by Dinu et al. [38], who studied the corrosion behavior of chromium-based films. They produced CrN, Cr(N,O), Cr(N,O)/CrN, and CrN/Cr(N,O) coatings over 304 stainless steel coupons. Their findings pointed out the crucial role of oxygen in the outer film layer leading to higher R_p values and consequently better corrosion resistance.

Table V-3. Fit parameters of Tafel plots and polarization resistances from coatings.

	β_A (mV/decade)	$\lvert\beta_c\rvert$ (mV/decade)	J_{corr} (nA/cm²)	E_{corr} (mV)	R_p (KΩ*cm²)*	Corrosion Rate (×10⁻³ mm/yr)
Cr	170 ± 58	193 ± 18	476 ± 67	−238 ± 11	82	5
gCrN	124 ± 7	309 ± 63	3471 ± 129	−258 ± 92	11	27
CrN	203 ± 38	139 ± 14	5075 ± 1335	−409 ± 15	7	35
CrO	127 ± 26	74 ± 15	321 ± 23	−505 ± 14	63	3
CrN/CrO	195 ± 30	94 ± 13	486 ± 19	−364 ± 7	57	-

* Substrate: R_P = 16.73 KΩ*cm².

Electrochemical impedance spectroscopy (EIS) results pointed out to a diminution of impedance modulus (|Z|) after 96 h systematic immersion, which denotes a diminution of corrosion resistance against artificial sweat of the obtained films (see Figure V-7). Nitride films consistently exhibited the worst anticorrosive properties. On the other hand, Cr and CrO exhibited the highest |Z| values, meaning the best corrosion resistance, along with corrosion rate forecasts (see Table V-3). The multilayered CrN/CrO sample could not be used to calculate the corrosion rate owing to the difficulty of estimating or assuming its density with a certain reliability. Also, the phase angle plots showed the largest differences at low frequencies (<10 Hz), which exhibited an increasing trend in angles with higher exposure time.

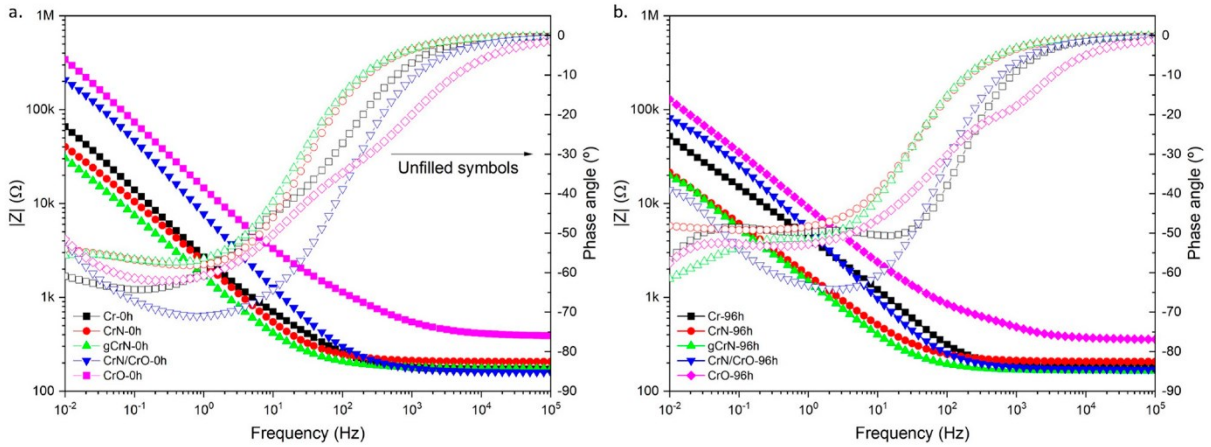

Figure V-7. Bode plots of obtained coatings to 0 h (a) and 96 h (b).

Additionally, Nyquist plots (Figure V-8) evidenced the capacitive nature of the films. At 96 h of exposure to the artificial sweat, the Nyquist plots evidenced the strong shrinking of initial semicircles shown by the films. Cr and CrO films displayed light steeping to low frequencies, which could indicate some degradation of the capacitive behavior. Nitrides and multi-layered CrN/CrO samples kept the same initial shape in Nyquist plots. All these measurements were adjusted according to the equivalent electrical circuit (EEC) exhibited in Figure V-9.

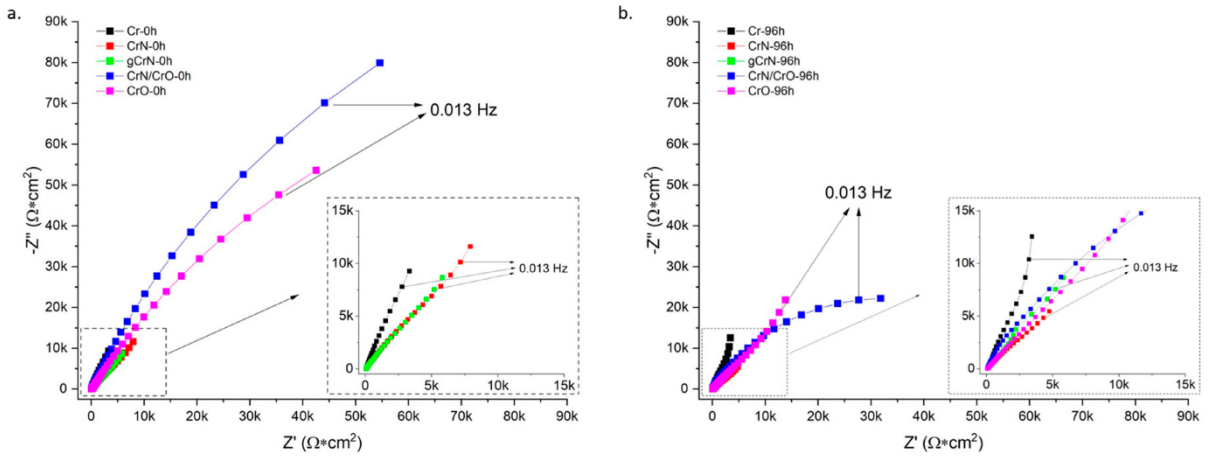

Figure V-8. Nyquist plots of obtained coatings to 0 h (a) and 96 h (b).

Regarding the EEC, the circuit is composed of five elements. R_{sol} represents the resistance of artificial sweat. Furthermore, R_{coat} and CPE_{coat} represent the coating's resistance and constant phase element, respectively. Commonly, CPEs are used to reproduce the electrochemical response of the surface when it is not working ideally. Defects like pores, pinholes, and heterogeneities in topography or chemical species along the surface (i.e., impurities) are common in sputtered films. These elements are classified according to a variable exponent α, which can vary between 1 and 0. When this exponent is closer to 1, the CPE behaves as a capacitor; between 0.6 and 0.4, it is considered as a resistor connected in series

with a capacitor (or a Warburg element); and 0 means that the CPE works like a resistor [39]. Lastly, R_p and CPE_{dl} represent the charge transfer resistance and the double-layer capacitance, respectively.

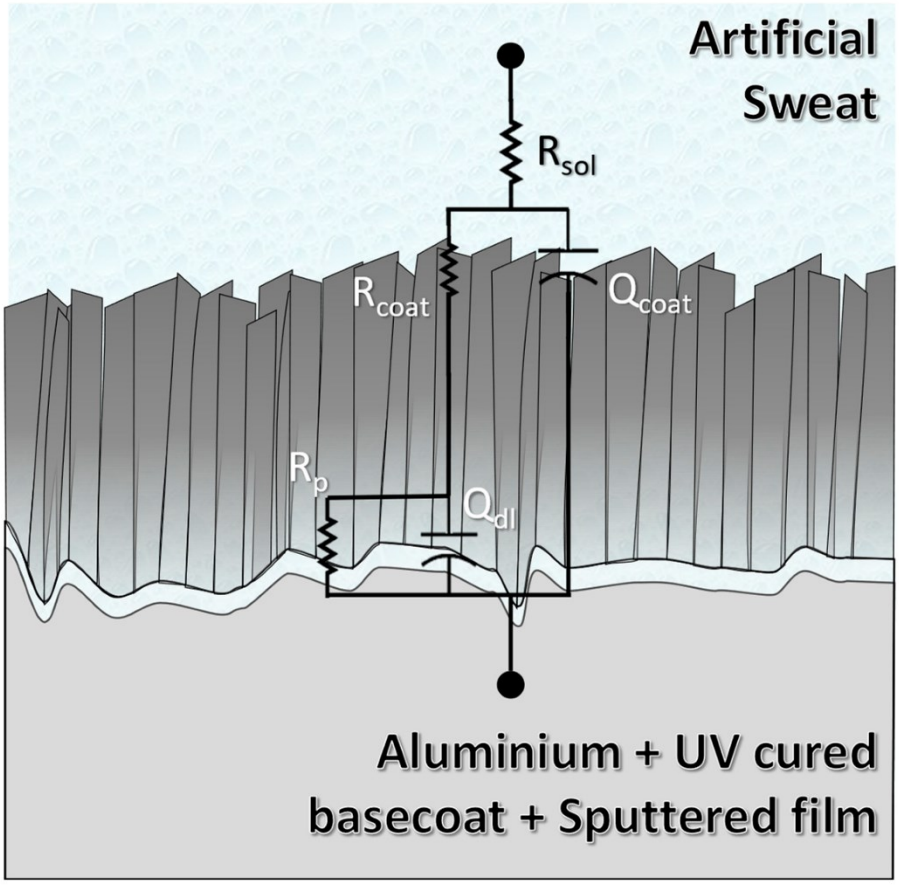

Figure V-9. Equivalent electrical circuits of obtained coatings.

The latter is related to the substrate/coating interaction. Table V-4 shows the highest R_p values in Cr and CrO for the obtained films. In fact, R_p value showed by Cr (~2.2 MΩ), the closest one to CrO (~7.8 MΩ), confirms the formation of the oxides in these films as the electrolyte/film interaction, and, hence, this sample has a self-protecting mechanism (passive layer) as was mentioned before. In contrast, nitride films showed the lowest values and, hence, less corrosion resistance, confirming the results obtained in polarization potentiodynamic tests. Another important aspect is the α exponent of CPEs. CrO was the only one which showed α value (~0.52) pointing to the CPE_{coat} behaving like a Warburg element (W), meaning that a slight diffusion process occurred but was not significant enough to replace the CPE for a W in the EEC [40]. The remaining α values in CPE_{coat} were between 0.66 and 0.84; hence, the remaining films were demonstrated to be far from the ideal capacitive behavior. These values are consistent with surfaces with a high grade of defects like voids, such as SEM and AFM results (see Figures V-4 and V-5). On the other hand, α values in CPE_{dl} were 0.62 and 0.79. These values reflect the substrates' high roughness and surface defects (Aluminium with UV-cured basecoat), expected in a painted metallic

surface. Fit parameters showed chi-square values in the magnitude of $10^{-3,}$ which could be considered a good fit [41]. All other fit parameters are shown in Table V-4.

Table V-4. EIS fit parameters of obtained coatings

	R_{sol} (Ω)	R_{coat} (Ω)	CPE_{coat} (μS*S$^{\alpha}$)	α_{coat}	R_p (kΩ)	CPE_{dl} (μS*S$^{\alpha}$)	α_{dl}	χ^2 (×10^{-4})
Cr	173 + 2	671 + 65	46 + 12	0.82 + 0.02	2205 + 1441	124 + 20	0.69 + 0.03	2.5
gCrN	167 + 1	4899 + 2450	267 + 55	0.73 + 0.02	190 + 77	169 + 41	0.72 + 0.06	1.8
CrN	198 + 2	3286 + 1092	314 + 94	0.66 + 0.04	44 + 17	322 + 36	0.75 + 0.03	23.8
CrO	195 + 3	3844 + 1166	23 + 7	0.54 + 0.05	7829 + 2660	9 + 2	0.79 + 0.02	25.6
CrN/CrO	167 + 5	20685 + 3535	31 + 4	0.84 + 0.03	275 + 195	24 + 11	0.62 + 0.02	7.6

EDS measurements were performed after corrosion tests to verify the chemical changes in the samples after artificial sweat interaction. Figure V-10 exhibits chemical composition and the O/Cr ratio between as-deposited and corroded conditions from all obtained films. The artificial sweat significantly oxidized the film surfaces, confirmed by the increase in all O/Cr ratios. The formation of oxides in some areas is probably due to the heterogeneity of the films, as mentioned before, which is exhibited in Figure V-5. The chemical kinetics of film after the electrolyte interaction was not measured in this study. However, some studies point out the possibility of CrN oxidation. Indeed, Gao et al. [42] established that the CrN films could oxidize in some hydroxide and oxide species. According to their XPS results after 4 h of electrolyte exposure (3 h in a buffer solution and 1 h in a 3.5 wt.% NaCl + buffer solution), CrN displayed strong superficial passivation with Cr_2O_3, $Cr(OH)_{3,}$ and CrO_3 species. The formation of Cr_2O_3 is plausible in the obtained films according to the EDS results after the corrosion tests, which exhibited a quasi-direct exchange between Cr and O without affecting the N content in the film. This phenomenon is possible due to the preferential formation of this oxide with free Cr in the film structure as is demonstrated by the Cr-O phase diagram [43] and the enthalpy of formation of these compounds ($\Delta_fH°_{CrN}$ = −117.15 KJ/mol & $\Delta_fH°_{Cr2O3}$ = −1134.70 KJ/mol [44]). Also, the EDS results before corrosion tests exhibited the substoichiometric conditions of the films, hence the possibility of having Cr free atoms which could react with an oxidizing media as the artificial sweat. It is possible that a mixture of free Cr crystals and CrN in the film's structure would be affected by the electrolyte, leading to an oxidation process promoted by OH^- and the dissolution of this passive layer provoked by the presence of Cl^- ions as proposed Gao et al. [45,46].

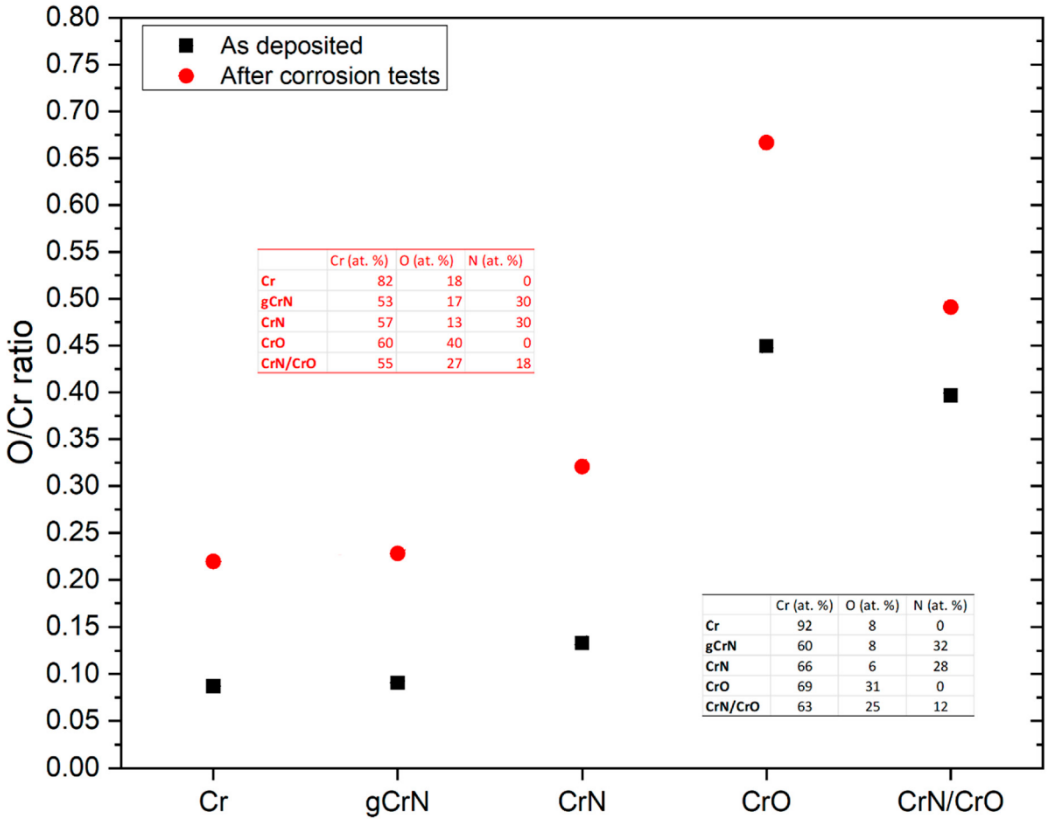

Figure V-10. O/Cr ratio and chemical composition of the obtained films before and after corrosion tests.

We further investigated the possible reactions involved at the coating–electrolyte interface for a better understanding of the chromium nitride morphology after corrosion tests.

In the presence of aqueous NH_3, a high concentration of OH^- ions will be present in the artificial sweat-like electrolyte (pH = 11.7), Equation (2):

$$NH_{3\,(aq.)} + H_2O_{\,(l)} \rightarrow NH_4^+{}_{\,(aq)} + OH^-{}_{\,(aq.)} \qquad (2)$$

Through EDS analysis, it is possible to see an increase in the oxygen content of the samples after corrosion tests. By naked eye visualization, it is possible to observe the coverage of CrN by a dark layer that can indicate the presence of chromium oxide. This allows us to identify the probable reaction pathway involved in the reduction–oxidation mechanism of CrN to Cr_2O_3 (Equation (3)) because the coatings will gradually oxidize to the thermodynamically stable oxides.

$$2\,CrN_{\,(s)} + 3\,OH^-{}_{\,(aq.)} \rightarrow Cr_2O_{3\,(s)} + N_{2\,(g)} + 3\,H^+{}_{\,(aq.)} \qquad (3)$$

The pitting in the chromium nitride samples observed by SEM analysis after electrochemical tests (Figure V-5) can be due to the release of molecular nitrogen from the coating to the electrolyte. In the presence

of a synthetic sweat electrolyte, nitrogen is released into the solution and does not remain trapped within the solid layer.

5.3 Partial conclusions

In an effort to develop hexavalent chromium-free coatings for frequently touched automotive parts, Cr(N,O) and multilayered CrN/CrO coatings were successfully deposited on aluminium substrates by reactive magnetron sputtering.

The chemical composition showed that all coatings had an excess of oxygen that can be related to high deposition pressure. Chemical and structural characterization of gCrN and CrN/CrO multilayered coatings showed a combination of the monolithic coating's characteristics.

Morphologically, Cr coating showed a columnar structure that turned denser with the addition of N_2 as a reactive gas. When oxygen was added as reactive gas (CrO coating), the coating increased in thickness, and, due to the deposition chamber setup, repeated layers of either O-deficient or O-rich material were deposited. Once again, CrN/CrO coating shows a mixture of both CrN and CrO morphology throughout the coating.

Regarding coating stability on the epoxy-coated aluminium substrates, all samples presented good adhesion to the substrates enhanced by the epoxy used and/or graded interlayer.

Corrosion behavior was induced using artificial sweat to simulate long exposure to human touch for 96 h. In potentiodynamic polarization tests, the coatings showed nobler behavior then the naked substrate. Cr almost does not possess a passivation region. Meanwhile, gCrN exhibited a passivation of the surface and its respective breakdown with several current fluctuations above +0.5 mV vs. E_{ref}, indicating the occurrence of pitting, which was confirmed by SEM micrography after the corrosion tests. The remaining films displayed two zones of passivation with their respective breakdown regions. Regarding EIS results, all films depicted a diminution of impedance modulus (|Z|) after 96 h, indicating a diminution of corrosion resistance against artificial sweat. Nitride films exhibited the worst anticorrosive features governed by film defects that cause electrolyte sinking. On the other hand, Cr and CrO exhibited the highest |Z| values. These results are corroborated by low the corrosion rates of both coatings.

Equivalent electrical circuits of obtained coatings are composed of five elements: R_{sol}, R_{coat}, CPE_{coat}, R_p, and CPE_{dl}. R_p, the charge transfer resistance was higher for Cr (~2.2 MΩ) and CrO (~7.8 MΩ), confirming oxide formation due to electrolyte/surface interaction and indicating a self-protecting mechanism. On the

other hand, nitride films showed the lowest values and less corrosion resistance, confirming the results obtained in polarization potentiodynamic tests.

The coatings developed in this work, namely Cr and CrO, showed promising behavior that could endure a lifetime of frequent human touch in various applications, either automotive or general appliances.

5.4 References

[1] Lu, R.; Miyakoshi, T. *Lacquer Chemistry and Applications*; Elsevier: Amsterdam, The Netherlands, 2015. https://doi.org/10.1016/C2014-0-04817-4.

[2] Chodun, R.; Skowronski, L.; Okrasa, S.; Wicher, B.; Nowakowska-Langier, K.; Zdunek, K. Optical TiO 2 layers deposited on polymer substrates by the Gas Injection Magnetron Sputtering technique. *Appl. Surf. Sci.* 2019, *466*, 12–18. https://doi.org/10.1016/j.apsusc.2018.10.003.

[3] Skowronski, L.; Chodun, R.; Zdunek, K. TiO_2-based decorative interference coatings produced at industrial conditions. *Thin Solid Film.* 2020, *711*, 138294. https://doi.org/10.1016/j.tsf.2020.138294.

[4] Ota, Y.; Masuda, T.; Kimura, S. Technical trends in aluminum alloy sheets for automotive body panels. *Res. Dev. Res. Dev. Kobe Steel Eng. Rep.* 2019, *69*, 15–18.

[5] Farfan-Cabrera, L.I.; Tapia-Gaspar, M.; Pérez-González, J. Tribology of Polymer Matrix Composites Within the Automotive Industry. In *Encyclopedia of Materials: Composites*; Elsevier: Amsterdam, The Netherlands, 2021; pp. 970–982. https://doi.org/10.1016/B978-0-12-819724-0.00029-X.

[6] Hattori, C.S.; Almeida, G.F.C.; Gonçalves, R.L.P.; Santos, R.G.; Souza, R.C.; da Silva, W.C., Jr.; Cunali, J.R.C., Jr.; Couto, A.A. Microstructure and fatigue properties of extruded aluminum alloys 7046 and 7108 for automotive applications. *J. Mater. Res. Technol.* 2021, *14*, 2970–2981. https://doi.org/10.1016/j.jmrt.2021.08.085.

[7] Hirsch, J. Automotive trends in aluminium—The European perspective. *Mater. Forum* 2004, *28*, 15–23.

[8] Sivanur, K.; Umananda, K.V.; Pai, D. Advanced materials used in automotive industry-a review. *AIP Conf. Proc.* 2021, *2317*, 020032. https://doi.org/10.1063/5.0036149.

[9] Liu, M.; Guo, Y.; Wang, J.; Yergin, M. Corrosion avoidance in lightweight materials for automotive applications. *Npj Mater. Degrad.* 2018, *2*, 24. https://doi.org/10.1038/s41529-018-0045-2.

[10] Mihora, D.J.; Ramamurthy, A.C. Friction induced damage: Preliminary numerical analysis of stresses within painted automotive plastics induced by large curvature counterfaces. *Wear* 1997, *203–204*, 362–374. https://doi.org/10.1016/S0043-1648(96)07452-2.

[11] Ramamurthy, A.C.; Lorenzen, W.I.; Bless, S.J. Stone impact damage to automotive paint finishes: An introduction to impact physics and impact induced corrosion. *Prog. Org. Coat.* 1994, *25*, 43–71. https://doi.org/10.1016/0300-9440(94)00502-8.

[12] Ryntz, R.A.; Everson, M.; Pollano, G. Friction induced paint damage as affected by clearcoat chemistry. *Prog. Org. Coat.* 1997, *31*, 281–288. https://doi.org/10.1016/S0300-9440(97)00082-9.

[13] Ramamurthy, A.C.; Charest, J.A.; Lilly, M.D.; Mihora, D.J.; Freese, J.W. Friction induced paint damage—A novel method for objective assessment of painted engineering plastics. *Wear* 1997, *203–204*, 350–361. https://doi.org/10.1016/S0043-1648(96)07453-4.

[14] Chami, A.; Benabbou, R.; Taleb, M.; Rais, Z.; El Haji, M. Analysis of survey data on corrosion in the automotive industry. *Mater. Today Proc.* 2021, *45*, 7636–7642. https://doi.org/10.1016/j.matpr.2021.03.113.

[15] Bing, L.; Zhou, X.; Zhang, X. Filiform corrosion behaviour on machined AA7150 aluminium alloy. *Trans. Nonferrous Met. Soc. China (Engl. Ed.)* 2020, *30*, 2056–2066. https://doi.org/10.1016/S1003-6326(20)65360-2.

[16] Rathish, R.J.; Rajendran, S.; Christy, J.L.; Devi, B.S.; Johnmary, S.; Manivannan, M.; Rajam, K.; Rengan, P. Corrosion Behaviour of Metals in Artificial Sweat. *Open Corros. J.* 2010, *3*, 38–44.

[17] Shimpi, K.C.; Ravindranath, K.; Jani, A.K.; Kothari, D.C.; Harindranath, C.S. Decorative coatings produced using combination of reactive arc evaporation and magnetron sputtering. *Surf. Coat. Technol.* 1997, *90*, 115–122.

[18] Suo, X.; Guo, C.; Kong, D.; Wang, L. Corrosion behaviour of TiN and CrN coatings produced by magnetron sputtering process on aluminium alloy. *Int. J. Electrochem. Sci.* 2019, *14*, 826–837. https://doi.org/10.20964/2019.01.81.

[19] Yadav, A.; Kumar, K.; Ambat, R. Statistical analysis of corrosion failures in hearing aid devices from tropical regions. *Eng. Fail. Anal.* 2021, *130*, 105758. https://doi.org/10.1016/j.engfailanal.2021.105758.

[20] Fenker, M.; Jackson, N.; Spolding, M.; Nicole, P.; Schönhut, K.; Gregory, G.; Hovsepian, P.E.; Münz, W.D. Corrosion performance of PVD-coated and anodised materials for the decorative market. *Surf. Coat. Technol.* 2004, *188–189*, 466–472. https://doi.org/10.1016/j.surfcoat.2004.08.054.

[21] Carneiro, E.; Parreira, N.M.G.; Vuchkov, T.; Cavaleiro, A.; Ferreira, J.; Andritschky, M.; Carvalho, S. Cr-Based Sputtered Decorative Coatings for Automotive Industry. *Materials* 2021, *14*, 5527. https://doi.org/10.3390/ma14195527.

[22] Hodgman, C.D.; Lange, N.A. Handbook of chemistry and physics. *J. Frankl. Inst.* 1930, *209*, 847. https://doi.org/10.1016/s0016-0032(30)91499-8.

[23] Ando, E.; Suzuki, S. Optical and mechanical properties of Cr and CrNx films by dc magnetron sputtering. *J. Non Cryst. Solids* 1997, *218*, 68–73. https://doi.org/10.1016/S0022-3093(97)00197-X.

[24] Rothhaar, U.; Oechsner, H.R.f. magnetron sputter deposition of Cr2O3 layers on ceramic Al2O3 substrates. *Surf. Coat. Technol.* 1993, *59*, 183–186. https://doi.org/10.1016/0257-8972(93)90080-8.

[25] Ponte, F.; Sharma, P.; Figueiredo, N.M.; Ferreira, J.; Carvalho, S. Decorative Chromium Coatings on Polycarbonate Substrate for the Automotive Industry. *Materials* 2023, *16*, 2315. https://doi.org/10.3390/ma16062315.

[26] Sharma, P.; Ponte, F.; Lima, M.J.; Figueiredo, N.M.; Ferreira, J.; Carvalho, S. Plasma etching of polycarbonate surfaces for improved adhesion of Cr coatings. *Appl. Surf. Sci.* 2023, *637*, 157903. https://doi.org/10.1016/j.apsusc.2023.157903.

[27] Nezhad, A.N.; Davoodi, A.; Zahrani, E.M.; Arefinia, R. The effects of an inorganic corrosion inhibitor on the electrochemical behavior of superhydrophobic micro-nano structured Ni films in 3.5% NaCl solution. *Surf. Coat. Technol.* 2020, *395*, 125946. https://doi.org/10.1016/j.surfcoat.2020.125946.

[28] Józwik, J.; Ostrowski, D.; Milczarczyk, R.; Krolczyk, G.M. Analysis of relation between the 3D printer laser beam power and the surface morphology properties in Ti-6Al-4V titanium alloy parts. *J. Braz. Soc. Mech. Sci. Eng.* 2018, *40*, 215. https://doi.org/10.1007/s40430-018-1144-2.

[29] Duboust, N.; Ghadbeigi, H.; Pinna, C.; Ayvar-Soberanis, S.; Collis, A.; Scaife, R.; Kerrigan, K. An optical method for measuring surface roughness of machined carbon fibre-reinforced plastic composites. *J. Compos. Mater.* 2017, *51*, 289–302. https://doi.org/10.1177/0021998316644849.

[30] Chipatecua, Y.L.; Olaya, J.J.; Arias, D.F. Corrosion behaviour of CrN/Cr multilayers on stainless steel deposited by unbalanced magnetron sputtering. *Vacuum* 2012, *86*, 1393–1401. https://doi.org/10.1016/j.vacuum.2012.01.016.

[31] Cassie, A.B.D.; Baxter, S. Wettability of porous surfaces. *Trans. Faraday Soc.* 1944, *40*, 546–551. https://doi.org/10.1039/tf9444000546.

[32] Jin, J.; Liu, H.; Zheng, D.; Zhu, Z. Effects of Mo content on the interfacial contact resistance and corrosion properties of CrN coatings on SS316L as bipolar plates in simulated PEMFCs environment. *Int. J. Hydrogen Energy* 2018, *43*, 10048–10060. https://doi.org/10.1016/j.ijhydene.2018.04.044.

[33] Barshilia, H.C.; Selvakumar, N.; Deepthi, B.; Rajam, K.S. A comparative study of reactive direct current magnetron sputtered CrAlN and CrN coatings. *Surf. Coat. Technol.* 2006, *201*, 2193–2201. https://doi.org/10.1016/j.surfcoat.2006.03.037.

[34] Creus, J.; Idrissi, H.; Mazille, H.; Sanchette, F.; Jacquot, P. Improvement of the corrosion resistance of CrN coated steel by an interlayer. *Surf. Coat. Technol.* 1998, *107*, 183–190. https://doi.org/10.1016/S0257-8972(98)00646-X.

[35] Ibrahim, M.A.M.; Korablov, S.F.; Yoshimura, M. Corrosion of stainless steel coated with TiN, (TiAl)N and CrN in aqueous environments. *Corros. Sci.* 2002, *44*, 815–828. https://doi.org/10.1016/S0010-938X(01)00102-0.

[36] *ASTM G3-14(2019)*; ASTM G3—Conventions Applicable to Electrochemical Measurements in Corrosion Testing. ASTM international: West Conshohocken, PA, USA, 2014; pp. 1–9. https://doi.org/10.1520/G0003-13.2.

[37] Dinu, M.; Mouele, E.S.M.; Parau, A.C.; Vladescu, A.; Petrik, L.F.; Braic, M. Enhancement of the corrosion resistance of 304 stainless steel by Cr-N and Cr(N,O) coatings. *Coatings* 2018, *8*, 132. https://doi.org/10.3390/coatings8040132.

[38] Yuan, X.; Song, C.; Wang, H.; Zhang, J. *Electrochemical Impedance Spectroscopy in PEM Fuel Cells Fundamentals and Applications*; Springer: London, UK, 2010. https://doi.org/10.1007/978-1-84882-846-9.

[39] Castro, J.D.; Lima, M.J.; Carvalho, S. Corrosion resistance of Cu-Zr(O) N films in a simulated seawater environment. *Surf. Coat. Technol.* 2022, *451*, 129050. https://doi.org/10.1016/j.surfcoat.2022.129050.

[40] Castro, J.D.; Pinto, B.; Ferreira, F.; Serra, R.; Carvalho, S. Wettability and corrosion resistance of zirconium nitride films obtained via reactive high-power impulse magnetron sputtering. *J. Vac. Sci. Technol. A* 2023, *41*, 023106. https://doi.org/10.1116/6.0002341.

[41] Gao, S.; Dong, C.; Luo, H.; Xiao, K.; Pan, X.; Li, X. Scanning electrochemical microscopy study on the electrochemical behavior of CrN film formed on 304 stainless steel by magnetron sputtering. *Electrochim. Acta* 2013, *114*, 233–241. https://doi.org/10.1016/j.electacta.2013.10.009.

[42] ASM International. *Alloy Phase Diagrams*, 1st ed.; ASM International: West Conshohocken, PA, USA, 1992; Volume 3.

[43] Chase, M.W., Jr. *NIST-JANAF Thermochemical Tables, Part I, A1-Co—Monograph No. 9*, 4th ed.; The American Chemical Society; The American Institute of Physics: New York, NY, USA, 1998.

[44] Nielsen, H.P.; Frandsen, F.J.; Dam-Johansen, K.; Baxter, L.L. The implications of chlorine-associated corrosion on the operation of biomass-fired boilers. *Prog. Energy Combust. Sci.* 2000, *26*, 283–298.

CHAPTER VI- Final Remarks and Future Developments

6 Final remarks and future developments

The implementation of Reach Regulation across the European Union served as the driving force behind this doctoral thesis. As the race to enhance human and environmental safety began, the substitution of hazardous chemicals with safer alternatives made it evident that processes involving hexavalent chromium required immediate and urgent attention.

We investigate two primary categories of functional properties involving Cr(IV) – hard chromium and decorative chromium applications. By means of PVD we explore several options trying to find the best alternative coating for achieving equivalent functional characteristics to those traditionally attained through chromium electroplating.

In the pursuit of eco-friendly and high-performance solutions to replace hexavalent chromium in minting dies, Cr(Al,Si)N coatings stand out as a possible good solution. We successfully deposited these coatings using reactive magnetron sputtering. Focused on both the mechanical attributes of our produced coatings and the required functional properties asked by the application, we achieved important outcomes. Among various coatings, the CrAlN sample outperforms others, closely followed by the CrAlSiN sample. This means you can rely on these coatings for robust mechanical performance and longevity. With the final application in mind, after nano-impact tests, these coatings demonstrate impressive behaviour. At lower loads CrAlN and CrAlSiN performed similarly, but with increasing load, the CrAlN sample takes the lead, achieving higher contact pressures. The reduced final depth achieved by CrAlN coatings signifies their superior toughness and endurance. In applications (such as minting) where fracture resistance is critical, these coatings offer a distinct advantage. Our innovative coatings are well-suited for applications characterized by the presence of high impact loads, and we believe that they can replaced electroplated hard chromium in such processes.

Nevertheless, and despite this doctoral work expanded our understanding of local fatigue wear phenomena in thin films specially when fracture is a crucial factor there remains the need to subject our coatings to real-world testing. The logical progression would involve applying the coatings to punching dies and evaluating their performance in an industrial facility across numerous running cycles.

Next, we explored the application of reactive magnetron sputtering for the deposition of hexavalent chromium-free coatings onto PC substrates, with a specific focus on their utilization within the automobile industry.

The sputtered coatings, notably CrON and CrN, exhibit remarkable mechanical properties, presenting good hardness values associated with good adhesion, making them highly suitable for various automotive applications. These coatings offer a spectrum of grey tones, enabling diverse decorative applications. In dry sliding tests, most coatings meet industry standards for wear rates, underscoring their practical suitability for the automotive sector – others where decorative parts may be heavily touched. By tuning chemical composition, we narrow down limits for grey decorative coatings.

Conscious of the importance of preserving decorative properties over time, we then emphasize the significance of studying corrosion behaviour. On aluminium substrates, another common material used in the automotive industry, we successfully developed hexavalent chromium-free coatings for frequently touched automotive components, employing Cr(N,O) and multilayered CrN/CrO coatings through reactive magnetron sputtering. The coatings exhibited strong adhesion to epoxy-coated aluminium substrates and demonstrated impressive corrosion resistance when subjected to artificial sweat, simulating extended human touch exposure. notably, Cr and CrO coatings exhibited exceptional resistance to corrosion, as evidenced by their low corrosion rates. EIS further supported the corrosion resistance findings, emphasizing the high charge transfer resistance (Rp) of Cr and CrO coatings, indicating the presence of self-protective mechanisms. Nitride films, in contrast, exhibited lower values and reduced corrosion resistance. The coatings, particularly Cr and CrO, are promising in withstanding the rigors of frequent human touch, making them suitable for various applications, including those in the automotive industry and general appliances.

Therefore, considering our findings the next natural course of action should be tribo-corrosion assessment. It would be important for applications like automotive parts regularly touched by individuals (handles or knobs), to understand the effects of perspiration on the coatings combined with the reciprocating contact of another body.

In summary, we have effectively achieved our research objectives. Although there is work to be undertaken within this domain. This doctoral thesis serves as a substantial contribution to the scientific knowledge for the effective replacement of electroplated hexavalent chromium coatings by safer alternatives.